The Influence of Negative Skin Friction on the Bearing Capacity of Timber Piles in Amsterdam

D.H.J.E. Jacobs

Delft University of Technology
Civil Engineering and Geosciences
MSc. Civil Engineering - Geo-Engineering

The Influence of Negative Skin Friction on the Bearing Capacity of Timber Piles in Amsterdam

by

D.H.J.E. Jacobs

to obtain the degree of Master of Science in Civil Engineering
at the Delft University of Technology,
to be defended publicly on 17-12-2021

Student number:	4570804	
Project duration:	February 1, 2021 - December 17, 2021	
Thesis Committee:	Dr. ir. M. Korff	TU Delft
	Dr. ir. R. Spruit	Ingenieursbureau Gemeente Rotterdam
	Prof. dr. K.G. Gavin	TU Delft
	Ir. D.A. De Lange	Deltares
	Dr. ir. G.J.P. Ravenshorst	TU Delft
	Ir. M.P. Felicita	TU Delft

Preface

The objective of this master thesis was to contribute to ongoing research by analysing test data. A master student from Delft University of Technology performed the study and fulfilled the requirements to acquire the title Master of Science in Geo-Engineering at the Civil Engineering and Geosciences faculty. The student completed the research at the engineering department of the municipality of Rotterdam, with support from Delft University of Technology, Deltares and the engineering department of the municipality of Amsterdam.

The topic of the master thesis was to study the influence of negative skin friction on the geotechnical bearing capacity of timber foundation piles in Amsterdam. According to the current safety norms, many bridges and quay walls in Amsterdam are considered structurally unsafe. Several types of tests were carried out in Amsterdam to increase the knowledge on the contribution of different factors to the bearing capacity of timber piles, where this thesis focused on the factor negative skin friction.

Delft, December 2021

Acknowledgements

This report contains the findings of nine months of graduate work at the engineering firm of the municipality of Rotterdam and Delft University of Technology. Deltares and the engineering department of the municipality of Amsterdam further supported the research. The input and feedback of the graduation committee have contributed to the quality of the thesis.

My gratitude goes to my daily supervisor, Rodriaan Spruit, who, with his many years of experience in geotechnical engineering, was a great source of help in the past months. I also want to express my gratitude to Dirk de Lange: you always took the time to give me constructive feedback and always checked whether I understood the concepts. Our discussions at Deltares were precious to me. I want to thank Mandy Korff for keeping control over the process and continuously checking in with me after the progress meetings. Ken Gavin, thank you for sharing your knowledge on residual loads and how these impact a pile load test. I want to thank Geert Ravenshorst and Maria Felicita for their input and help in interpreting the material properties of timber. It was valuable to have feedback from geotechnical and structural engineering perspectives. I am also grateful to Willem van Bommel, Erwin de Jong and Aziz Cherkaoui for their support and feedback with their knowledge on the 'Programma Bruggen en Kademuren' project.

Concluding on my study time, I would like to express my gratitude to my parents, Willy and Yvonne, for their continuous support. My grandmother, Annie, has been a great inspiration with her drive and dedication. My gratitude goes to my sister, Pauline, for showing interest and giving support. I want to express my appreciation for my friends and roommates from Enschede for giving me a great time while studying in Enschede. And I want to thank my roommates and friends from Delft, for also making my time studying in Delft a pleasure. Finally, my best friend Anaïs: thank you for your continuous support and friendship through the years and for making my student life great.

I hope you will enjoy reading this thesis report.

Dianne Jacobs,

Delft, December 2021

Abstract

In the city of Amsterdam, many bridges and quay walls have a timber pile foundation. The bridges and quay walls were built many years ago, and there is limited insight into these timber pile foundations' original design and bearing capacity. The project 'Programma Bruggen en Kademuren' was established with several research divisions. One division focused on studying the bearing capacity of timber piles, and one group performed tests on new timber piles using optical fibre sensors to measure the pile behaviour along with the entire pile. The results of four piles tested in tension are used to study the influence of negative skin friction from these new piles.

The bearing capacity of pile foundations is calculated with the CPT method, using parameters from a Cone Penetration Test to estimate the bearing capacity. When evaluating the net bearing capacity, one should include the contribution of negative skin friction. The contribution from negative skin friction for a single pile and a pile group can be calculated in the current NEN code. In old bridges and quay walls with timber pile foundations, this load from negative skin friction was not considered during the original design. This research compared the negative skin friction developed around new timber piles to the value resulting from the NEN code.

The tensile load test measured the applied load, displacement of the pile at head level, and strains through the entire pile. Before the tests, the geometry and initial strains within the piles were determined. The results were combined to establish axial and shear force distributions and then create the mobilisation of shear forces in the different soil layers. Initially, the stiffness of the pile was based on strain readings in the pre-drilled top sand layer. When the compression load tests were performed on small sections of the piles in the timber laboratory of Delft University of Technology, these values were used in further analysis. Two scenarios have been analysed: based on relative strains, where the strains measured at the start of the tensile load test were zeroed out, and based on absolute strains, without zeroing out strain readings, but subtracting the initial strains present in the pile that were measured before the piles were driven into the soil.

The most interesting results of the analysis are the mobilisation curves of the different soil layers. According to the NEN 9997-1, the maximum shaft friction is expected to be mobilised at a displacement of 10 mm for driven piles. The combined mobilisation curves confirm this value: after 10 mm displacement, the maximum shaft friction was mobilised. Some curves showed an even softer response: 20 mm of displacement was needed.

It is the first time in the Netherlands that an α_t factor is calculated for a timber pile directly derived from an instrumented pile. According to the procedure in NEN 9997-1, one should perform more tests at another test site to validate the alpha factors before they are allowed to be mentioned in the NEN. The comparison of the α_s from the compression load test with the α_t from the tensile load tests showed that in 87 % of the cases, α_t was smaller than α_s, thus confirming the influence of tapering on the mobilisation of shaft friction.

The comparison of expected negative skin friction based on NEN 9997-1 and the calculated negative skin friction based on the maximum shaft frictions mobilised during the tensile load test confirmed that the tensile load test was a good method to quantify the negative skin friction to be expected. Based on the comparison, it was shown that using 0.25 for the $K_{0,j,k} * \tan(\delta_{j,k})$ term overestimates the negative skin friction. From the test data, an average factor of 0.22 was found, with a range of 0.21 to 0.23.

In conclusion, the variability of geometry and stiffness greatly influences the resulting forces

measured in the piles. The influence of negative skin friction was simulated based on the mobilisation curves derived from the test data and showed that the maximum influence of negative skin friction on the total bearing capacity was about 40 %. This research also verified whether optical fibre sensors apply to timber foundation piles since it was not tested before. The results show that the method effectively measures the pile behaviour and has high accuracy when analysed correctly. A minimum of two fibres should be applied to the timber pile, thus measuring at four locations in the cross-section of the pile.

The pile test history increased the complexity of the interpretation of the test data. The test history increased the number of uncertainties around the analysis, so if further pile tests were to be performed on timber piles, the complexity of this pile test history should be avoided if possible.

List of Figures

List of Tables

Contents

1. Introduction

This chapter will introduce the project in Amsterdam that is currently in progress. The student will explain the objectives, followed by establishing a scope for this Master Thesis.

1.1 Problem Description

Over the years, traffic loads on bridges and quay walls have increased. Also, sand fills were added to keep the street level constant. The elevation of the street level with sand fills has caused an increase in load on the timber foundation piles of these bridges and quay walls. It is thought that this has caused a rise in negative skin friction on the timber piles, a phenomenon that was not taken into account while designing the piles (Korff 2013). Also, the maintenance of the bridges and quay walls was not sufficient in the past years. Rather than maintaining the structures in a preventive way, one chose to repair the structures when severe damage existed. (*Programmaplan Bruggen en Kademuren* 2020) These two cases have led the municipality of Amsterdam to question the remaining bearing capacity of timber foundation piles under these structures. The program 'Bruggen en kademuren' was established to investigate this matter thoroughly.

1.2 Project Background

The document 'Actieplan bruggen en kademuren' mentions that Amsterdam has 829 traffic bridges and 205 kilometres of quay walls on timber piles. What was also mentioned in the document: according to the NEN code of 2012, all these bridges are structurally insufficient. The document says that the structural integrity of all these bridges and quay walls will have to be re-evaluated in the coming years. If needed, one will replace the entire structure, but if only minor repairs suffice, this is prefered.

Part of this action plan is to test the bearing capacity of timber piles, since it is thought that some conservative assumptions are made in the current calculation methods that need to be updated. (*Programmaplan Bruggen en Kademuren* 2020) It is mentioned in the action plan that according to the NEN code of 2012, most of the bridges involved in the project could be structurally unsafe and collapse immediately, but this has not happened. It is thought that the influence of the negative skin friction on the bearing capacity of timber piles is unfavourable. In Amsterdam Overamstel 27 new timber piles were tested, either during a compression load test or a tensile load test. Honardar (2020) analysed the compression load tests and derived alpha factors from the test data. His analysis showed that the alpha factors are too conservative in the current design methods. The alpha factor is a design factor that correlates the Cone Penetration Test readings and pile geometry to the pile's bearing capacity. From these tests in Amsterdam Overamstel, one did not yet analyse the data of the tensile load tests. During a tensile load test the movement of the soil relative to the pile is the same as when negative skin friction is occurring. It is expected that the results of the tensile load tests will contain information about the development of negative skin friction.

1.3 Research Objectives and Questions

In this thesis, one tries to answer the main research question: **'What is the load of negative skin friction on the piles tested in Amsterdam?'** The objective of this thesis is to find out how

negative skin friction develops around new timber piles. Since the timber piles are instrumented with fibre optics, it is expected that one can gain detailed insight into the negative skin friction development. To answer that, the following research questions are formulated:

1. How realistic are the current pile design methods in determining the bearing capacity of timber piles?
2. What is the influence of tapering on the soil stresses around the pile?
3. What is the influence of the variation in E-modulus over the length of the pile in the interpretation of the measurement data?

This thesis aims to recommend how the negative skin friction can be included in a more realistic way than is now the case in the calculation methods when proven that the current code is off too much. This improved method can then be used to assess the structural integrity and bearing capacity of the timber pile foundations.

1.4 Scope and Limitations

This thesis will quantify the negative skin friction developed around timber piles during a tensile load test. These piles are made of new timber since it was considered impossible to attach fibre cables for testing to the existing timber foundation piles. The piles would need to be pulled out of the soil first and then driven into the soil again, and it is thought that this will change the surrounding soil so that it is not representative anymore of the initial soil conditions. The influence of wood degradation could not be quantified during these tests. Since the test was performed in about five hours, degradation may occur, but this will be small for a short period.

The results from tensile load tests will be used as input for the simulation of negative skin friction development over the years. Negative skin friction develops over several years, but one could not take this parameter into account within the test framework.

The conclusions of this thesis on the development of negative skin friction around timber piles can initially be applied to timber foundation piles in Amsterdam. Still, it might also apply to other cities with timber pile foundations. Since the geotechnical profile will differ from the profile in Amsterdam, it is essential to look at the influence of individual soil types on negative skin friction.

1.5 Outline

The thesis will first describe the literature study needed to analyse the research topic properly. The literature study is followed by explaining the method used to find the proper results. The results will be presented, followed by a discussion and presentation of conclusions. Finally, recommendations will be given for further research.

2. Literature Study

This chapter includes the literature study that was done to prepare for the research. The study starts with an explanation of Amsterdam's geotechnical profile and the challenges this geotechnical profile has. Then a general description of the bearing capacity of pile foundations will be given, followed by a more in-depth elaboration for timber piles, including how decay occurs. Then the current assessment methods for timber piles will be explained. Field studies have previously been done on timber piles, so the results of these studies are also included. The last section of the literature study will explain how to measure strains using fibre optic sensors.

2.1 Geotechnical History Amsterdam

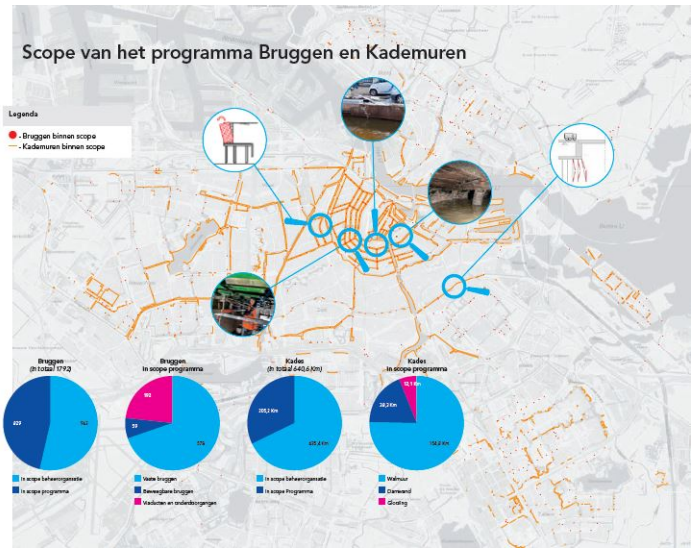

Figure 2.1: Bridges and Quay walls within scope of project (*Programmaplan Bruggen en Kademuren* 2020)

Figure 2.1 shows the bridges and quay walls involved in the research 'Programma Bruggen en Kademuren'. The city of Amsterdam is built around the river Amstel. Being built around a river means that thick peat and clay layers have accumulated over the decades. After men started to intervene with the natural conditions of this area, two circumstances changed. Firstly, dikes were built to make the land inhabitable. Since most of the land is situated below sea level and there used to be marshland, pump systems have to pump to keep the groundwater table below surface level continuously. It has caused peat to oxidise: it will react with oxygen and turn into carbon dioxide. A result is that the ground will start to subside. The second change is the application of a sand fill on top of the original peat layer. It was easier to construct sewerage and other structures in sand. But by applying this sand layer, the load on the soil layers below increased, thus increasing the amount of settlement these layers experienced. (De Gans 2011)

2.1.1 Geotechnical Profile

To conclude on the pile behaviour in the city centre of Amsterdam based on the tests in Overamstel, the soil conditions of both locations should be similar. Figures A.5 and A.6 shows a borehole taken at the Overamstel site.

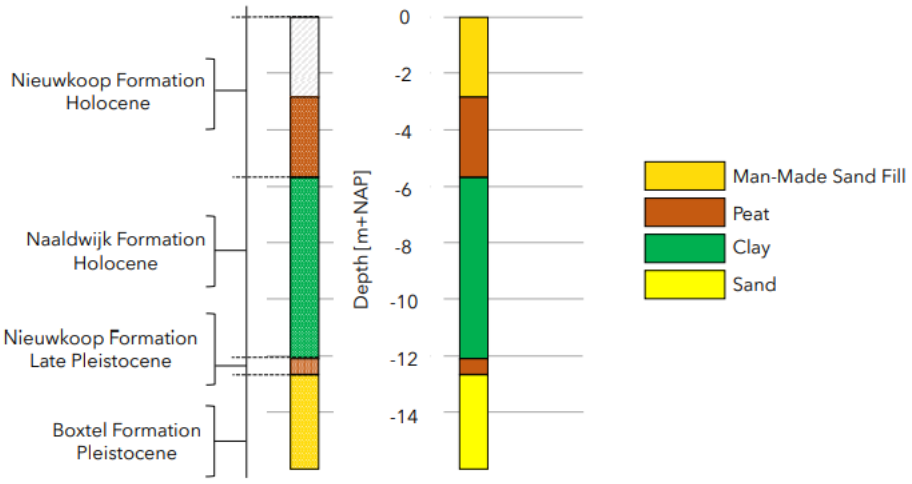

Figure 2.2: Soil profile and formations in Amsterdam
reprinted from Honardar (2020)

Figure 2.2 shows the typical soil profile found in Amsterdam. It was mentioned by De Gans (2011) that the parts of the city centre that are constructed close to the original Amstel river are built on a clay top layer. This clay layer was deposited on top of the peat layer during tides of the Amstel river. Further expansion of the city meant structures needed to be constructed on a peat top layer after a sand fill was applied on top of the peat. The fill caused settlement of the peat layer, and thus additional sand was needed to keep the street level constant. A sand fill was also added on top of the clay layer in the city centre, but due to differential settlements, this top sand layer has a varying thickness. The top sand fill at Overamstel is thicker than in most city-centre locations and was predrilled. This thicker layer can create higher friction along the pile shaft during soil settlement. However, during the tensile load test, the pile is pulled out, so the friction created results from the pile shaft moving along the soil, not the soil along with the pile. The test was also performed in a short period - one day- so it is assumed that no friction was created due to soil settlement during the test.

2.1.2 Bridge and Quay Wall Design

Figure 2.3 shows a typical design of a bridge in Amsterdam that was constructed with a timber pile foundation. Over the years, the traffic intensity has increased, so the bridges were reinforced. In many cases, additional piles were placed near the already present piles in the abutments. As a result, the piles will behave like a pile group, which should be considered. Another feature of the timber founded bridges is that they also contain piles installed under an angle. Especially in the abutments, piles are installed inclined.

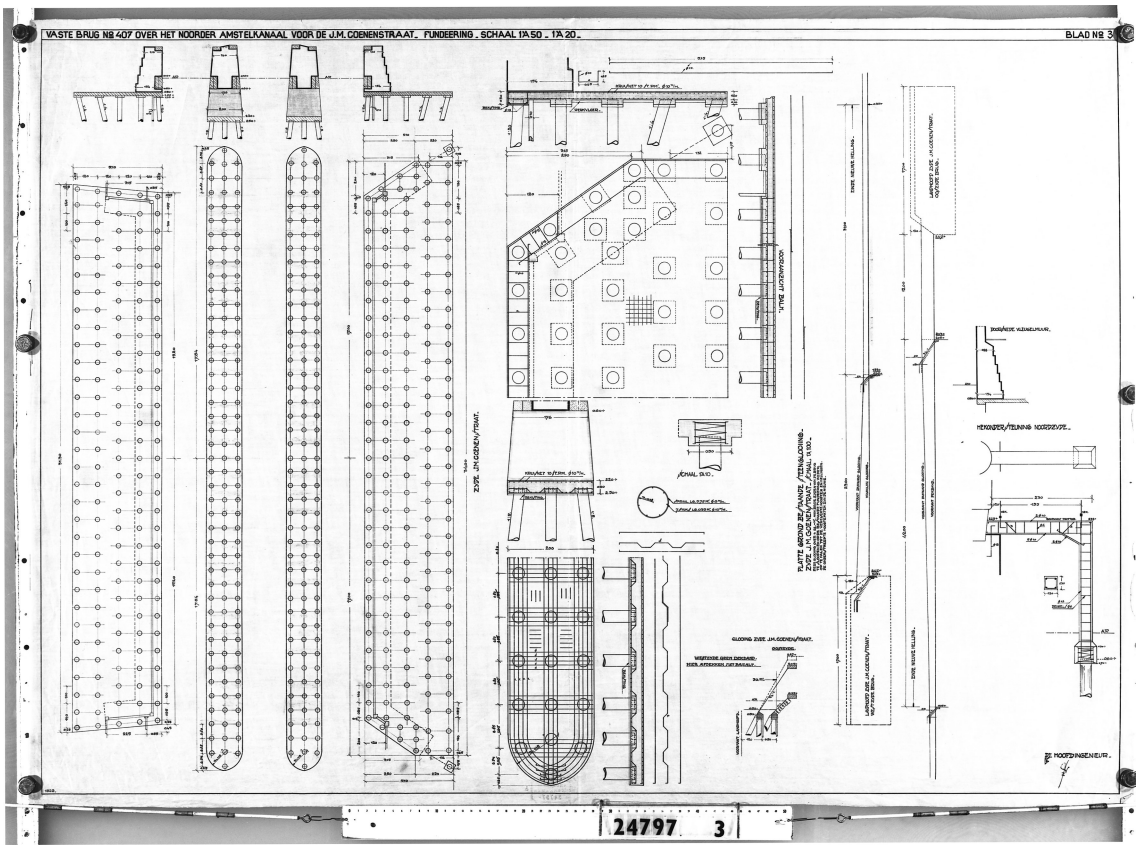

Figure 2.3: Floor plan Bridge 407 (1925) in Amsterdam (Gemeente Amsterdam, 2021)

Figures 2.4 and 2.5 show the design of a timber founded quay wall in Amsterdam. As for timber founded bridges, some of the foundation piles are installed under an angle. The biggest challenge for these timber founded quay walls is the increased loads on the piles due to the constant addition of the top sand fill.

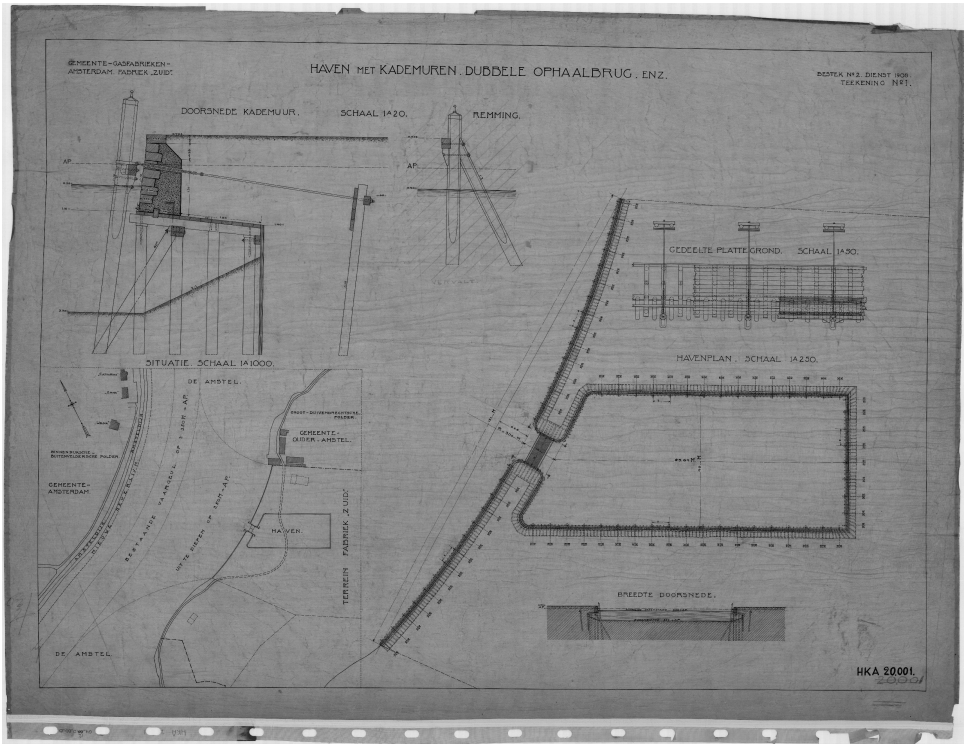

Figure 2.4: Design plan Quay wall Amsterdam, part 1 (Gemeente Amsterdam, 2021)

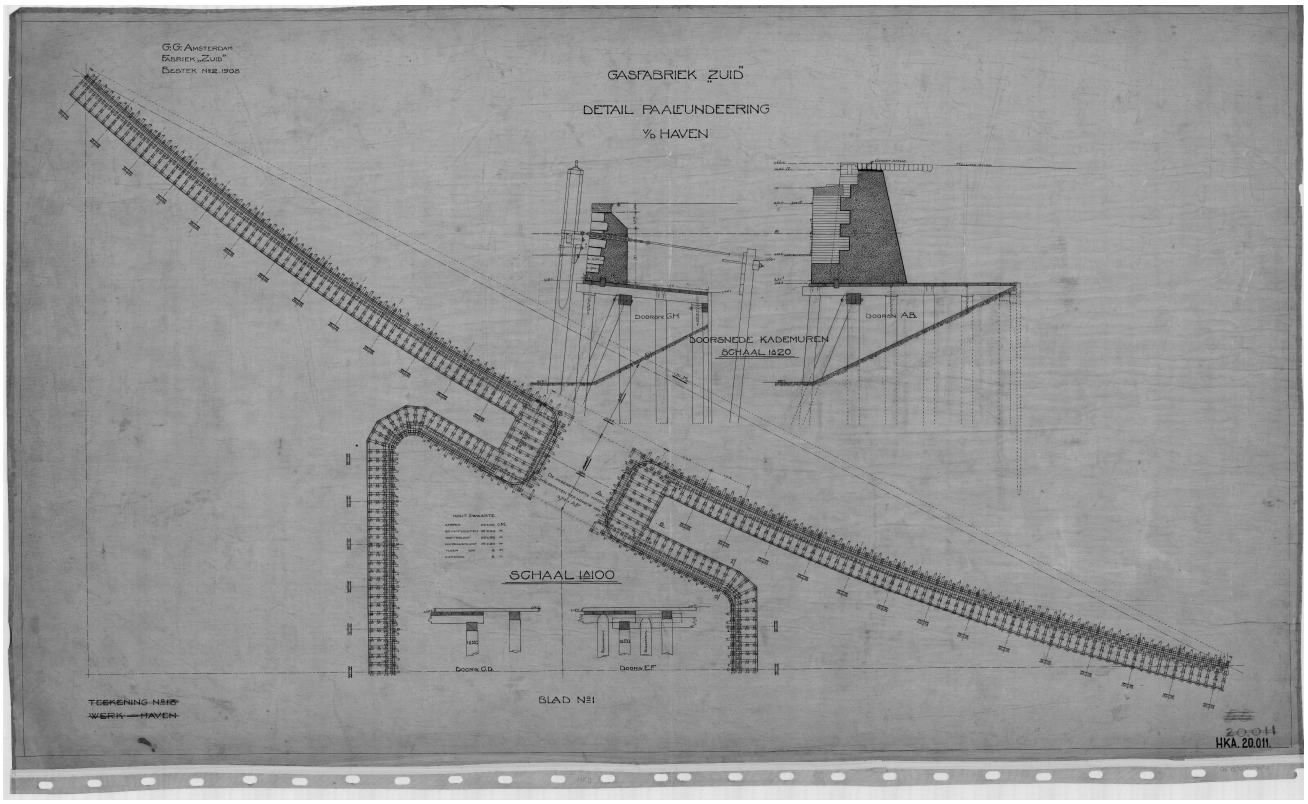

Figure 2.5: Design plan Quay wall Amsterdam, part 2 (Gemeente Amsterdam, 2021)

2.2 Bearing Capacity of Pile Foundations

In this section, the common Dutch method to calculate the bearing capacity of a pile foundation will be explained.

There are two different types of pile foundations: the end-bearing pile and the friction pile. The end-bearing pile mobilises most of its bearing capacity from resting into a load-bearing soil layer: theoretically - based on pile tests in Amsterdam - 60 percent of the total bearing capacity comes from the capacity that is created at the pile tip by resting in the bearing layer (Korff 2013). The total bearing capacity is mobilised in combination with shaft resistance created around the pile shaft with the surrounding soil layers. In this thesis, the end-bearing pile is considered only.

2.2.1 CPT based method

In the Netherlands, the CPT-based method is the most common method to determine the bearing capacity of pile foundations. In particular, the Koppejan method. The total bearing capacity can be calculated based on parameters retrieved from Cone Penetration Tests and correlation factors. The following formula is used:

$$R_{total} = R_{base} + R_{shaft,pos} - F_{shaft,neg} \tag{2.1}$$

Where R_{base} is the tip resistance [kN] in the load-bearing soil layer. $R_{shaft,pos}$ is the shaft resistance [kN] mobilized by the friction between the shaft of the pile and the surrounding soil. $F_{shaft,neg}$ is the load [kN] applied on the pile by negative skin friction, which acts in the opposite direction of the shaft resistance. In the next subsections, these three terms will be explained in detail.

Recently there has been a transition in pile design methods: rather than designing on ultimate capacity; now the design is based on maximum allowable displacements (Bersan et al. 2018). This means instrumented pile load tests are performed more frequently to find the load-displacement behaviour. Performing these tests also gives a better insight into the actual behaviour of pile foundations under loads, such as how individual soil layers contribute to the bearing capacity.

2.2.2 Base Capacity

The base capacity of the pile foundation can be calculated using the following formulas of the Koppejan method:

$$R_{base} = A_b * q_{b,max} \tag{2.2}$$

$$q_{b,max} = \frac{1}{2} * \alpha_p * \beta * s * (\frac{q_{c,I,gem} + q_{c,II,gem}}{2} * q_{c,III,gem}) \tag{2.3}$$

- R_{base} = pile tip resistance [kN]
- A_b = pile tip area [m^2]
- α_p = correlation factor for pile tip. Values depend on material and shape of the pile, and mode of installation. Factors are mentioned in NEN 9997-1.
- β = pile tip shape factor
- s = pile tip shape factor
- $q_{c,I,gem}$, $q_{c,II,gem}$, $q_{c,III,gem}$ = average cone resistance based on 8 * $D_{piletip}$ above and a minimum of 0.7 to 4 * $D_{piletip}$ below the pile tip level.

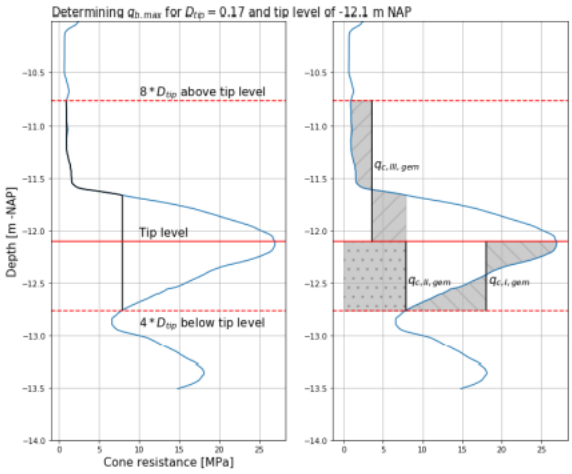

Figure 2.6: Determining $q_{b,max}$ with Koppejan method
reprinted from (Daatselaar 2019)

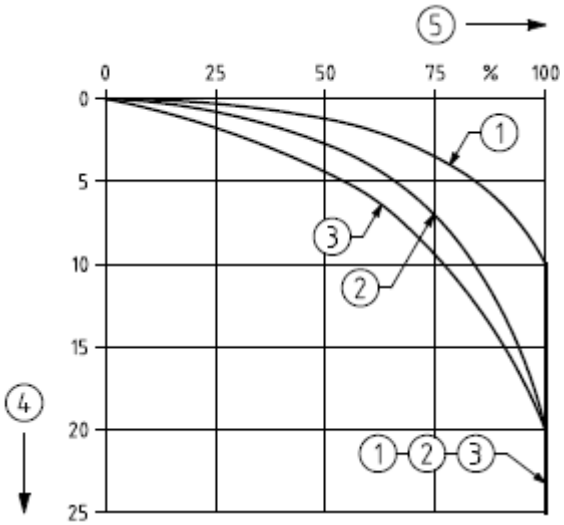

Figure 2.7: Mobilisation pile tip resistance as percentage of maximum pile tip resistance against pile tip settlement
reprinted from (*NEN 9997-1 + C2* 2017)

Figure 2.6 shows how the average cone resistance of the different terms can be determined. First, the minimum cone resistance on the interval 0.7 to 4D below the pile tip is determined. This should be $q_{c,II,gem}$. Then $q_{c,I,gem}$ is determined based on that minimum cone resistance and the maximum cone resistance on the interval. $q_{c,III,gem}$ is determined based on the interval of 8D above the pile tip. Figure 2.7 shows the mobilisation of the pile tip resistance against the pile tip settlement. Timber piles behave along curve 1, so the maximum pile tip resistance is expected at a pile tip settlement of 10 mm.

2.2.3 Shaft Capacity

The shaft capacity is created by combining all the friction that occurs along the pile shaft due to local soil stresses and friction properties of the soil. Since the pile displaces the soil, friction develops between the soil and the pile shaft, creating positive skin friction. The shaft capacity

can be calculated using the following formulas:

$$R_{shaft} = O * \int_{\delta L} p_{max,shaft}\, dz \tag{2.4}$$

$$p_{max,shaft} = q_c * \alpha_s \tag{2.5}$$

- R_{shaft} = pile shaft resistance [kN]
- O = circumference pile shaft [m]
- q_c = cone resistance [MPa]
- α_s = correlation factor for pile shaft. Values depend on the material and shape of the pile, and mode of installation. Mentioned in NEN 9997-1. α_t should be used for piles loaded in tension.

The pile shaft resistance is calculated using the maximum shaft friction that is expected to occur. The shaft resistance can only occur when a friction is mobilised, thus displacement between the pile and soil is needed.

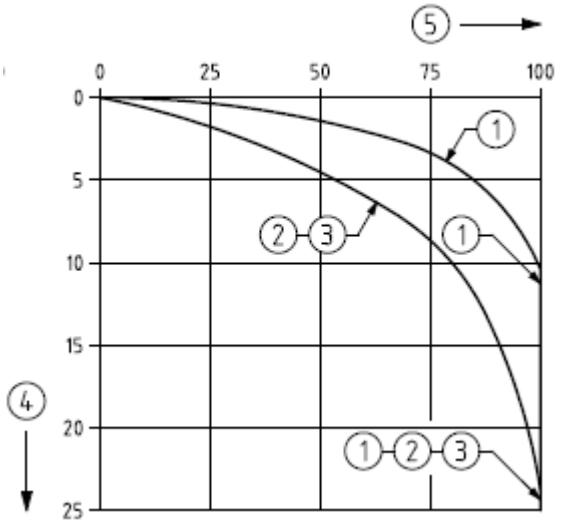

Figure 2.8: Mobilisation shaft resistance as percentage of maximum shaft resistance against pile tip settlement
reprinted from (*NEN 9997-1 + C2* 2017)

Figure 2.8 shows the mobilisation of shaft resistance against the displacement of the pile tip in millimeters. Timber piles are supposed to behave along curve 1. This means that at a pile tip displacement of 10 mm the maximum shaft resistance is expected.

2.2.4 Negative Skin Friction in Bearing Capacity Calculation

After calculating the base and shaft capacity using the CPT parameters and correlation factors, other phenomena that develop over time, such as negative skin friction, need to be included in the bearing capacity calculation. According to *NEN 9997-1 + C2* (2017), the negative skin friction along a single pile can be calculated using to the following formulas:

$$F_{nk,d} = \gamma_{f,nk} * F_{nk,k} \tag{2.6}$$

$$F_{nk,k} = O_{s,gem} * \sum_{j=1}^{j=n} d_j * K_{0,j,k} * tan(\delta_{j,k}) * \frac{\sigma'_{j-1,k} + \sigma'_{j,k}}{2} \tag{2.7}$$

- $F_{nk,d}$ = design value for load due to negative skin friction [kN]
- $\gamma_{f,nk}$ = partial factor, for the formula used 1.0
- $F_{nk,k}$ = characteristic value for load due to negative skin friction [kN]
- $O_{s,gem}$ = average circumference pile [m]
- d_j = soil layer thickness [m]
- $K_{0,j,k}$ = earth pressure coefficient of specific layer, equals 1 - sin($\phi_{j,k}$) [-]
- $\phi_{j,k}$ = internal friction angle of soil j
- $\delta_{j,k}$ = friction angle between pile shaft and soil layer j. For timber piles $\delta_{j,k}$ = 0.75 * $\phi_{j,k}$
- $\sigma'_{j,k}$ = effective vertical pressure at the bottom of soil layer j [kPa]

The negative skin friction can be calculated by adding the influence of all soil layers that experience downward movement along with the pile due to settlements. So the load-bearing soil layer is not included since it is assumed this layer will barely settle, thus not contributing to negative skin friction. The values of the internal friction angle and volumetric weight of the soil types are mentioned in Table 2b from *NEN 9997-1 + C2* (2017). In this calculation, one value is used for the circumference of the pile. As is mentioned above, it is assumed that the friction angle between the pile shaft and soil layer can be determined using the internal friction angle of the soil. How negative skin friction develops and how it influences the pile will be explained in detail in the section on ground behaviour.

$$F_{nk,k} = A * \sum_{j=1}^{j=n} (\sigma'_{v;j;sur;k} - \sigma'_{v;j;m;k}) \tag{2.8}$$

- $F_{nk,k}$ = characteristic value for load due to negative skin friction [kN]
- A = area covered by one pile [m^2]
- $\sigma'_{v;j;sur;k}$ = effective vertical pressure at the bottom of soil layer j as a consequence of a surcharge load, without the influence of other piles [kPa]
- $\sigma'_{v;j;m;k}$ = characteristic value of reduction of effective vertical pressure in layer j, caused by negative skin friction be transferred to other piles in pile group [kPa]

This equation calculates the expected negative skin friction occurring in a pile group. The difference with the equation for a single pile is that effective vertical pressure is reduced since part of the negative skin friction will be transferred to the other piles in the pile group.

2.2.5 Residual loads

Fellenius (2002) discusses the presence of residual loads. These loads can be created during different processes: during the installation of the pile, during reconsolidation of the surrounding soil, a time-dependent phenomenon, or due to previous loading conditions. These residual loads should be included in the interpretation of load test results because otherwise, this will lead to a false representation of the stress distribution along with the pile. Where negative skin friction occurs, there will be an overestimation of shaft resistance. There will be an underestimation of shaft resistance where positive skin friction occurs.

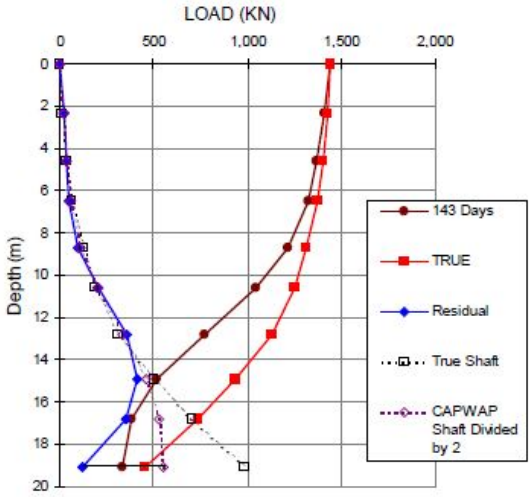

Figure 2.9: True and residual load distributions, (Fellenius 2002)

Figure 2.9 illustrates this false representation when residual loads are not taken into account. The brown line is the measurement when the strains at the test start are reset to zero. But the true distribution is the red line, which is found when the blue line - residual loads - is added to the brown line.

When including residual loads, negative skin friction will occur during a compression pile load test on the upper part of the pile, and on the lower part, positive skin friction is occurring. The negative skin friction is not fully mobilised in the lower part. Between the negative and positive skin friction, there should be a transition zone according to Fellenius (2002). This is observed in ideal conditions only, so it might not always be observed. In conclusion, the residual loads should be considered in a compression load test since these loads contribute to the overall capacity. It was found by Honardar (2020) that there is an increase in base and shear force when residual loads are included compared to when residual loads are not included.

2.3 Soil behaviour

The pile foundation is located in the soil, which means that the structure on top of the foundation influences the piles and the soil surrounding the piles. If the soil were to stay unchanged during the structure's lifespan, the soil would not affect the piles. But the soil will change over time, so the soil's influence has to be taken into account. This section will explain what happens to the soil and how this impacts the pile foundation.

2.3.1 Time Effect

The soil will settle over time. Either due to loads at the surface level or loads induced by the self-weight of soil layers on top of the specific soil layer. The load-bearing layer is assumed to settle only a small amount compared to the soft layers on top of that layer. The soft layers will settle, caused by different reasons, explained in the subsection on negative skin friction. While the soil is settling, it moves down along the pile shaft, mobilising friction between the soil and the pile. If the pile settled too, the friction created by the soil settlement would be reduced.

2.3.2 Positive skin friction

When a pile is driven into the ground, all the skin friction will be positive. Since the pile displaced the soil, there will be an upward reaction to the driving. The skin friction is positive since it has a positive contribution to the bearing capacity of the pile: it acts upwards, combined with the pile tip capacity compensating the load induced by the structure on top of the foundation. This positive skin friction contributes to the total resistance of the pile to the load applied on top of the pile.

2.3.3 Negative skin friction

Over the years, negative skin friction around the pile shaft can create an additional load on the pile, influencing the capacity of the pile foundation.

Three different events can induce negative skin friction:

1. Reconsolidation of remolded soil
2. Groundwater draw down
3. Surcharge loading

The reconsolidation of the remoulded soil happens right after the driving and is caused by the self-weight of the soil. In this situation, a soil settlement of less than 2 mm can already cause a total mobilisation of the negative skin friction (Ruifu 2008). The second event - groundwater drawdown - first causes an upward movement since the water drawdown reduces the effective vertical stress. But then this movement is compensated by the increase in effective vertical stress after consolidation. So adding these two events together leads to an effective downward movement of the soil.

The last event is adding a surcharge load on top of the soil. This leads to a consolidation of the underlying soil layers. However, while for the first two events, only small settlements of soil are needed to mobilise the maximum negative skin friction, for this event, a much bigger settlement is required for negative skin friction to mobilise fully. According to Ruifu (2008) after a settlement of 100 mm and in some literature, even 400 mm was needed for the full mobilisation of negative skin friction. In the case of Amsterdam, a surcharge load is added to the ground every time sand is added to the top fill to keep the street level constant.

There is a significant difference in the amount of soil settlement needed to mobilise the negative skin friction in the different events fully. Ruifu (2008) explained that during the events with small settlements the test conditions restricted the maximum amount of negative skin friction that could develop. The soil strength was either unchanged during the test or confined to a few pile diameters around the pile, which means that soil settlement cannot develop in a large area. In the case that large soil settlement is needed for full mobilisation - after applying a surcharge load -, there was a continuous dissipation of excess pore water pressure, which resulted in significant settlements. Thus the effective stress in the soil kept increasing, and so also the shear strength around the pile shaft.

Negative skin friction has also been researched in laboratory and model testing. Kong et al. (2013) performed a parametric analysis, using a mathematical model developed for the analysis of negative skin friction in consolidating soil.

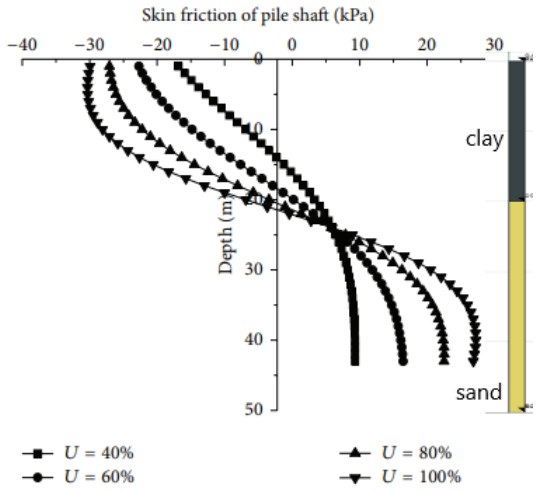

Figure 2.10: Curves of skin friction versus pile depth influenced by soil consolidation degree reprinted from Kong et al. (2013)

Figure 2.10 shows the influence of the soil consolidation degree on the development of negative skin friction along the length of the pile. The geotechnical profile consisted of different types of clay, and below 20 metres depth, a sand layer was present. It can be observed that at the maximum consolidation degree, the negative skin friction stops at the start of the sand layer. And at the lower consolidation degree, the negative skin friction shows linear behaviour but becomes non-linear when the degree increases.

Leung (2009) simulated the negative skin friction on piles using centrifuge testing. It was found that the amount of negative skin friction developed along a single pile depends on the magnitude of soil movement along with the pile, not on the settlement mode. Unlike to what Ruifu (2008) mentioned.

Negative skin friction greatly influences the remaining geotechnical capacity of the timber foundation piles in Amsterdam. Since there are many settlements in Amsterdam, it is expected this phenomenon plays a significant role. Based on the current NEN codes, a lot of the bridges and quay walls in Amsterdam are considered structurally unsafe (*Programmaplan Bruggen en Kademuren* 2020). However, it is thought these codes are too conservative for timber piles, and additional research should be done into the influence of negative skin friction on the bearing capacity. By doing so, a better insight can be obtained, and a better estimate can be made on the remaining bearing capacity of timber pile foundations.

2.3.4 Group Effect

When piles are placed close enough, the piles can be considered a pile group: forces on the pile will have different effects since part of the effect will be covered by the other piles. Kong et al. (2013) developed a mathematical model for the analysis of negative skin friction in pile groups. A pile group effect coefficient was calculated based on results from case studies, both field and model tests. The following formula was found to estimate the drag load for a pile group:

$$F_G = \eta * n * F_S \tag{2.9}$$

- F_G = dragload of pile group [kN]
- η = pile group effect coefficient [-]
- n = number of piles [-]
- F_S = dragload of single pile [kN]

Leung (2009) found that for a pile group with more than five piles, the group effect can be beneficial in reducing the negative skin friction. However, the corner piles still experienced more negative skin friction than the inner ones. Preliminary studies suggested that this reduction of negative skin friction decreases when soil settlement is increased. But further research is needed to confirm this.

As was mentioned in section 2.1.2, the foundation of most old bridges in Amsterdam can be considered as a pile group. It is thus of importance to consider the group effect on the resulting negative skin friction and the impact for one pile.

2.4 Timber Pile Foundations

This section will explain in more detail how timber pile foundations deviate from concrete and steel pile foundations. According to Borello et al. (2010), timber piles have an indefinite service life under ideal conditions. Unfortunately, ideal conditions do not occur. One of the significant differences between concrete and steel pile foundations is the order of magnitude of the nominal capacity: timber piles on average have an axial capacity that is one magnitude smaller than concrete piles. Timber pile foundations have been used for a long time and are still used nowadays, although now they are often used in combination with a concrete cap. Even though timber piles have been used for centuries, certain phenomena - such as negative skin friction - were not considered during the piles' design.

2.4.1 Tapering

A significant difference compared to other pile foundations is that timber piles are almost always tapered. This means that the diameter at the top of the pile is bigger than at the bottom. This is caused by the natural taper, depending on the shape of the tree that was used for the pile foundation (Borello et al. 2010). Tapering increases the frictional capacity of the pile in compression loading.

In the Netherlands, the Koppejan method is often used. It correlates the cone resistance found during a Cone Penetration Test to the shaft resistance using the α_s or α_t factor for a pile loaded in compression or tension, respectively. Tapering needs to be considered to find the true force acting on the pile. One can include tapering by measuring the taper at several pile heights. In the city of Amsterdam, it is assumed that the timber foundation piles have an average taper of 8 mm/m (Daatselaar 2019).

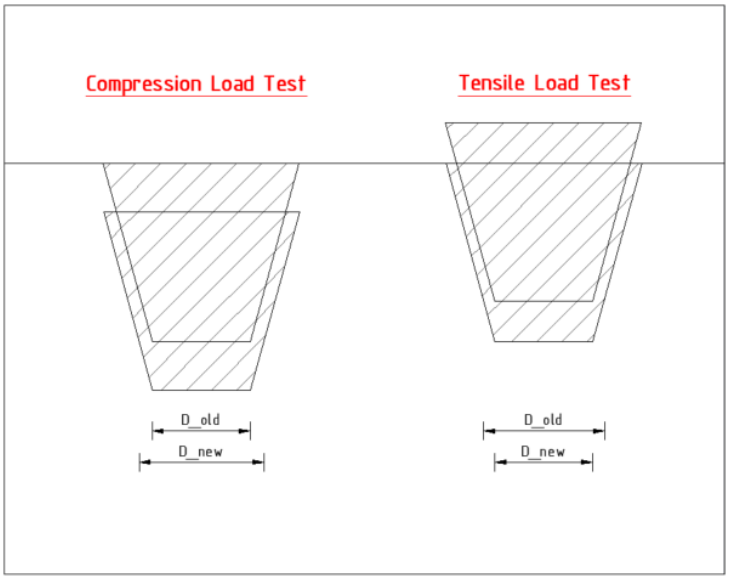

Figure 2.11: Difference in diameter during tests

Different friction along the pile shaft is expected to be measured during a compression and tensile load test. During a tensile load test, the pile moves upwards, meaning that a smaller diameter pile will be present where there used to be a bigger diameter. So a small relieve of horizontal stresses between the soil and pile shaft is expected, meaning smaller friction. (Figure2.11) This moving upwards for a tensile load test and downwards for a compression load test can only occur when slippage occurs. Before slippage happens, the pile itself will take

up the stresses created. After slippage, soil relaxation will arise, and the measured strain should be lower than the strain measured during a compression load test on the same elevation.

2.4.2 Variation in E-modulus

Another difference between concrete and steel pile foundations is that a timber pile does not have one single value for stiffness. The inner part of the timber pile contains younger wood than the outer part, and thus it is expected that the stiffness in the younger parts is lower (Daatselaar 2019).

Wood cells consist of three main components, with properties comparable to concrete piles. The first component is lignine, which is responsible for the compressive strength of the timber pile. Then cellulose is the reinforcement of the timber pile because it can withstand tensile forces. The hemicellulose binds the two other components together (Daatselaar 2019).

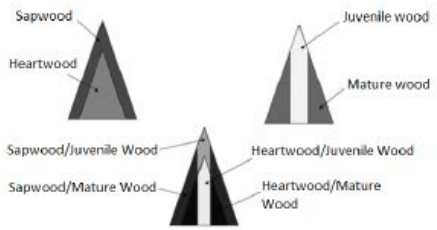

Figure 2.12: Properties over length of Pile
reprinted from Daatselaar (2019)

Figure 2.12 shows the different properties within a tapered timber pile. As can be seen in the picture on the right top, juvenile wood is present in the tree's core, and the top - which becomes the tip when used as a foundation pile - consists solely of juvenile wood. This juvenile wood has a lower stiffness than mature wood.

2.4.3 Bacterial Growth

Daatselaar (2019) mentions that fungi and bacteria cause wood degradation. Fungi can only grow in the top part of the pile, since they need oxygen to survive. But bacteria can grow along the complete length of the pile. They can break down cellulose and hemicellulose, thus especially influencing the tensile strength of the pile. The more open the wood structure, the easier it is for bacteria to occupy the space and break down the components. The tests analysed in this thesis did not measure the influence of bacterial growth; it was not in the scope of the pile load test: new timber piles were used. Thus bacterial growth was expected not to occur already, and the fibre optic cables could only measure strains or temperature differences, but no bacteria.

2.4.4 Loading conditions

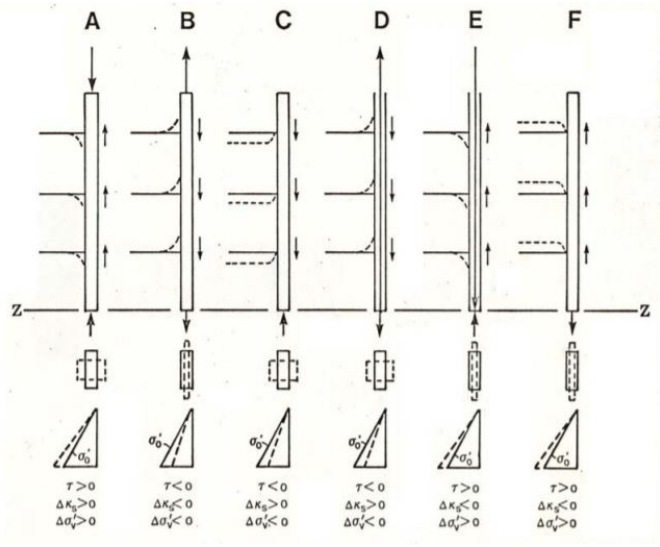

Figure 2.13: Behaviour modes of a pile subjected to different loading conditions reprinted from Fellenius (1984): Negative skin friction and settlement of piles

Figure 2.13 from Fellenius (1984) shows the difference in behaviour pile foundations may show under different loading conditions. Fellenius argued that the behaviour of the pile during a tensile load test is not completely similar to the behaviour of the pile during the occurrence of negative skin friction. Indeed, the direction of movement of the soil relative to the pile is the same, but when negative skin friction is happening, the pile is most likely loaded in compression rather than in tension. It should be mentioned that the piles tested by Fellenius were concrete piles. Concrete might have a different reaction to tensile and compression forces than timber has. Since timber has a smaller stiffness than concrete, being subjected to tensile and compression forces could have a larger effect on timber piles. Finding out how big the difference is between these two components is out of the scope of this thesis. Thus I assume that the maximum shear stresses found after a tensile load test can be related to the friction occurring along with the pile during soil settlement.

2.5 Decay of Timber Piles

Although the timber piles are situated in saturated soil - which means that the decay is minimised - still several phenomena develop during the lifetime of a timber pile that can influence its bearing capacity. Daatselaar (2019) mentioned that next to bacteria, the soil conditions have a significant influence on the degradation. Around peat and clay, less degradation is found since less water, and thus less oxygen is present. For peat in particular, the oxygen is already used for oxidation, so barely any oxygen is left for the degradation process.

In the following subsections, the decrease in stiffness and the creep effect will be explained further since it is expected they will have a significant impact on the remaining bearing capacity of old timber piles.

2.5.1 Decrease E-modulus

Over the years, and under the influence of different factors, the stiffness of a timber pile can decrease. A set of 12 old timber foundation piles of bridges 30 and 41 in Amsterdam were removed from the soil and tested in the laboratory. This gave an average static modulus of elasticity of 8100 N/mm^2, with a coefficient of variation of 0.32.

Tests on new timber piles - 30 spruce and 30 pine piles -, found a mean dynamic modulus of elasticity of 14300 N/mm^2 (and a CoV of 0.14) for spruce piles and 12000 N/mm^2 (and a CoV of 0.20) for pine piles. The static modulus of elasticity is 95 per cent of the dynamic modulus of elasticity, which gives a mean static modulus of elasticity of 13585 and 11400 N/mm^2 for spruce and pine, respectively (G.J.P. Ravenshorst, personal communication, September 27, 2021). So the piles that were part of the foundation of a bridge for several years showed a much lower stiffness than new timber piles.

2.5.2 Creep Effect

Creep is an ongoing permanent deformation of the timber, while the stress is constant. On the other hand, relaxation is a stress reduction, while the deformation stays the same. Especially creep is expected to significantly influence the properties of the timber pile during its lifespan.

Insight into creep and relaxation behaviour is essential for analysing the tensile load tests. Some of the piles were also tested in compression before the tensile load test, which might have influenced the timber's internal structure. Under the influence of the compressive load of the pile load test and the load developed by settling soil, the new timber piles might have developed a certain amount of creep between their instalment in July 2019 and the tensile load test in October 2020. If so, the compression resulting from this creep is partly responsible for the strain measured by the fibre optic sensors at the beginning of the tensile load test. It is difficult to define the contribution of stress in the first strain reading, but it is possible during one load step. Since the load is kept constant during the load step, creep must be responsible for a difference in strain during that load step.

2.6 Current Assessment Method for Existing Timber Piles

In the Netherlands, the F30 guideline is used to determine the current structural state of a structure on timber piles (*Richtlijn Houten Paalfunderingen onder gebouwen* 2016). Four assessment steps are needed to determine the condition. In this section, these steps will be discussed, and the last step - testing the geotechnical bearing capacity of the foundation - will be discussed in detail.

1. Stability of foundation construction: a visual inspection whether the construction shows any abnormalities that hamper the foundation piles to take on the loads from the upper part of the construction.
2. Bearing capacity timber piles: the design value of compressive load from the structure $\sigma_{c,d}$ needs to be compared to the design value of remaining compressive strength of the timber pile $f_{c,d}$, where $\sigma_{c,d} \leq f_{c,d}$.
3. Bearing capacity timber horizontally placed on piles: the design value of compressive loads acting perpendicular on the wood fiber $\sigma_{c90,d}$ needs to be compared to the design value of remaining compressive strength of the timber pile $f_{c90,d}$, where $\sigma_{c90,d} \leq f_{c,d}$.
4. Geotechnical bearing capacity

2.6.1 Geotechnical bearing capacity

The geotechnical bearing capacity can be determined based on two methods. The first method is a consideration based on the proven strength of the structure. The proven strength can be calculated based on the measured settlements, differences in settlements and the rate of settlements.

The second method is a consideration based on calculating the geotechnical bearing capacity. The formula mentioned in NEN 9997-1, which was also explained in section 2.2, should be used for this method. But as is stated in NEN 8700, the actual settlements need to be used in the formula instead of the calculated settlements. And NEN 8701 says that the load factors of an existing building are lower than the factors of new structures. The calculated load on the pile head and the load from negative skin friction together should not exceed the calculated bearing capacity of the pile (*Richtlijn Houten Paalfunderingen onder gebouwen* 2016).

2.7 Previous Field Studies

In 1974 tests were performed in Dapperbuurt, Amsterdam. The project included both timber piles from demolished houses and additional new piles driven into the soil. The piles of the houses were about 70 to 100 years old. All piles were first tested in compression and then tested in tension. The additional piles consisted of a reference pile, similar to the old timber piles, but then new. And there was a new timber pile, with a casing attached to it, so it is assumed that no shaft friction will be mobilised in the soft Holocene layer (Korff 2013).

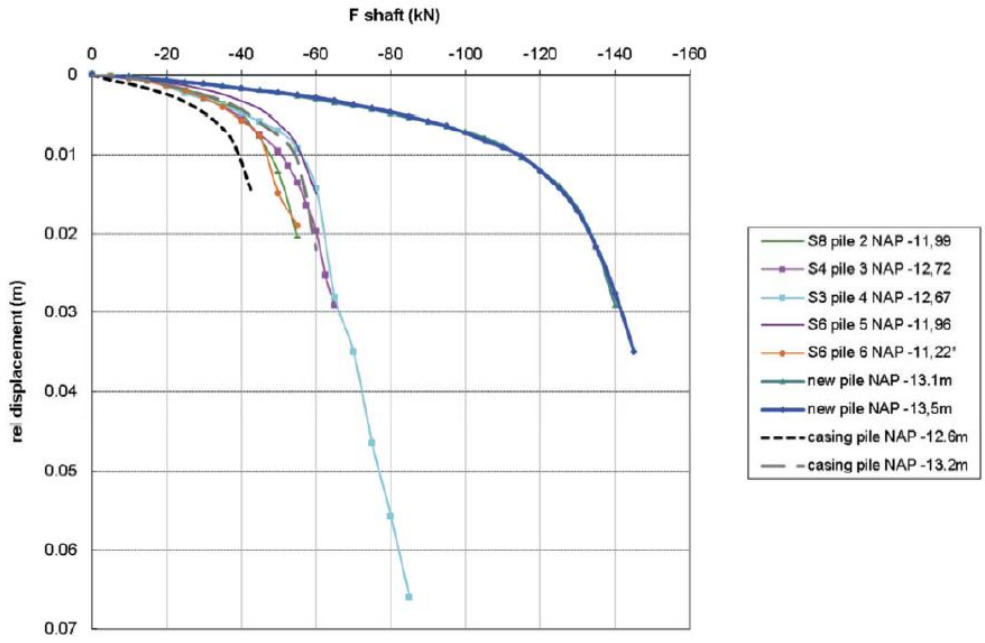

Figure 2.14: Shaft capacity after tensile load tests on old and new timber piles (Korff 2013)

The test results of the old timber piles compared to new ones showed a reduction of 40 per cent in shaft friction needed to fit the load-displacement curve. And as mentioned earlier, the old timber piles had a much lower stiffness - 0.6*10^7 to 0.8*10^7 kN/m^2 - compared to the new ones - 2*10^7 kN/m^2. However, Daatselaar (2019) critiqued the results of these tests. The first critique is that there was only one day between the compression and tensile tests for some of the tests. This might have influenced the test results of the tensile load test. Another critique is that the tests performed on 37 additional piles have not been reinterpreted. It is thought that since 1974 the calculation methods have improved, thus that a reinterpretation would give new insights. It needs to be mentioned that these piles could not be instrumented with fibre optic sensors, which has hindered the correct interpretation of the tests. The technique was not available yet.

These tests can help analyse the tensile load tests on the timber piles in Overamstel. An advantage is that the timber piles in Overamstel were instrumented with distributed fibre optic sensors, so it is expected that a better insight can be acquired in the development of negative skin friction.

2.8 Fibre Optic Sensors for Strain Measurements

Starting from the late 1990's, a development has taken place in measuring strain. Bersan et al. (2018) mentioned: one of the newest equipment of instrumentation for pile loads tests are Fibre Optic Sensors. They have a lot of advantages: amongst others, they can survive in extreme weather conditions, and production costs are relatively cheap compared to other test equipment. The only expensive part of the test is the equipment to send the light through the cables: the more frequently the measurements should be, the more expensive the equipment becomes. However, this method has a significant advantage over older types of instrumentation since it can give a fully distributed development of strains inside the pile.

2.8.1 Principle of Fiber Optic Sensors

Light is transmitted through the Fibre Optic Sensors. Three scatter forms are occurring in the sensors: Rayleigh, Raman and Brillouin scattering. Rayleigh and Brillouin scattering are sensitive to both temperature and strain, so one of the parameters should be kept constant during a test. During a pile load test, the temperature of the upper soil up to one-metre depth can only be influenced by variations in temperature. But when the test continues for several days, the temperature variations can also be found more profound in the soil (Bersan et al. 2018).

Light is sent through the cables during a pile load test, which interacts with the acoustic waves inside the optical fibre. The analysis can be performed using two different methods. Brillouin Optical Time Domain Analysis (BOTDA) is based on the stimulated pump-probe technique. One end of the glass fibre is connected to the pump of the reading equipment, and the other end is connected to the probe. Light is sent through the fibre from both sides during the strain reading. Since the power of the backscattered signal is greater than the Brillouin scattering, this method of analysis is faster than the other method, which uses unstimulated Brillouin scattering. The second method is the Brillouin Optical Time Domain Reflectometer (BOTDR) analysis. It detects the Brillouin backscattered light and measures the peak frequency. Only one end of the glass fibre needs to be connected to the reading equipment for this analysis.

2.8.2 Application in Geotechnical Engineering

As mentioned by Bersan et al. (2018), the strain measurements can be processed to create the resistance-displacement curves that are needed to determine the capacity of a pile. Before using the raw data, some averaging should be done since a lot of the variability is caused by load eccentricity. Averaging the strain measurements on all sides of the pile will solve this variability considerably. The following four steps were described to find the curves:

1. Integration of strain profile from top to bottom to determine vertical displacements. The displacement recorded at the pile head is a boundary condition.
2. Multiplication strain with local axial stiffness EA to determine load distribution.
3. Determining the tip resistance q: q = F(L)/A(L). The integral of the force along the entire length of the pile (L) should be divided by the pile tip area A(L).
4. Differentiation of the load for depth.

3. Method

This chapter will explain the several steps undertaken to answer the research questions. First, the initial data will be described, followed by how this data will be assessed and what will be done with the results.

3.1 Overview of Available Data

This section will give an overview of the available data for the analysis of this thesis. It will be explained how this data will be valuable towards the conclusions for the project.

3.1.1 Derivation Soil Parameters

Before the timber piles were driven into the soil at the test location, three CPT readings were done around every pile. Based on the average of the three CPTs, the location of the soil layers around that specific pile could be determined.

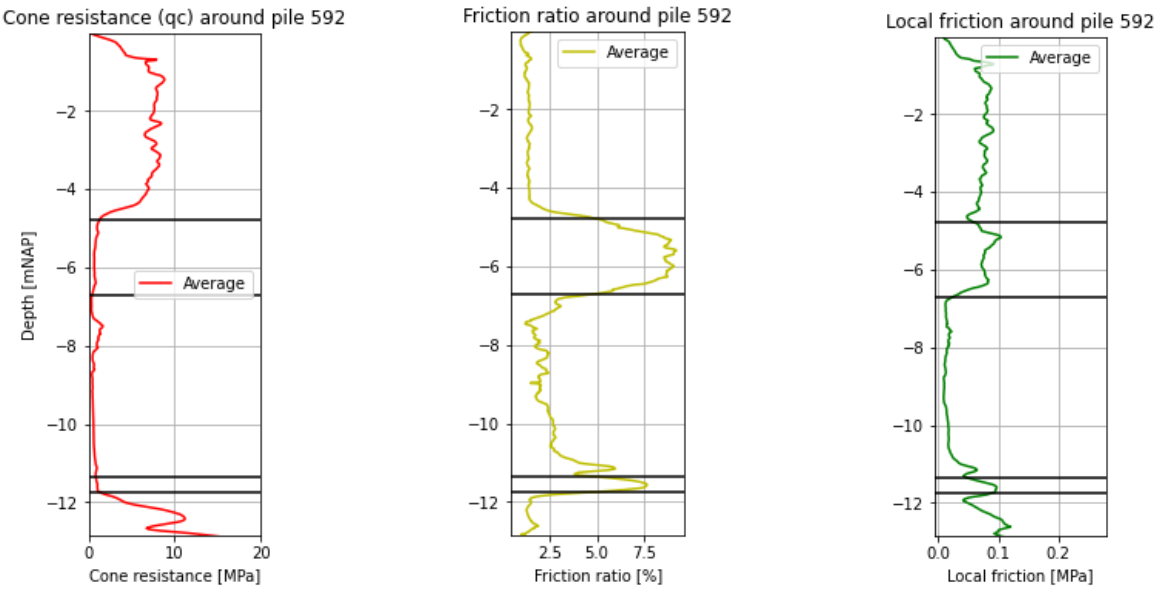

Figure 3.1: Parameters from CPT of pile 592

Figure 3.1 illustrates the cone resistance, friction ratio and local friction measured in the CPTs around pile 592. The average values of the distribution are illustrated. The soil boundaries were determined based on the cone resistance and friction ratio: the black lines illustrate the soil boundaries. The CPTs of the other piles can be found in section A of the Appendix. Combining the CPT results with the results of the borings done at the Overamstel site led to a final interpretation of the soil profile for each pile.

	P175	P187	P576	P592
Start Topsand	0.02 mNAP	0.04 mNAP	0.03 mNAP	0.03 mNAP
Start Peat1	-4.68 mNAP	-4.71 mNAP	-4.80 mNAP	-4.80 mNAP
Start Clay1	-6.56 mNAP	-6.63 mNAP	-6.70 mNAP	-6.70 mNAP
Start Peat2	-11.47 mNAP	-11.43 mNAP	-11.36 mNAP	-11.36 mNAP
Start Sand1	-11.71 mNAP	-11.75 mNAP	-11.74 mNAP	-11.74 mNAP

Table 3.1: Soil Boundaries derived from Cone Penetration Tests

The highest ground level that was measured by the CPTs was used as the start of the top sand layer. The location of the soil boundaries differs for some piles significantly from the soil boring, but it is thought that the depth registration of the CPTs are more accurate, and thus these values should be used in the further analysis of the thesis.

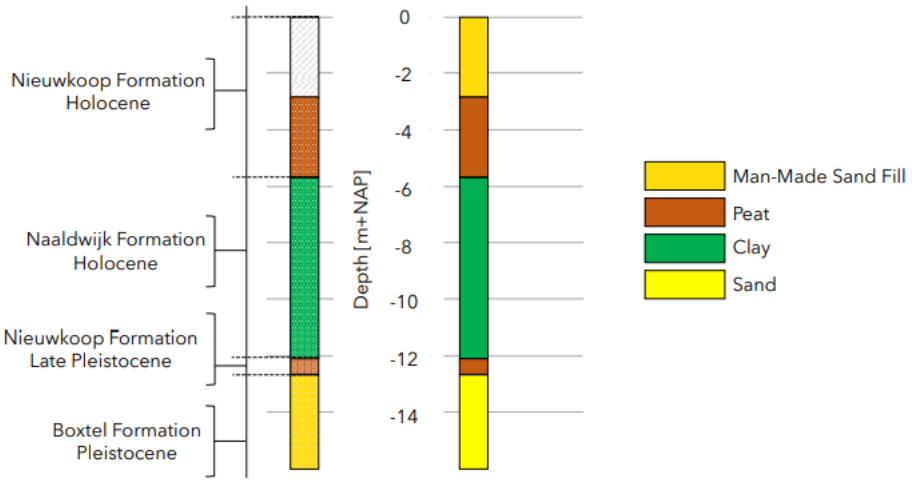

Figure 3.2: Typical soil profile and formation in Amsterdam
reprinted from Honardar (2020)

Figure 3.2 shows the typical soil profile of Amsterdam. The boring taken at Overamstel is illustrated in section A: it confirms the profile of Figure 3.2. Because the soil boring has to be interpreted manually, and tubes of one metre each are used for the boring, there is an uncertainty in the exact location of the soil boundaries.

3.1.2 Load and Displacement Data

Figure 3.4 illustrates the test set-up. At location 1, the load cell was placed on top of the jack. The jack pushed upwards to create a tensile force on the pile; the load was then measured by the load cell. The load and pile head displacement data were captured by the Daisylab program. Section A.1 shows the location of the LVDT (Linear Variable Differential Transducer): at ground level.

3.1.3 Reference Strain Readings

Reference strain readings were measured before the piles were driven into the soil, to find out the strain already present in the fibres before the pile was influenced by the soil. The reference measurements were tested on another day than the tensile load test, so the fibre loop could

be located elsewhere. In further analysis, the averaged strains from the hanging test were subtracted from the absolute strains. Sometimes it was not possible to determine the fibre loop based on the data from the hanging test: in those cases, the fibre loop was determined based on another reference test. It was assumed that the fibre loop location does not differ significantly between the different reference tests.

3.1.4 Test Strain Readings

During the test, strain readings were acquired using the OmniSens, which used either the BOTDA (Brillouin Optical Time Domain Analysis) or BOTDR (Brillouin Optical Time Domain Reflectometer) to measure the strain within the fibres. Whether one or two fibres were measured during the test, the time between two succeeding measurements in a fibre differed. How the strain readings were acquired is described in detail in section 2.8.

Every pile was instrumented with two fibers, attached in groves on the side of the pile, then looping through the pile just above the pile tip.

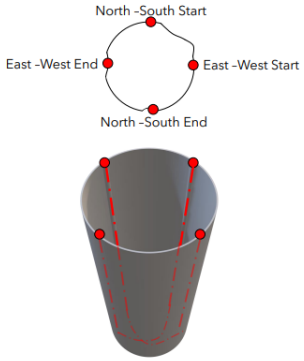

(a) Fibre orientation in pile reprinted from Honardar (2020)

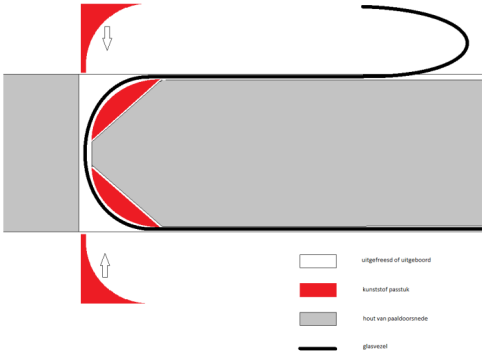

(b) Conceptualisation fibre loop through pile tip reprinted from Spruit (2020)

Figure 3.3a gives an illustration of how the fibres are attached to the pile. This configuration will decrease the influence of bending effects on the strain readings. In further analysis, the readings of the four sides are averaged to make sure bending effects have a limited impact.

The strains measured are absolute. This means that strains already present in the fibre at the beginning of the test are included. For some parts of the analysis, one only wants to include the strains developed during the test. For these parts, the relative strains will be used. The first strain readings of the tensile load test are subtracted from the absolute strains to calculate these relative strains.

3.1.5 Pile Test History

Before, the timber piles used for these tests were subjected to compression load tests. This means that there is already strain present from these previous tests. It is essential to take this aspect into account for the analysis. Table 3.2 shows an overview of the pile test history. Another important factor is that the piles are new. It is thus assumed that the influence of bacterial growth, as mentioned in section 2.4.3, that accumulates over the years, is negligible. Also, the measurement equipment used could not measure bacterial growth, so it is impossible to give conclusions based on the data used.

Pile ID	Type	Debarking	Com.Test	80perc.	Fill	Tens.Test
175	Spruce	Man.	Yes	No	No	Yes
187	Spruce	Man.	No	Yes	No	Yes
195	Spruce	Mech.	Yes	No	Yes	No
397	Spruce	Man.	Yes	No	Yes	No
398	Spruce	Man.	Yes	No	Yes	No
566	Spruce	Mech.	No	Yes	No	No
567	Spruce	Man.	No	Yes	No	No
576	Pine	Mech.	Yes	Yes	No	Yes
592	Pine	Mech.	Yes	No	No	Yes

Table 3.2: Tests performed on timber piles

Table 3.2 shows the type of timber, the debarking method used and the tests performed on the piles mentioned. A different timber type might result in different stiffness values, and a different debarking method can influence the shaft friction mobilised during a test. Appendix section G shows a picture of both a manually debarked pile and a mechanically debarked pile. After manually debarking the bark is still visibly present. Thus the pile has a more rough contact area with the soil than the mechanically debarked piles. The bold pile numbers represent the piles included in further analysis. A description of the different tests follows now.

- The compression tests were performed between September and November of 2019. The piles were driven into the soil in July 2019. The objective of this test was to apply an axial compressive load on the pile head until geotechnical failure was experienced. The NPR guidelines were followed during these tests, which means that there was first unloading between two subsequent load steps before the higher load was applied.
- In June 2020, four timber piles were subjected to a rapid loading test. This meant that an axial compressive load was applied on the pile head, and the load was increased more rapidly than the standard procedure during a load test. Then when the failure load was reached, the axial load was decreased to 80 per cent of that failure load. This load was kept on the pile heads over the summer. Strain readings were conducted a few times over the summer.
- Also, during the summer of 2020, three timber piles of the selection were loaded with an extra sand fill, which was kept on top of the soil surrounding the piles for six months. During this period, strain readings were conducted to monitor the strain developing in a pile due to the increased top load.
- The tensile load tests were performed on four piles in September and October 2020. The following section will give a more detailed description of these tests since these tests will have the main focus during this thesis.

3.2 Experimental Framework

This section will explain the set-up of the tensile load tests performed on four timber piles in September and October 2020.

3.2.1 Test Method

Steel profiles were attached to the pile head to accommodate the tensile load test. First, the upper 1 metre of the pile was cut such that the cross-section of the pile would be rectangular. Then two steel profiles were attached to this part of the pile, fixating this part of the pile fully. A structural engineer calculated the entire test set-up, and a certain amount of bolts were needed to attach the steel profiles while making sure the timber would not split because of a too high force on one bolt.

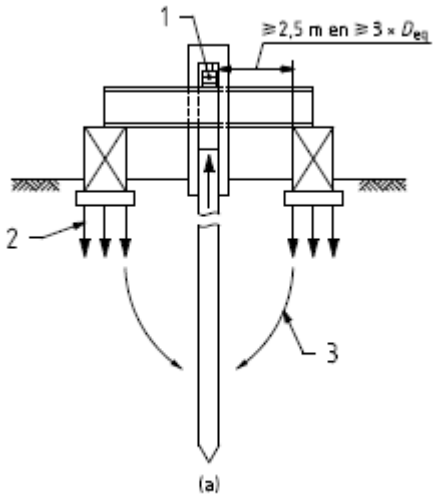

Figure 3.4: Schematization of test set up
reprinted from *NPR 7201* (2017)

On top of these two steel profiles, a steel beam was placed horizontally, and to this beam again, two steel profiles were attached vertically. The two profiles go around the test load frame, and then again, a horizontal steel beam was attached to the profiles. The load cell was placed on top of the load test frame, and during the test, it was pushed against the upper horizontal beam. Figure 3.4 shows a simple schematization of the test. As was mentioned in section 2.1, the bridges and quay walls contain piles that are installed under an angle, and some parts of the bridge foundation are to be considered as a pile group. These two aspects were not tested in this test set-up. It is difficult to test a pile group properly, so it was chosen to test single piles.

3.2.2 Pile Geometry and Instrumentation

Before the piles were driven in the soil, the pile tip was cut to have a diameter of 15 centimetres. Then every metre, the circumference was measured. It was not possible to measure the circumference at some points, for example, because the pile was resting on support at that location.

Loc [m]	175 [cm]	187 [cm]	576 [cm]	592 [cm]
14	-	95.0	-	-
13	90.5	89.5	65.0	-
12	89.0	85.5	64.0	70.5
11	83.5	83.5	61.0	69.5
10	84.0	79.5	56.5	68.0
9	80.0	77.0	55.0	65.5
8	77.0	75.0	54.0	65.5
7	-	-	-	-
6	71.0	71.0	51.0	62.0
5	69.0	66.5	49.0	58.5
4	-	64.0	50.0	57.0
3	61.5	61.5	47.5	53.5
2	58.0	55.0	46.0	51.5
1	53.5	50.5	44.0	51.0
0	50.0	-	-	-

Table 3.3: Circumferences of piles
reprinted from (Gemeente Rotterdam, 2019)

Table 3.3 shows the circumferences found on different locations of the piles. The first column shows the distance till the pile tip. The following method was used to assign a cross section to every centimeter in the pile:

- If the pile tip circumference was not measured - as is the case for piles 187, 576 and 592 -an area was assigned to the pile tip based on a circumference of 15 centimetres, as was mentioned earlier in this section.

- Between two succeeding values, a linear interpolation was used to assign a circumference to all sections.

- If halfway in a pile there were no measurements, the interpolation was done over 2 metres instead of 1 metre.

- To find the circumference of the pile head of piles 175, 576 and 592, the step increase of the segment below was used to extrapolate until the pile head.

All piles were instrumented with two optic fibre cables. Small groves were cut into the sides of the pile, such that the fibres would just fit into the grove without experiencing tension from being placed in a too narrow grove. Then the grove was filled with glue that had a stiffness comparable to the timber. The fibre would loop just above the pile tip, such that readings could be conducted on two sides of the pile. So with two fibres, four locations on the sides of the pile would be tested. Some fibres were damaged during the previous tests or the tensile load test set-up. In Table 3.4 you can find an overview of the fibres that were included with the location of the loop of that specific fibre. The loop of the North-South fibre was placed 2 centimetres above the actual pile tip, and the loop of the East-West fibre was placed 2 centimetres above the loop of the North-South.

	North-South	East-West	Pile Tip
175	-12.25 mNAP	-	-12.27 mNAP
187	-	-12.42 mNAP	-12.46 mNAP
576	-12.57 mNAP	-12.55 mNAP	-12.59 mNAP
592	-12.80 mNAP	-12.78 mNAP	-12.82 mNAP

Table 3.4: Pile tip and fiber loop locations per pile

3.3 Assessment of Strain Readings and Load Cell Data

This section will describe how the raw strain readings were assessed and what assumptions were used to come to the results.

3.3.1 Acquiring Strain Readings

The Omnisens Dual device is used to acquire the strain readings from the fibre optic sensors. Either Brillouin Optical Time Domain Analysis (BOTDA) is used, or Brillouin Optical Time Domain Reflectometer (BOTDR). The principles of these methods are explained in section 2.8. Independently of what method is used, the Omnisens uses a 'moving window' to read the scatter over a distance of one metre. For this metre of fibre, an average strain is calculated. Then the window is moved 25 centimetres further and again calculates an average strain.

3.3.2 Determination of Loop Location

It is essential to know the exact location of the loop in the fibre to average the measurements of the four different sides. The Omnisens averages the strains over 25 centimetres and gives them the average value. It is possible that this location is not exactly in the loop. It depends on the length of the extension cable and the fibre itself where the measurement points will be during that test. An arbitrary value was first given to the location of the loop, based on the length of the pile, to find the location of the loop. The extension cable plus extra fibre outside the pile was about 103 metres, and if the pile were 14 metres long, one would set the loop location to 117 metres. Then, a plot of the original strain readings was checked to see whether this gave symmetry in strain readings on both sides.

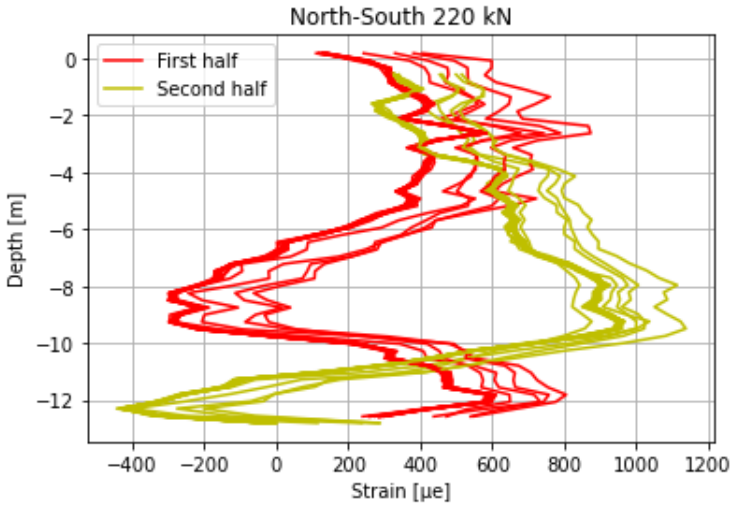

Figure 3.5: North-South fiber of Pile 592

Figure 3.5 shows the strains in the North-South fibre of pile 592 during the load step of 220 kN. For this fibre, one would need to try to locate the minimum and maximum around -8 mNAP and -12 mNAP at the same level, such that the location of the measurements of opposite sides would be on the same level. It was chosen to check the symmetry of the fibre based on the absolute strain readings so before the residual loads are subtracted. Because the absolute strain readings still include possible bending effects, which are needed to see where compression and tension occur.

3.3.3 Load Cell and Displacement Data

The Daisylab device recorded the values of the load cell and the LVDT's. Initially, the load cell data will be most important to use because this data can be used to create different time frames for the load steps. To create the time frames, it was checked when the next load was first reached by the load cell. Then 90 seconds was added to this time because fluctuations might still occur in the first 90 seconds, which means that the resulting strain readings are not entirely reliable to be based on a constant load. The same was done for the end of the load step, so 90 seconds was subtracted from the start of the succeeding load step to find the end of the time frame. 90 seconds were chosen, since one measurement cycle through both fibres takes 90 seconds in total. So it is thought the increase in load will influence the correctness of the strains measured in the first measurement cycle of the new load step. Thus this measurement is disregarded from further analysis.

3.3.4 Combining two Data Sets

Different devices gathered the strain readings and load cell data. Daisylab - which measures the load and the displacement of the LVDT's - was started earlier than the Omnisens device - which measures the strain readings -, because one first had to check whether the LVDT's were not showing strange values. In that case, it might be that one was still stuck, which needed to be solved before the test started. Before starting the new test files for both devices, the time was reset simultaneously, such that both devices would show the same timestamp in their datasheets.

3.3.5 Averaging strain readings

The report explained earlier that the Omnisens device could measure a strain reading every 25 centimetres. This value for that point is based on averaging over a length of 25 centimetres. Since the measurement locations are every 25 centimetres, it was found that it rarely occurs that the measurement locations of the four sides are at the same height in a pile. It was chosen to oversample the original strain data to prevent mistakes from averaging the strains from four sides since they are not at the same height, and thus a skewed value might develop. This means that now the pile will be divided into elements of one centimetre. The 12.5 centimetres above and below one measurement point are all assigned that original strain value. So blocks of 25 centimetres are created. Then at every centimetre in a pile, the average strain, following the normal and shear force, can be calculated.

3.4 Determination of Pile Stiffness

The stiffness of the pile is needed as input to convert the strain readings to forces. This section will elaborate on the different methods used to determine pile stiffness.

3.4.1 Static Modulus of Elasticity

The static modulus of elasticity can be determined when a known force is applied to the timber, inducing a deformation. This static modulus is measured over a longer time than the dynamic modulus, so the static modulus resembles the tensile load test better. Compression load tests on parts of the piles were performed in the timber laboratory of the TU Delft in July 2021. The cutting in sections of piles 576 and 592 can be found in Figures F.1 and F.2. Some parts of the piles were not tested, as seen in the figures. It was chosen to calculate an average stiffness based on the two adjacent parts assigned to this part. The upper part of pile 592 was not tested: the modulus of elasticity of the part below it was assigned to this part. The total length of the individual sections tested does not equal the total length of the pile when it was still one piece. Two discs of 50 mm were taken from each pile to determine the moisture content via the dry oven method (Pagella 2021). Moreover, cutting losses occurred when making the surface parallel for the compression test (G.Pagella, personal communication, October 8, 2021). The cutting losses were distributed evenly over the pile to assign the found modulus of elasticity to the entire pile. The values of the tests in the timber laboratory can be found in Figure F.3 for piles 576 and 592.

3.4.2 Calculated Stiffness from Strain Readings

Before the dynamic and static modulus of elasticity of the parts of the piles were found in the timber laboratory, another method was used to find the stiffness to perform the analysis.

The strain readings acquired during the tensile load test were used to determine a modulus of elasticity. The following formulas were used:

$$F = E * \epsilon * A \tag{3.1}$$

$$E = \frac{F}{\epsilon * A} \tag{3.2}$$

F is the tensile force applied, thus the value measured by the load cell. The force fluctuated slightly (2 kN) during a load step, but it is assumed that the force was constant. The following steps were performed to find a value for the pile stiffness:

1. The first strain reading of the tensile load test was subtracted from the strain readings to find the relative strain readings. These strains were accumulated during the tensile load test only.
2. During one load step, multiple cycles of strain readings were acquired. For every cycle, an average strain was calculated. First, an average strain was calculated for every side based on four measurement locations, thus a section of one metre. Those four values were then combined to find one average value for the cycle. This was repeated for every cycle in the load step and the other load steps.
3. The average cross-section of the pile based on the cross-section at the four measurement locations was calculated.
4. The average strains calculated were multiplied with the average cross-section. The values were then plotted against the load step.

5. Both a linear fit and quadratic fit between the points was calculated. Based on the R2 found for the fits, what type of fit is best to use will be decided.
6. The value found for the pile stiffness will be further used in the analysis. The tests in the timber laboratory showed that the stiffness decreases till the pile tip, but it is very variable how much. Thus, the pile stiffness found from the strain readings will be assigned to the entire pile.

When no load is applied to the pile head, zero strains should be present in a pile. So the fit of the graphs should pass through 0,0. However, even when the strains measured at the start were subtracted, some piles still showed a strain and did not pass through the origin. The student is uncertain what might have caused this strain.

3.5 Determination of Normal and Shear Forces

In this section, the strain readings will be processed to create the distribution of normal forces in the pile and the shear forces around the pile. The shear forces will be used to compound the mobilisation curves of the different soil layers.

3.5.1 Normal forces

Since the strain readings are oversampled to give every centimetre strain, the normal force will also be calculated for every centimetre. A linear or quadratic fit was found in the previous section for each pile, depending on what fit gave the best root mean square score. Piles with a linear fit or where the stiffness was determined in the timber laboratory, the following formula is used:

$$F = E * \epsilon * A \tag{3.3}$$

Where E is the stiffness found based on fitting the strain readings or the compression tests in the timber laboratory. ϵ is the averaged strain from two or four sides of the pile - depending on whether one or two fibres were measured during the test -, and A is the cross-section of the pile at the location of the node. When a quadratic fitting was found to fit the strain readings best, the following formula is used:

$$F = a(\epsilon * A)^2 + b(\epsilon * A) \tag{3.4}$$

Where a and b are the coefficients determined during the quadratic fitting.

3.5.2 Shear Forces

From the calculated force at every node, the shear stress can be calculated for each element. The following formula was used:

$$\tau[i + 0.5] = \frac{F[i + 1] - F[i]}{O[i + 0.5] * L} \tag{3.5}$$

Since the strain readings were oversampled to show an average strain (and force) every centimetre, this means on a small scale, the shear stress can be both positive and negative. This alternation in sign is not expected when looking at the physical behaviour of the pile. So to take away this alteration in sign, it was chosen to use more significant intervals in which the shear stress would be calculated. The shear stress is calculated for every soil layer, so i in the formula is the i-th soil layer. F[i+1] is the force at the top of the soil layer below or the bottom of the current soil layer. F[i] is the force at the top of the current soil layer. The following steps were taken to calculate the shear stress:

1. Find top and bottom levels of the current soil layer.
2. For both top and bottom level, determine the force calculated at that level.
3. Calculate the length of the interval.
4. Calculate the contact area between the soil and pile of the interval by appending the area of all the elements within the interval.
5. Subtract the force at the bottom of the soil layer by force at the top of the soil layer and divide this by the contact area of the interval.
6. Repeat for every soil layer and every load step.

3.6 Assessment of Residual Loads

All four piles were tested in compression before the tensile load test was conducted, so it is assumed that loads applied on the pile before are still partially present in a pile. Also, it is assumed that creep has occurred in a pile over the months, which contributes to the strain measured at the beginning of the tensile load test. At the beginning of the test, there was already a non zero strain reading.

3.6.1 Reference Readings before Driving

Before the piles were driven into the soil, strain readings were measured with two different methods:

1. Hanging: the pile was hung from a crane. In this situation, the pile should not experience any strain apart from self-weight from an external influence because it just hangs in the air.
2. Standing: the pile was placed standing on the ground, using a crane to keep the pile straight.

For the analysis based on absolute strains, the strains measured during hanging are subtracted from the measurement. Since the strains from hanging were already present in the pile before it was driven in the soil, it does not influence the strains developed when the pile was in the soil.

3.6.2 Comparison Absolute and Relative Strains

To compare the influence of the residual loads present inside the pile, in the further analysis, the results based on the absolute strains will be compared to the results based on the relative strains.

3.7 Compounding Mobilisation Curves

For the simulation of negative skin friction, mobilisation curves are needed as input. Compounding the mobilisation curves involves plotting the development of mobilised shaft friction against the load steps and plotting the settlement of different soil layers against the load steps. The method will be explained in the following sections.

3.7.1 Mobilised Shaft Friction

The steps described in section 3.5.2 will be used again to calculate the mobilised shaft friction in every soil layer. The shaft friction will be based on the average strains of one load step to exclude the possibility of fluctuations or deviations in the measurement. The calculated shaft friction is then plotted against the load. It is chosen to plot the friction against the load instead of the time since some load steps took longer than others.

3.7.2 Relative Pile Settlement

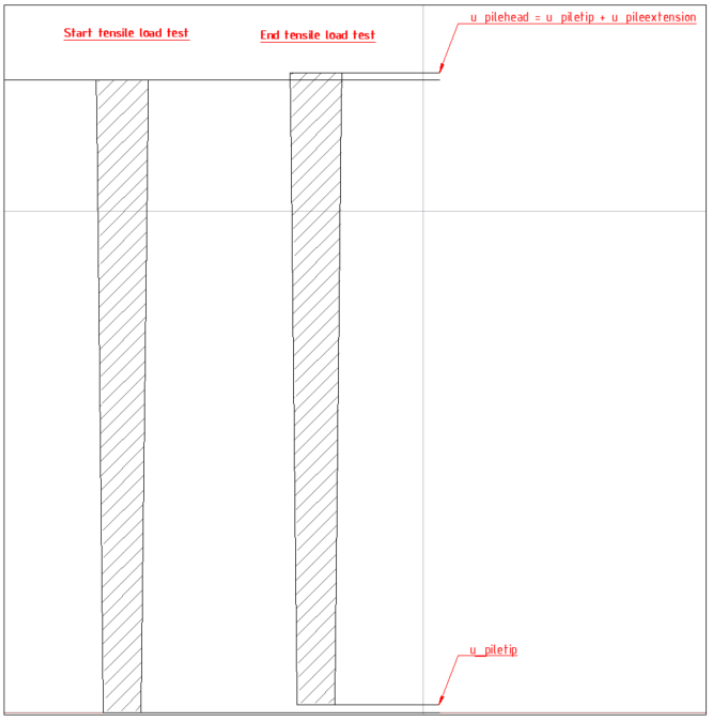

Figure 3.6: Illustration measured displacements in pile

Figure 3.6 shows the different components that the LVDT measures at ground level: it measures the displacement of the pile tip plus the extension of the pile under the influence of the tensile force. To create the mobilisation curves, only the displacement of the pile at that level is needed, not the extension.

First, verification is needed to check that the strain readings show the same displacement at the beginning of the test as the LVDT. This can be done by integrating the strain readings of the entire pile. When the LVDT and strain readings are verified, the displacement of every single soil layer can be derived. In every soil layer, the pile displacement was determined halfway the pile. Strain readings were done every 25 centimeter, so to find the extension in a soil layer, the

following formulas need to be used:

$$\epsilon[\mu e] = \int \epsilon - \int \epsilon_0 \tag{3.6}$$

$$\epsilon_{avg}[\mu e] = 0.25 * (\epsilon_{north} + \epsilon_{south} + \epsilon_{east} + \epsilon_{west}) \tag{3.7}$$

$$u_{extension}[mm] = \frac{\epsilon_{avg}}{10^3} * 0.25 \tag{3.8}$$

$$u_{rel}[mm] = u_{LVDT} - u_{extension} \tag{3.9}$$

All strains until halfway through the soil layer need to be summed in the first equation. Since the extension of the pile can only be calculated based on measurements during the test, the strains present at the beginning of the test need to be zeroed out. In the second equation, the average strain will be calculated based on the integrals of all four sides - the fibre optic sensors measured on four sides of the pile.

As explained earlier, the strain can be converted in a displacement by a factor of 0.25 - the length between two adjacent strain readings. Then to get millimetres instead of micrometres, a division of 10^3 is needed. This gives the pile extension under the specific tensile load in millimetres. The last step - to get the relative pile displacement of the particular soil layer - the extension of the pile needs to be subtracted from the displacement measured by the LVDT at ground level.

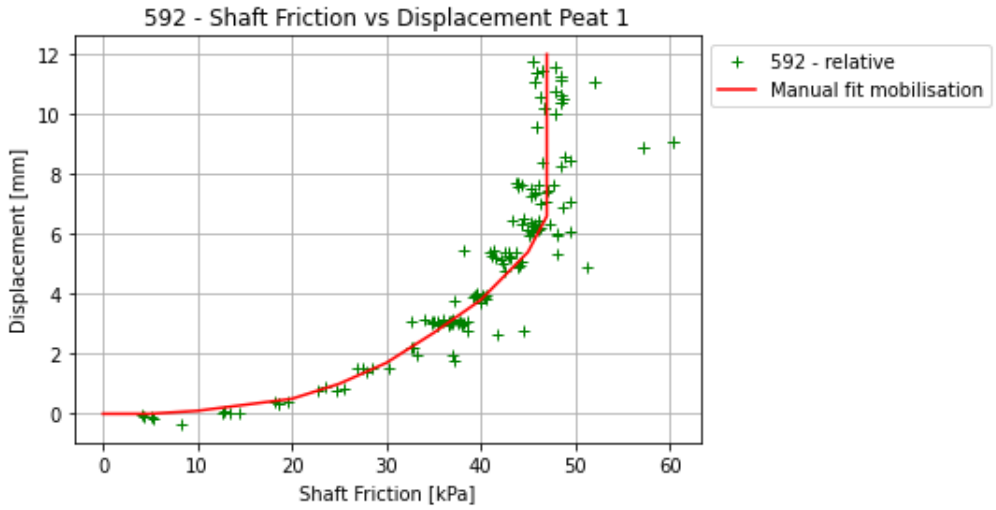

Figure 3.7: Mobilisation Curve in Peat 1 of Pile 592

Figure 3.7 shows the compounded mobilisation curve in Peat 1 of pile 592, before it was combined with the other piles. A manual fit was made from the distribution, since the automated fits did not represent the mobilisation correctly.

3.8 Comparing Influence of Tapering

One of the research questions is to investigate the influence of tapering on the mobilised shaft friction of the timber piles. The mobilised shaft friction during the tensile load test should be compared to the compression load test's to answer this research question. As was described and illustrated in section 2.4.1, during a tensile load test, the pile is pulled out of the soil, meaning that when it moves upwards, a smaller diameter will be at the location where there used to be a bigger diameter of pile. So it is assumed that this will cause smaller shaft friction since there will be less friction with the soil. The compression load test is considered to behave the other way since a bigger diameter will be at the location where there was a smaller pile diameter.

3.8.1 Calculation Alpha Factors

The alpha factors are a correlation factor to correlate the cone resistance from the CPT to the shaft resistance of the pile. During a compression load test, an α_s can be derived for the pile shaft. A tensile load test gives an α_t, which can be calculated with the following formula:

$$\alpha_t = \frac{\tau_{max}}{q_c} \tag{3.10}$$

Where τ_{max} is the maximum shaft friction, found during the tensile load test, and q_c is the cone resistance found at the level of the soil layer, retrieved from the CPT.

The α_t of the tensile load test will be compared to the α_s found during the compression load tests, which were calculated before by Honardar (2020). Since the α_s values are calculated using a calculated E modulus from the strain readings, the α_t will also be calculated with a stiffness based on strain readings.

3.9 Simulation of Negative Skin Friction

The last step of the analysis is to use the mobilisation curves of the test data in the simulation of the development of negative skin friction. The simulation will be performed in Deltares Pile Group. A disadvantage of Deltares Pile Group is that a variable EA cannot be applied yet, needed since the timber piles are tapered. So now, an average value of the pile diameter and pile stiffness will be used.

The objective of the thesis is to conclude the development of negative skin friction based on the results of the tensile load tests. As is explained earlier in the report, the direction of the soil relative to the pile is the same during a tensile load test as to when negative skin friction is developing. However, when negative skin friction develops, the pile is loaded in compression instead of tension.

3.9.1 Soil Parameters

The soils will be defined based on t-z curves retrieved from the mobilisation curves. Both longitudinal and lateral mobilisation can be specified, but only the longitudinal mobilisation was measured during the tensile load tests. Thus the lateral mobilisation is disregarded. The top sand layer will be defined with the mobilisation curve of pile 576 since there was no mobilisation in that layer around pile 592. It needs to be mentioned that the top sand layer was pre-drilled, and this might have influenced the mobilised shaft friction. The other three layers are defined with the mobilisation curves of pile 592.

The soil displacement profile is defined with 1 cm of settlement at ground level, then linearly decreasing till no settlement at the top of the bearing sand layer.

3.9.2 Pile Characteristics

D Pile Group cannot assign a variable cross-section to a pile so that an average cross-section will be applied. The pile stiffness can only have one value, so initially, a weighted average pile stiffness will be assigned based on the results of the laboratory tests. The pile tip curve from NEN 9997-1 will be assigned as pile tip curve.

3.9.3 Load Scheme

One simulation will simulate the complete pile test history. The part of the tensile load test can be verified with the results from the LVDT.

1. Apply compressive load till 392 kN
2. Decrease compressive load to 0 kN
3. Apply soil displacement
4. Apply tensile load till 220 kN
5. Decrease tensile load to 0 kN

The simulation is performed for pile 592. Honardar (2020) found that geotechnical failure was reached at a compressive load of 392 kN. The maximum end bearing load, including residual loads, was 218 kN. These values are applied in the simulation. Then in the city of Rotterdam, it is customary to assume a ground-level settlement of 1 cm per year, so the ground level settlement applied between the compression and tensile load test - about one year apart - is 1 cm, and no settlement at the top of the bearing sand layer. A maximum tensile force of 220 kN was reached during the tensile load test, so this value is also included in the simulation.

Then after the verification of the pile behaviour with the simulation of the pile test history, the same pile and soil information can be used to simulate the situation when the pile is part of a foundation. The following steps are done:

1. Apply compression load up until 50 per cent of maximum bearing capacity
2. Keep compression load on the pile head
3. Apply a soil displacement of 1 cm at ground level

Since the compression load test showed a maximum capacity of 392 kN for pile 592, a compressive load of 196 kN was applied. This load was kept on the pile head, and then a soil displacement was applied. By altering the factor used for the application of the soil displacement, the influence of ground-level settlement on the development of negative skin friction can be studied. In the next chapter, the results of the simulation will be discussed.

4. Results

This chapter will explain the results that were found during the analysis of the data. The observations will be discussed, and interpretations will be made in the following chapters.

4.1 Load Cell Assessment

It was written down what the different load steps were during the tests. These values were used in the script to select time frames for the different load steps. When the desired load was reached, 90 seconds was added to this timestamp. Then to find the end of the time frame, 90 seconds was subtracted from the start of the next load step. Filtering out these first and last 90 seconds makes sure that fluctuations in load are not considered in the analysis. The strain readings must be based on a constant load.

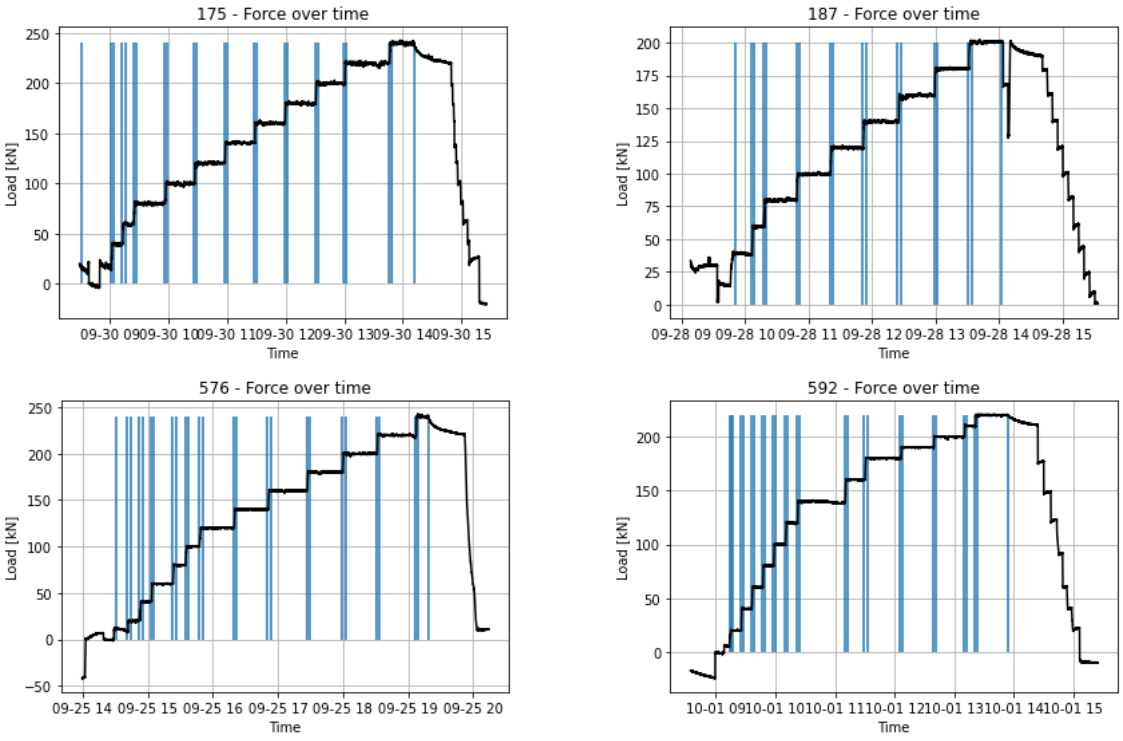

Figure 4.1: Force in Load Cell for 4 piles, including created time frames

In Pile 187, according to the notes, relaxation was started five minutes later than what is now assigned to in the code, but as can be seen in the plot of pile 187 (top right), there is a significant drop in load on the pile head. So it was chosen not to take these strain readings into the analysis since the load was not constant on the pile head.

In the graphs of piles 175 and 187 (top left and right), it is observed that there was already a load on the pile head at the start of the measurements. This load was already on the pile because the setup needed to be fixated. At the beginning of the test, the load was first decreased before the first load step was started.

On the other hand, piles 576 and 592 (bottom left and right) start with a negative load at the beginning of the test. This has probably something to do with the configuration of the Daisylab

program. The first load step of pile 592 (10 kN) was disregarded in the further analysis: since the load step was so short, the end of the time frame was located before the start of the time frame, which means that no strain readings were assigned to the load step.

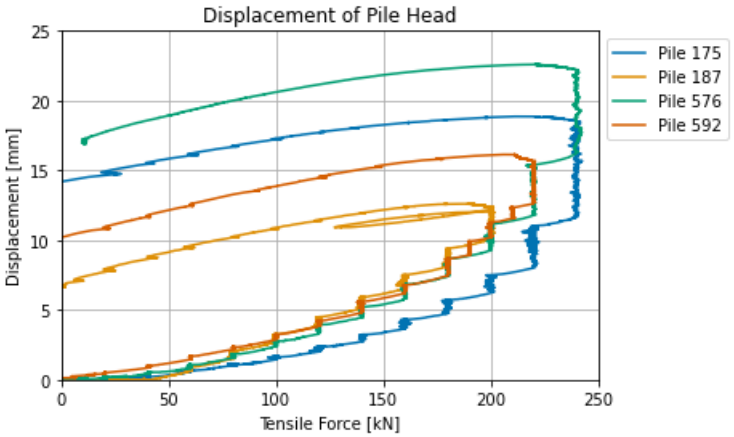

Figure 4.2: Pile Head Displacement

Figure 4.2 shows the pile head displacement measured by the LVDT under the tensile load for all four piles. There were no unloading and reloading steps included in the tensile load test since this was not a requirement from the *NPR 7201* (2017). When geotechnical failure was reached, the force was reduced to zero.

4.2 Strain Reading Assessment

This section describes how the strain readings acquired by the Omnisens are assessed and what results it gave.

4.2.1 Measurements around Fiber Loop

After finding symmetry in the strain readings of one fibre, the development of strains in the individual measurement locations around the fibre loop was looked into in detail. It was found that there seems to be a decrease in strain development in some fibres after a specific load step. The pile could have lost contact with the soil after that load step. A detailed explanation of this check can be found in Appendix E.

4.2.2 Original Strain Measurements

This section will explain the original strain measurements, after the location of the loop was optimised.

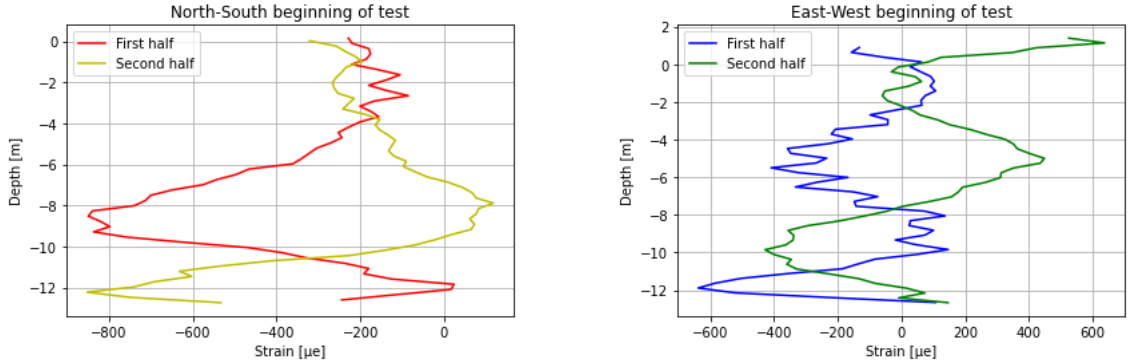

Figure 4.3: First Strain Reading both fibers of pile 592

Figure 4.3 shows the original strain readings of the North-South and East-West fibre after the location of the loop was optimised. The negative strain means compression is already present in the pile; positive strain implies tension. These figures show that the piles are not entirely straight inside the soil. At the start of the tensile load test, residual loads were already present in the pile, caused by the pile test history.

The blue line in the right plot of Figure 4.3 shows some fluctuation in the strain reading between two consecutive readings. The other lines do not display this behaviour. There could be a deviation in the fibre, or the pile has some fluctuations at this location.

4.2.3 Creating Continuous Strain Distribution

The Omnisens device calculates an average strain based on the strain readings measured in several blocks of the fibre; see section 3.1.4 for the explanation. In the end, every 25 centimetres, a strain reading is given.

Oversampling was done by assigning the value of the strain reading to the 12.5 centimetres above and below the location of the strain reading. So for over 25 centimetres, every centimetre was assigned the same strain value: basically, blocks of 25 centimetres were created. At the pile tip, the strain value of the last measurement above the loop was assigned until the location of the pile tip.

4.2.4 Average Strain Distributions

This section shows the average strain distributions that were found for the piles, comparing the results based on absolute strains and relative strains.

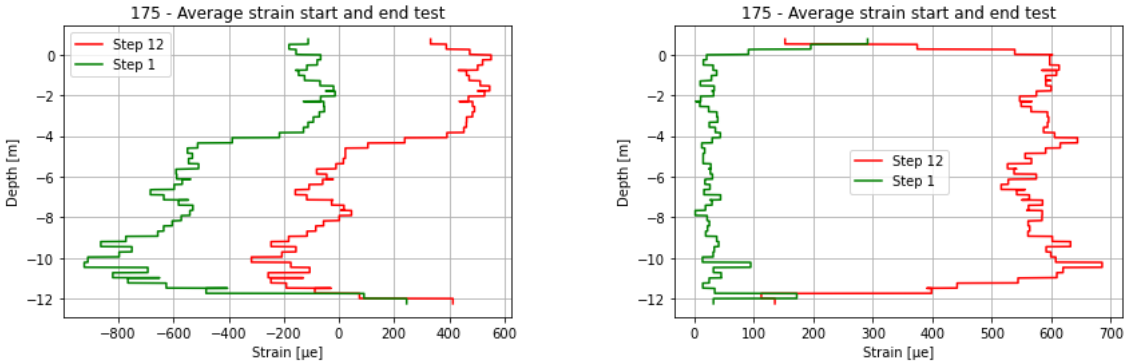

Figure 4.4: Pile 175 - Absolute Strains (left) and Relative Strains (right)

Figure 4.4 shows the average strain in pile 175 at the maximum load step of 240 kN, including residual loads on the left side, excluding residual loads on the right side.

- In the left plot of Figure 4.4, above 0 mNAP, the strain is still increasing. It is thought that this part should be disregarded for further analysis since this part of the pile is outside the soil, and thus it might be more susceptible to bending effects. Then the first four metres in the soil show the almost continuous strain value. Then just before the soft soils are reached (-4.68 mNAP), the strain decreases. Below -11 mNAP, the strain increases again. At the pile tip, the difference between the strain measured during the first load step and the last load step is small compared to other locations in the pile. At the end of a tensile load test, there should be zero force at the pile tip, but the plot shows that there is still a force present.
- In the right plot of Figure 4.4, the measurements inside the pile (below 0 mNAP) show a constant strain value at the first load step. At the last load step, there is more fluctuation in the strain value along with the depth: the sharp decrease around -6 mNAP could be caused by the transition from the sand to peat layer, but the other fluctuations do not correspond with a soil boundary.

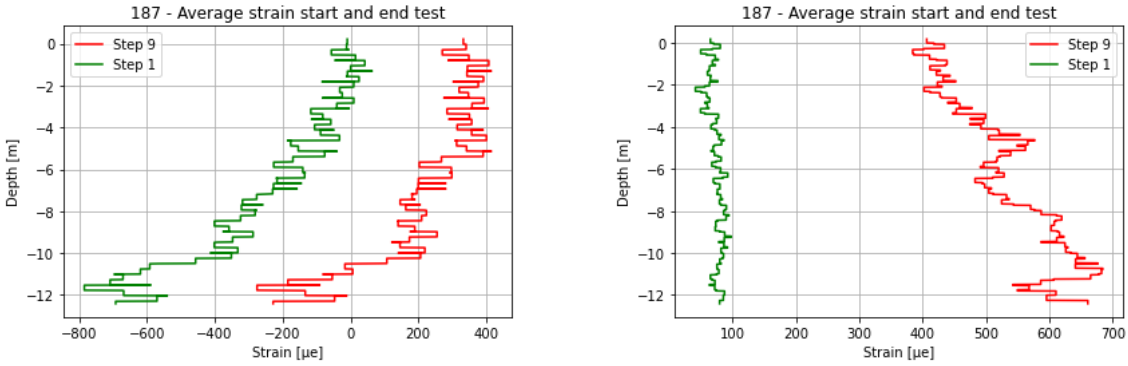

Figure 4.5: Pile 187 - Absolute Strains (left) and Relative Strains (right)

Figure 4.5 shows the average strain in pile 187 at the maximum load step of 200 kN, including residual loads on the left side. The right side shows the average strains when residual loads are excluded.

- In the left plot of Figure 4.5, there is some fluctuation in the average strain measured, but the overall trend is decreasing. This behaviour is expected since a lot of the load will be transferred to the soil in the top layers, which means less strain remains for the lower soil layers. When the sand layer (-11.75 mNAP) is reached, the strain becomes constant. There should be no load anymore at the pile tip at the end of the test, but there is still a negative strain present. This pile was tested during the extended compression load test, so there could be compression left in the pile after this long compression period, even when a tensile load test is performed afterwards.

- The first load step in the right plot of Figure 4.5 shows a continuous strain development along with the depth of the pile. There is already a positive strain measured at the first step since there is already a tensile force of 40 kN pulling at the pile head. Because of fluctuations in the force on the pile head, 40 kN was the first load step included in the analysis. The last load step shows an increasing strain along with the depth of the pile, which is not expected to occur during a pile load test. The transition from the top sand layer to the peat layer (-6.63 mNAP) and the transition from the second peat layer to the bearing sand layer (-11.75 mNAP) seem to coincide with a local decrease in strain.

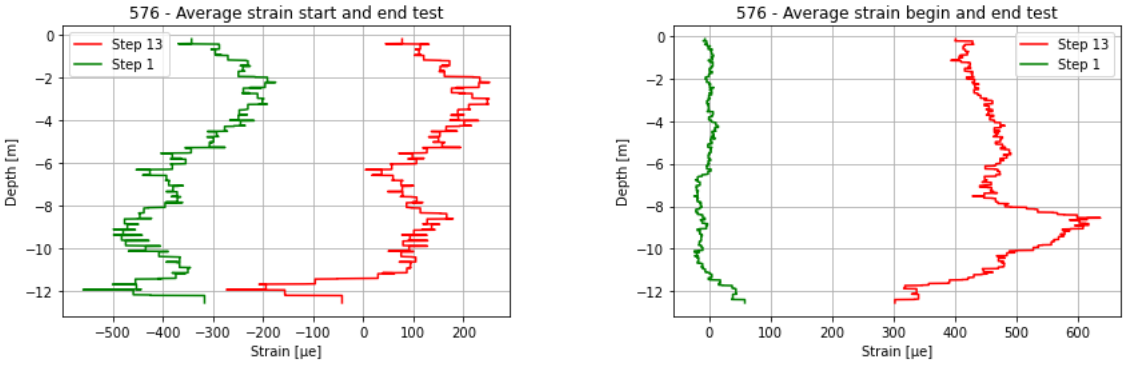

Figure 4.6: Pile 576 - Absolute Strains (left) and Relative Strains (right)

Figure 4.6 shows the average strain in pile 576 at the maximum load step of 240 kN, including residual loads in the left plot. The right plot shows the average strains in pile 576 when the strains measured at the beginning of the test are subtracted.

- In the left plot in Figure 4.6 the strain increases, then around -2 mNAP starts to decrease. At the bottom of the first peat layer (-6.70 mNAP), the strain increases slightly, but halfway the clay layer decreases again. The strain increases slightly in the bearing sand layer (-11.74 mNAP): during the last load step, a -50 microstrain is measured. No strain should be measured at the pile tip at the end of the tensile load test; the pile test history could have caused the deviation. This pile was also tested in the extended compression load test, which could explain why compression is still measured at the end of the test.

- The right plot in Figure 4.6 shows a continuous strain development along with the depth at the first load step, only at the pile tip there is already a small amount of positive strain present. In the last load step, between -8 and -10 mNAP, there is a significant increase of strains. This is in the middle of the clay layer, so a transition of soil layers cannot cause it. When the bearing sand layer is reached (-11.74 mNAP), the strain becomes constant.

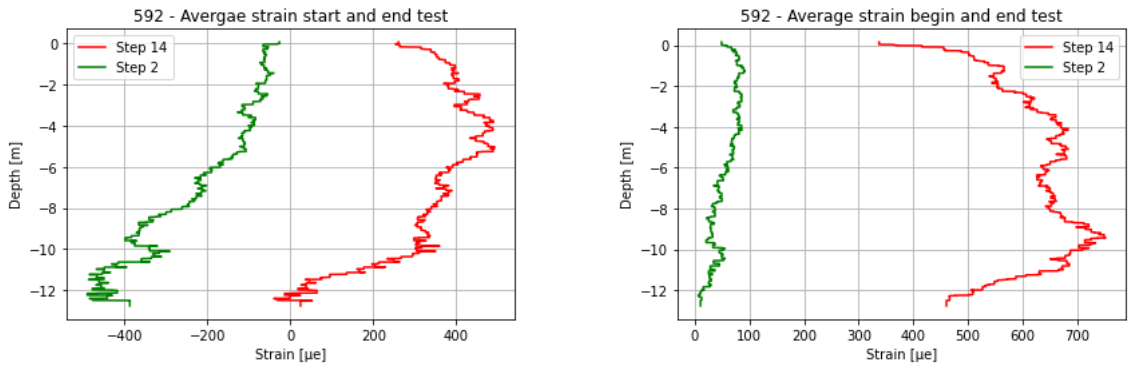

Figure 4.7: Pile 592 - Absolute Strains (left) and Relative Strains (right)

Figure 4.7 shows the average strain in pile 592 at the maximum load step of 220 kN, including residual loads in the left plot. The average strain when the strain at the test's beginning is subtracted is shown in the right plot.

- The first load step in the left plot in Figure 4.7 shows a continuous decreasing strain. When the bearing sand layer is reached (-11.74 mNAP), the strain becomes constant. The last load step deviates from the first load step in two locations: at the top, the strain increases to -2 mNAP before decreasing. And in the second peat layer (-11.36 mNAP), there is a sharper decrease in strain.
- The first load step in the right plot of Figure 4.7 shows a decreasing strain distribution at the first load step of 20 kN. The last load step shows fluctuations in the strain distribution along with the depth and seems comparable to the plot of pile 175.

4.2.5 Creep Effect Assessment

A consideration was done into the effect of creep on the strain readings. As mentioned before, it is expected that creep has contributed to the first strain reading of the tensile load test, but it is impossible to quantify the influence of creep on this first reading. Therefore, for a few measurement points inside the piles, the strain value measured at the beginning and end of each load step was plotted in one graph. The consideration is explained in detail in the Appendix section E.

In some locations, a difference between the strain at the beginning and end of the load step was observed, but this difference was not the same in every load step. (Figure E.2) So it is hard to conclude whether the difference is caused by creep or just an accidental shift in strain reading. The measurement points show a strain development that is expected to happen - the strain becomes more positive continuously with increasing load -, there is barely any difference between the start and end of the load step observed. See Figures E.4, E.5 and E.6.

Figure E.1 shows a constant increase in strain readings in the first load steps, but at 140 kN, a scatter seems to have developed, and on average, there is a decrease in strain. These two measurement points are located near the pile tip of pile 175, and thus a possible explanation of this behaviour is that the pile tip starts to lose contact with the soil. When the pile loses contact, there is no friction development anymore, resulting in a decrease in strains.

4.3 Load Distributions Assessment

The strain readings were combined with the pile geometry and the pile stiffness, resulting in a distribution of the normal force along with the depth of the pile. These distributions were then used to derive the shear force development in the different soil layers.

4.3.1 Normal Force Distribution

This section shows the results of the normal force distributions for all four piles, based on absolute and relative strains.

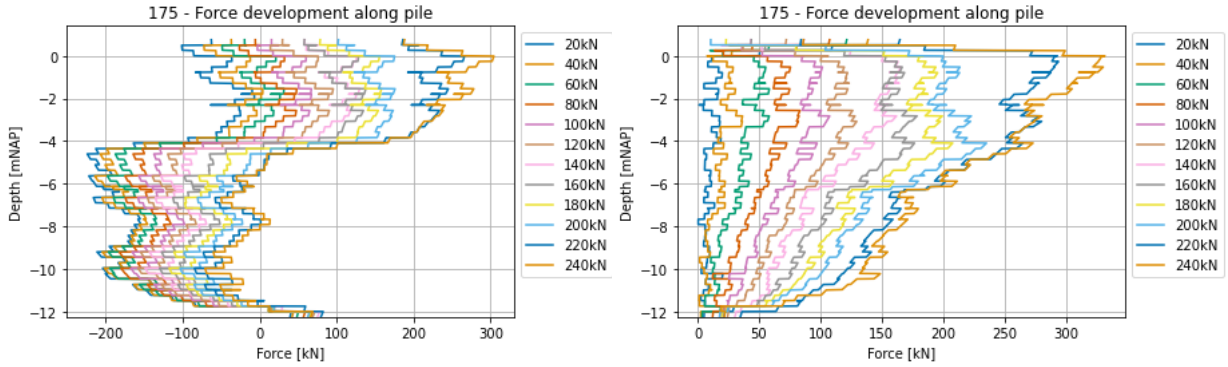

Figure 4.8: Pile 175 - Normal Force with Absolute Strains (left) and Relative Strains (right)

Figure 4.8 shows the force development in pile 175.

- In the left plot, it is clear that there is compression along with the entire depth of the pile at the start of the test. The force distribution is rather constant in the top sand layer, around -4 mNAP. When the peat layer is reached, a decrease in force is observed. In all soft layers, the force distribution stays rather constant, but when the bearing sand layer is reached, there is an increase again. This distribution is also observed in the next load steps. In the top sand layer, the last two load steps show a bigger force increase than the previous steps. At the end of the tensile load test, zero force is expected at the pile tip, but there is still a positive force.

- In the right plot, the distribution of the first load step is vertical. There is much increase in force in the top sand layer in the next load steps, but in the layer below, the increase is smaller.

- In both plots, the force measured in the top sand layer at the maximum load step does not correspond with the force applied on the pile head. They should have been the same; residual loads might have been left inside the pile that influenced the measured force distribution.

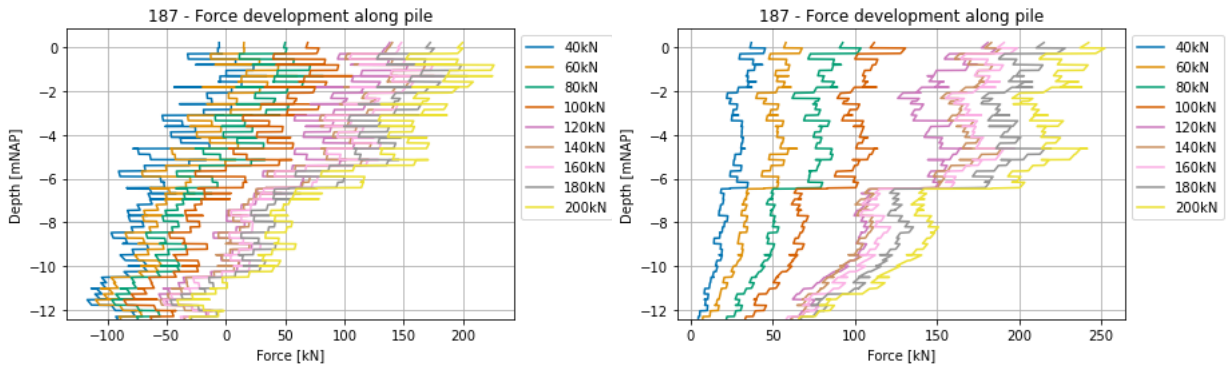

Figure 4.9: Pile 187 - Normal Force with Absolute Strains (left) and Relative Strains (right)

Figure 4.9 shows the force development for pile 187.

- In the left plot, a strong fluctuation in the force distribution is observed. This was also observed in the reference measurements, so the fluctuations are probably caused by how the fibre was attached to the pile. At the start of the load test, the entire pile experiences an increasing compression with depth. The pile was tested in the extended compression load test in the summer before the tensile load test, so it is no surprise the entire pile is still experiencing compression. The distribution seems similar in all soil layers; only when the bearing sand layer is reached the distribution becomes constant. The pile tip should experience zero force at the end of the tensile load test, and this is almost the case.
- In the right plot, the first distribution is not equal to zero. There was already 40 kN tensile force on the pile head at this step since the previous steps could not be included in the analysis. This was explained earlier in the report. Around -6.5 mNAP, there is a horizontal line in the distribution caused by the assigned pile stiffness. At -6.46 mNAP, there is a change in pile stiffness. Between 100 and 120 kN, there is a more considerable increase in the force distribution than in other load steps. It is unclear what might have caused the deviation.
- The force measured in the top sand layer at the last load step is a better match with the applied force on the pile head compared to pile 175.

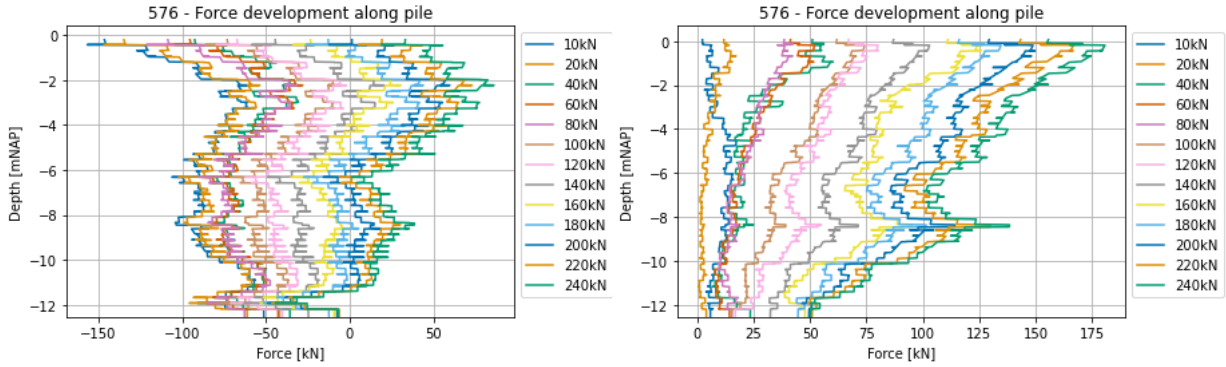

Figure 4.10: Pile 576 - Normal Force with Absolute Strains (left) and Relative Strains (right)

Figure 4.10 shows the force development for pile 576.

- In the left plot, there is an increase in force in the first two metres below ground level. The force is expected to decrease with depth inside the soil, not increase. Subtracting the reference strain readings from the absolute strain readings could have caused the deviation. At the start of the load test, the entire pile is in compression. The pile was recently tested in the extended compression load test before the tensile load test. Towards -8 mNAP, there is an increase in force halfway through the clay layer and cannot be explained by a transition of soil layers. In the second peat layer (-11.36 mNAP), there is a sharp decrease again; in the bearing sand layer, the force increases slightly. At the end of the tensile load test, the force at the pile tip should be zero, and this is almost the case.

- In the right plot, the first load step has a more significant force distribution than the second load step. In the next load steps, this difference is solved. At the load step of 40 kN, a deviation from the force distribution develops around -8 mNAP. This deviation was also observed in the left plot at the exact location; no explanation could be found for this deviation.

- The force measured in the top sand layer at the last load step in the right plot does not correspond with the tensile force applied on the pile head. Since this pile was tested in the extended compression load test, it is possible that residual loads were left in the pile after that test, which could have influenced the strain readings during the tensile load test.

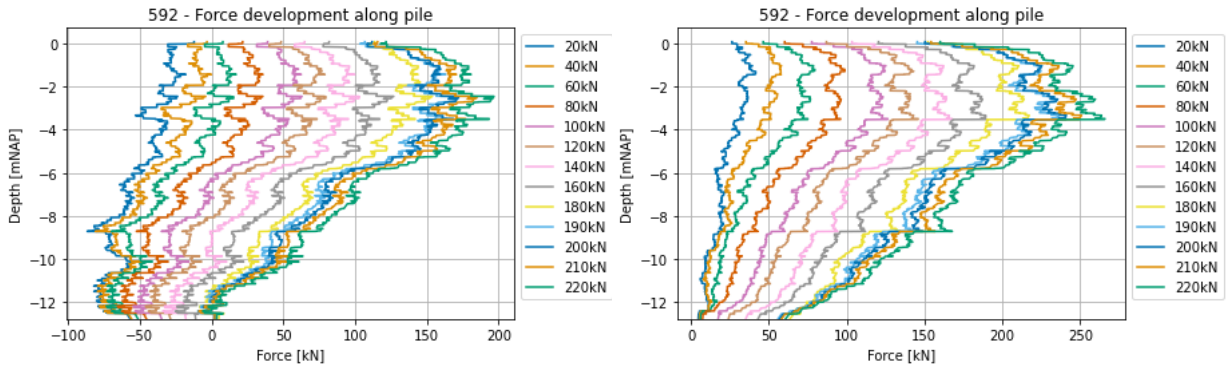

Figure 4.11: Pile 592 - Normal Force with Absolute Strains (left) and Relative Strains (right)

Figure 4.11 shows the force development for pile 592.

- In comparison to the previous piles, there is almost no difference in the pile distribution between the absolute and relative strains. Both figures show a continuous force distribution in the sand layer until -4.80 mNAP, then a continuous decrease in force is observed in the soft layers. There is no significant difference observed between the peat and clay layers. Also, between 0 and -1 mNAP, an increase in force is observed. The averaging of the fibre optic cable might be the reason for this increase: still, a part of the pile above ground is included in this strain reading. A decrease in force is observed in the second sand layer below -11.74 mNAP, contrary to the sand layer's behaviour in the other piles. However, pile 592 has the most friction with the sand layer of all piles since it is placed one metre in the layer. The other piles are more shallow in the sand layer. In the left plot, there should be zero force in the pile tip at the last load step, which is the case.

- The force measured in the top sand layer at the last load step is almost the same as the tensile load applied on the pile head.

4.3.2 Shear Stresses Distribution

This section shows the distribution of shear stresses mobilised in the different soil layers for the four different piles. Since the second peat layer is too small, the averaging of strains also includes readings from the upper and lower layer. So this second peat layer is combined with the clay layer on top of the peat layer.

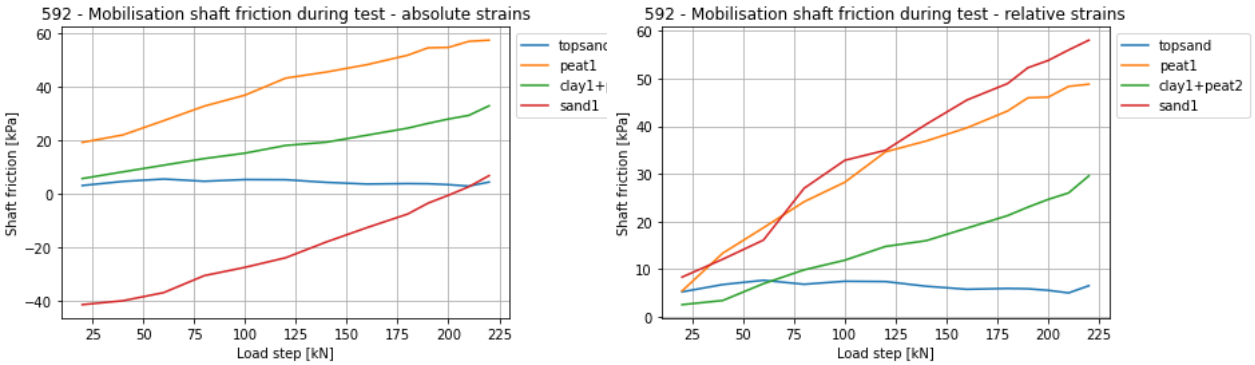

Figure 4.12: Pile 592 - Shaft Friction with Absolute Strains (left) and Relative Strains (right)

- In the left plot, the top sand layer does not seem to mobilise shaft friction. The top sand layer was pre-drilled, explaining why no mobilisation was observed. Sand 1 starts with negative shaft friction; just before the last load, the shaft friction becomes positive. So during most of the load test, Sand 1 still experiences positive skin friction; only at the end a small amount of negative skin friction is mobilised. According to the plot, the other two soils already experienced negative skin friction at the start of the load test, which was only increased during the test.

- The right plot shows the mobilisation of shaft friction based on relative strains. A similar mobilisation is observed compared to the left plot; only now can the top sand layer observe that a small amount of shaft friction is mobilised until 60 kN, then the shaft friction increases.

Appendix section A.1 shows an overview of the measurements points in pile 592 together with the location of the soil layers. In the North-South fibre, the lowest measurements on both sides (-12.541 and -12.548 mNAP) are 80 cm below the boundary with the peat layer. In the East-West fibre, the lowest measurements (-12.647 and -12.657 mNAP) are 87.5 cm below the boundary with the peat layer. Since the lowest measurement points are this far away from the peat layer, it is assumed that the peat layer has no influence on the strain readings and that the shaft friction derived for Sand 1 is based on enough measurements in that sand layer. It is assumed that the bending of the loop does not affect the strain reading since the fibre was installed so that this should not have an influence.

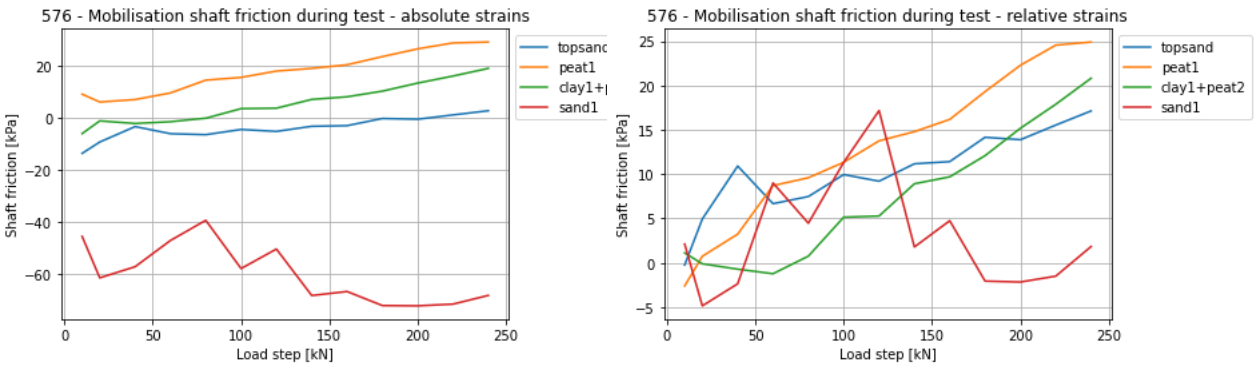

Figure 4.13: Pile 576 - Shaft Friction with Absolute Strains (left) and Relative Strains (right)

- In the left plot, the shaft friction in Sand 1 deviates from the shaft friction in the other soil layers. It is possible there was shaft friction of -50 kPa at the start of the tensile load test - so positive skin friction -, but it is expected that this positive skin friction is reversed in negative skin friction during the tensile load test, as was the case in pile 592. On the contrary, there is some fluctuation in the shaft friction, with a decreasing trend. Since there first is an increase in shaft friction, then decrease, it is possible there was friction mobilised with Sand 1, but the pile soon lost contact with the soil. Figure **??** confirms this: at a tensile force of 100 kN, the displacement measured based on strain readings already starts to differ from the displacement measured by the LVDT. The other soil layers show a continuous increasing strain during the test; also, shaft friction is mobilised in the top sand layer.

- In the right plot, the shaft friction of Sand 1 also deviates. Here it can be better observed that there is an increase in shaft friction, then after 120 kN, the shaft friction decreases.

Appendix section A.1 shows an overview of the measurements points in pile 576 together with the location of the soil layers. In the North-South fibre, the lowest measurements on both sides (-12.33 and -12.29 mNAP) are located 59 and 56 cm below the boundary with the peat layer. In the East-West fibre, the lowest measurements (-12.31 and -12.28 mNAP) are located 57 and 54 cm below the boundary with the peat layer. Since the lowest measurement points are this far away from the peat layer, it is assumed that the peat layer has no influence on the strain readings and that the shaft friction derived for Sand 1 is based on enough measurements in that sand layer. A continuous increase in friction is needed to create a mobilisation curve, which is not the case for Sand 1. It is thus expected that no mobilisation curve can be derived for this layer.

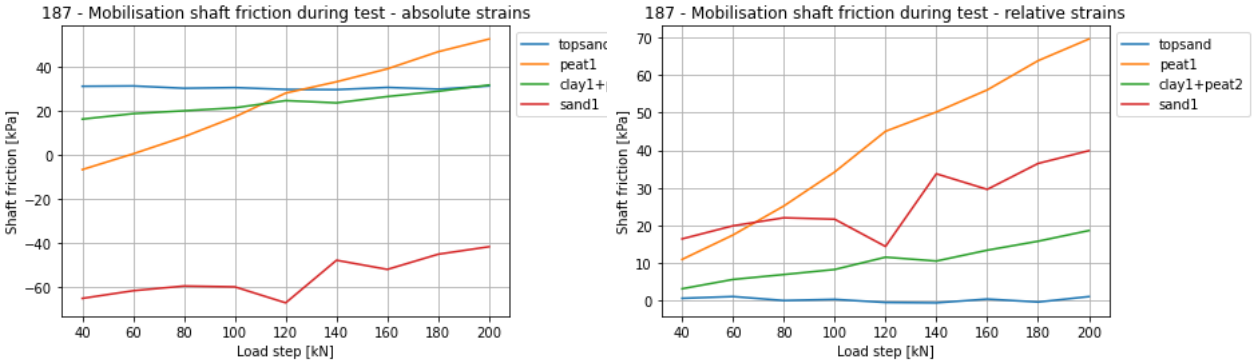

Figure 4.14: Pile 187 - Shaft Friction with Absolute Strains (left) and Relative Strains (right)

- The left plot in Figure 4.14 shows that the shaft friction in Sand 1 differs from the other soil layers. A negative shaft friction at the start of the test is possible: positive skin friction has developed around the pile after the compression load test. Then there is an positive increase in shaft friction during the test, but at the end of the test there is still a negative shaft friction. This means that at the end of the test - when geotechnical failure is reached and the pile is pulled out of the soil -, still positive skin friction is experienced. This is not likely to have been the case.
- The right plot shows that in Peat 1, the most shaft friction is mobilised during the tensile load test. The shaft friction in the top sand layer continuously keeps around 0 kPa.

Appendix section A.1 shows an overview of the measurements points in pile 187 together with the location of the soil layers. In the East-West fibre, the lowest measurements (-12.28 and -12.30 mNAP) are located 53 and 55 cm below the boundary with the peat layer. Since the lowest measurement points are this far away from the peat layer, it is assumed that the peat layer has no influence on the strain readings and that the shaft friction derived for Sand 1 is based on enough measurements in that sand layer. Only since little friction has mobilised during the tensile load test, and at the end of the test still negative shaft friction is measured, it is expected that the mobilisation curve of Sand 1 shows a soft response compared to *NEN 9997-1 + C2* (2017).

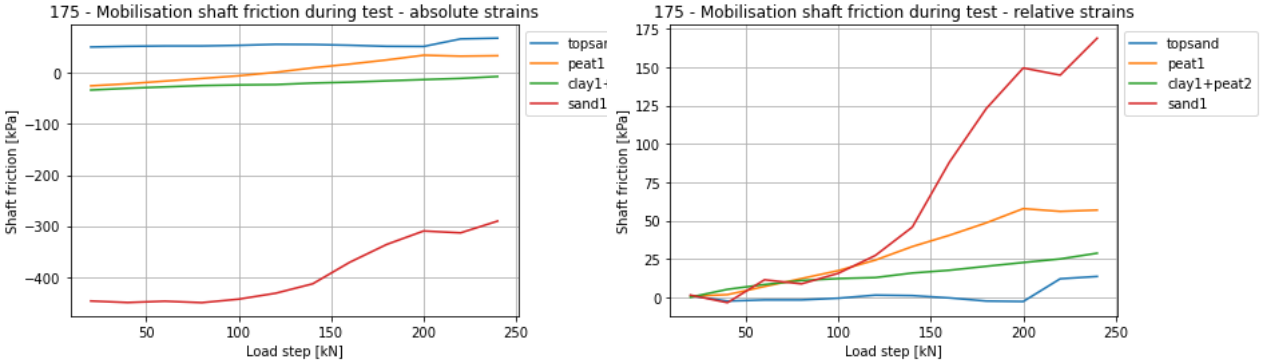

Figure 4.15: Pile 175 - Shaft Friction with Absolute Strains (left) and Relative Strains (right)

- In the left plot of Figure 4.15, the value of the shaft friction in Sand 1 is 10 times bigger than the friction measured in the other soil layers. This difference is not expected looking at the results of the other piles. The shaft friction does however increase positively during the test, but at the end of the test still a negative shaft friction is measured, which is not

expected. The other three soil layers do show more reasonable values of shaft friction: in the top sand layer there seems to be a small mobilization of shaft friction. Peat 1 reaches a maximum shaft friction at 200 kN, then the friction becomes constant.

- The right plot shows that Sand 1 first mobilises only a little friction, but after 120 kN, the shaft friction rapidly increases.

Appendix section A.1 shows an overview of the measurements points in pile 175 together with the location of the soil layers. In the North-South fibre, the lowest measurements (-12.13 and -12.12 mNAP) are located 42 and 41 cm below the boundary with the peat layer. So the peat layer on top of Sand 1 should not have affected the strain readings. Still, the value of the shaft friction in Sand 1 at the start of the test is strange.

Piles 175 and 187 were manually debarked, piles 576 and 592 were mechanically debarked. Figure G.4 in the Appendix shows the difference between the piles that are manually debarked and mechanically debarked. The mechanically debarked piles have a smoother contact area with the soil, and thus less friction is expected to develop. No significant difference could be found between manually and mechanically debarked piles when observing the mobilised shaft friction around the different piles.

4.4 Comparison Calculated and Measured Modulus of Elasticity

Before the compression load tests in the timber laboratory of the TU Delft were done, a modulus of elasticity was used in the analysis based on the average strain readings of four points on every side of the pile. In this section, the results of the calculated and measured stiffness of all four piles will be compared.

4.4.1 Calculated E modulus

Both fibers of pile 576 could be measured, so the average strains are based on four sides of the pile. To calculate the stiffness, the relative strains are used. The method explained in subsection 3.4.2 was used to calculate the pile stiffness.

Fibre	Start [mNAP]	End [mNAP]
North	-0.32	-1.09
South	-0.313	-1.08
East	-0.305	-1.07
West	-0.292	-1.06

Table 4.1: 576 - Locations calculation E modulus

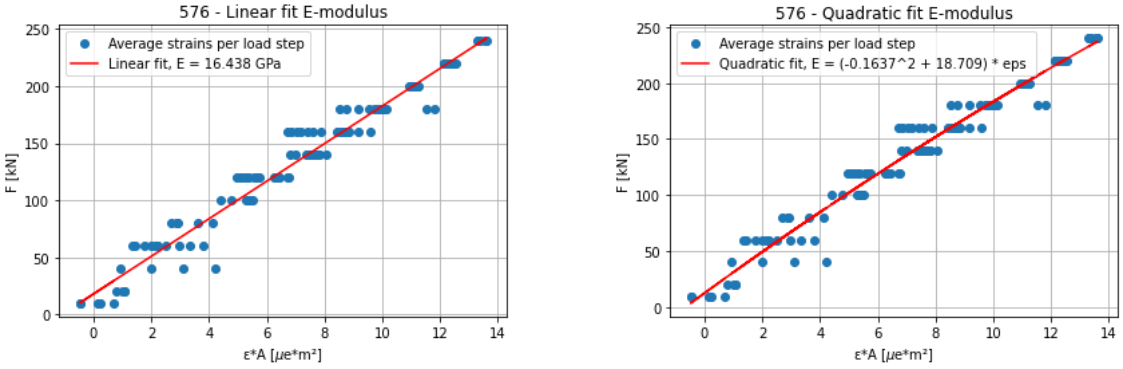

Figure 4.16: 576 - Calculated E modulus based on strain readings

Type fit	Stiffness	R^2 score
Linear	16.438 GPa	0.9701
Quadratic	$(-0.1637^2 + 18.709)\epsilon$	0.9715

Table 4.2: 576 - Results fitting E modulus

Table 4.1 shows the locations of the measurement points that were included in calculating the E modulus. Combining the average strains of the four sides and multiplying the average cross-section of the pile at the location of the four measurement points with these values resulted in the blue dots plotted in Figure 4.16. All measurement cycles within one load step were plotted, showing that there was a spread in strains measured during some load steps. This spread can be caused by a certain shift in the strain reading, which was observed a few times in the original strain readings. See Figures E.9 and E.10 in the Appendix. The red line is the fit between the data, and it is observed that the red line does not cross the origin. It is expected this should have happened since the strains are relative, but during the first load step of 10 kN, a negative $*A$

was found. A data point was added to the origin in the iteration process, but this did not lead to a better root mean square score. Also, omitting some of the last steps did not increase the score. The best fits and their scores are shown in Table 4.2.

Fibre	Start [mNAP]	End [mNAP]
North	-0.289	-1.056
South	-0.297	-1.062
East	-0.395	-1.161
West	-0.406	-1.172

Table 4.3: 592 - Locations calculation E modulus

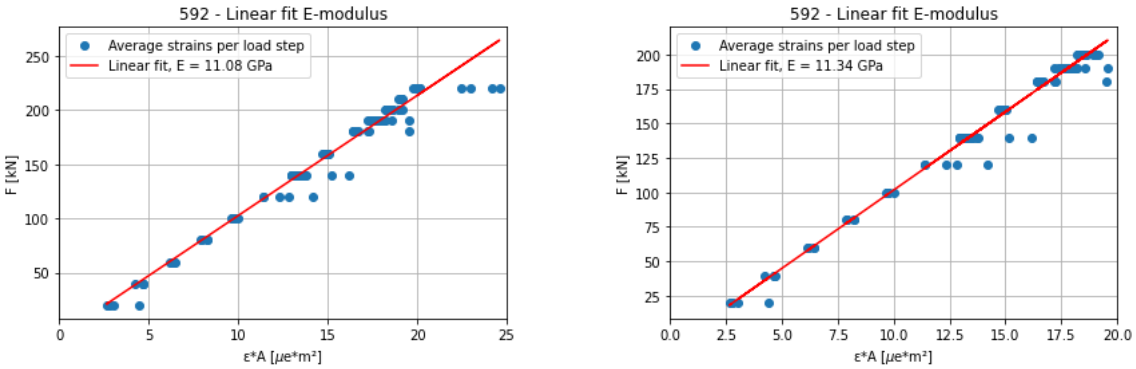

Figure 4.17: 592 - Calculated E modulus based on strain readings

Type fit	Stiffness	R^2 score
Linear (all)	11.08 GPa	0.9711
Linear	11.34 GPa	0.9816

Table 4.4: 592 - Results fitting E modulus

Pile 592 has two fibres, so the average strains are based on four sides of the pile. Table 4.3 shows the measurements included to determine the E modulus. The best root mean square scores were found with a linear fit. Figure 4.17 shows the linear fit on the left side when all load steps are included, and on the right side, the linear fit when the last two load steps are excluded. The left figure shows a significant deviation from the other strain readings observed in the last load steps. The linear fits resulted in a stiffness shown in Table 4.4.

Comparing the strain distribution in the graph between pile 592 and 576, pile 576 shows a more extensive spread of strain readings per load step than pile 592. A difference between the two piles is that pile 576 was tested in the extended compression load test only a month before the tensile load test was performed. The plot includes relative strains, so the influence of the pile history would be minimised, but it is still possible that the extended compression load test might have influenced pile 576, responding differently than pile 592.

Piles 175 and 187 were also tested in the laboratory, but only on three pieces instead of nine. Only one fibre could be measured in both piles. A consideration of the stiffness used in these two piles is explained.

175	North	South
Start	-0.385 mNAP	-0.378 mNAP
End	-1.151 mNAP	-1.143 mNAP

Table 4.5: 175 - Locations calculation E modulus

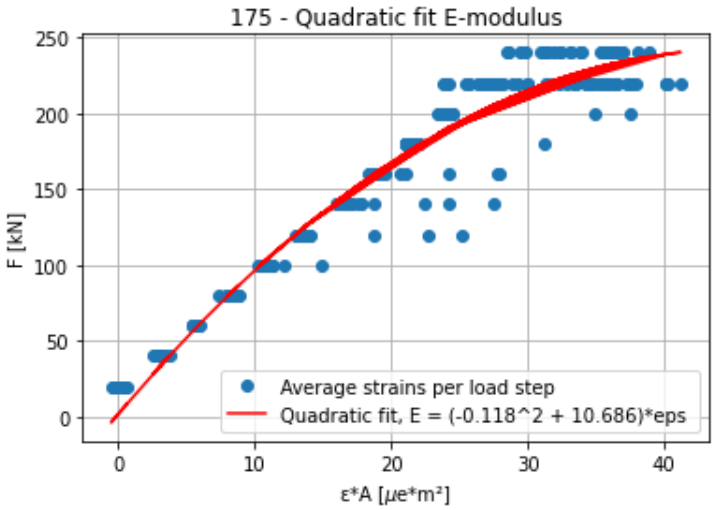

Figure 4.18: 175 - Calculated E modulus based on strain readings

In Pile 175, only the North-South fibre could be measured. A difference in the root mean square score was found compared to piles 576 and 592 since different configurations all resulted in a score slightly lower than the score of 576 and 592. The best score was found when using a quadratic fit, including all load steps. Despite the large spread in the last load steps, a root mean score of 0.9487 was found.

187	East	West
Start	-0.426 mNAP	-0.422 mNAP
End	-1.191 mNAP	-1.188 mNAP

Table 4.6: 187 - Locations calculations E modulus

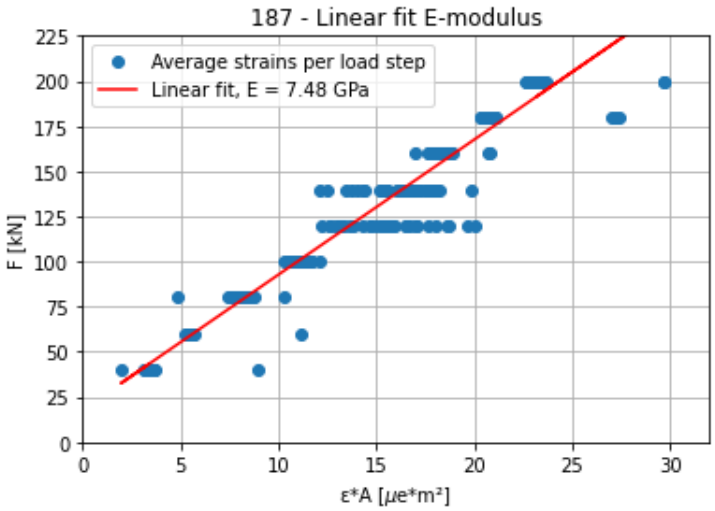

Figure 4.19: 187 - Calculated E modulus based on strain readings

In Pile 187, only the East-West fibre could be measured. Also, this pile showed a lower root mean square score compared to piles 576 and 592, suggesting that using two fibres increases the score and reduces the error. Figure 4.19 shows a large spread in strain readings at 120 and 140 kN. A linear fit without forcing the fit through the origin gave the highest root mean square score: 0.937. The E modulus found is 7.479 GPa: significantly smaller than the values found in piles 576 and 592.

4.4.2 Measured E modulus

The distribution of E moduli found during the compression load tests on piles 592 and 576 in the timber laboratory can be found in Figure F.3 in the Appendix. The tests on piles 175 and 187 were done in another test, where only three pieces of the pile were tested instead of nine.

Pile	E_{TU} [GPa]	E_{fiber} [GPa]	E_{fiber}/E_{TU}
592	11.489	11.34	98.7 %
576	12.963	16.438	126.8 %
187	8.666	7.48	86.3 %
175	9.69	10.686	110.3 %

Table 4.7: Pile stiffness comparison

Table 4.7 shows the different values of pile stiffness found for all four piles. The last column shows the under or overestimation of the pile stiffness based on the strain readings. This gave an average of 105.5 %, meaning that on average the calculated E modulus overestimated the measured E modulus with 5.5 %. But looking at the individual piles, only pile 592 got an accurate estimate, where the stiffness in pile 187 differed 13.3 %. The method has thus been proven accurate for pile 592, but not for the other piles.

Figure F.3 shows that at lower levels in the pile, the modulus is much lower than at the top of the pile. In one of the other piles tested in the laboratory, a decrease of 7 GPa between the pile head and pile tip was found (Pagella 2021), which shows that assigning a value based on the pile head can be inaccurate and thus leads to errors in the further analysis. On average, a reduction of 32 % in stiffness was measured, with a range between 13 and 52 %.

4.5 Mobilisation Curves Assessment

This section explains how the mobilisation curves were created. For every pile and per soil layer, separate mobilisation curves were created. Since the second peat layer was too small, this peat layer was added to the overlying clay layer for further assessment.

4.5.1 Shaft friction development

The shaft friction calculated in section 4.3.2 was used to compose the mobilisation curves. In section 4.3.2 it was discussed that especially in the bearing sand layer, the shaft friction developed showed different results to other soil layers. In all piles - except in pile 592 - there were only a few measurement points in the bearing sand layer. It was explained earlier that when calculating the shear friction over a small interval, the values of shaft friction can fluctuate quickly, with a reversal of sign. This might explain the sizeable negative shaft friction in the bearing sand layer. The mobilisation curves were composed for all soil layers, but further in the analysis, it was chosen to not use all mobilisation curves for the combined curves.

4.5.2 Relative settlement

First the displacement measured by the LVDTs was compared to the integrated strain readings of the Omnisens. The relative strain readings were used, since one wants to know the strains that are developed during the test only, to properly compare it to the LVDT measurements. These results will be explained shortly.

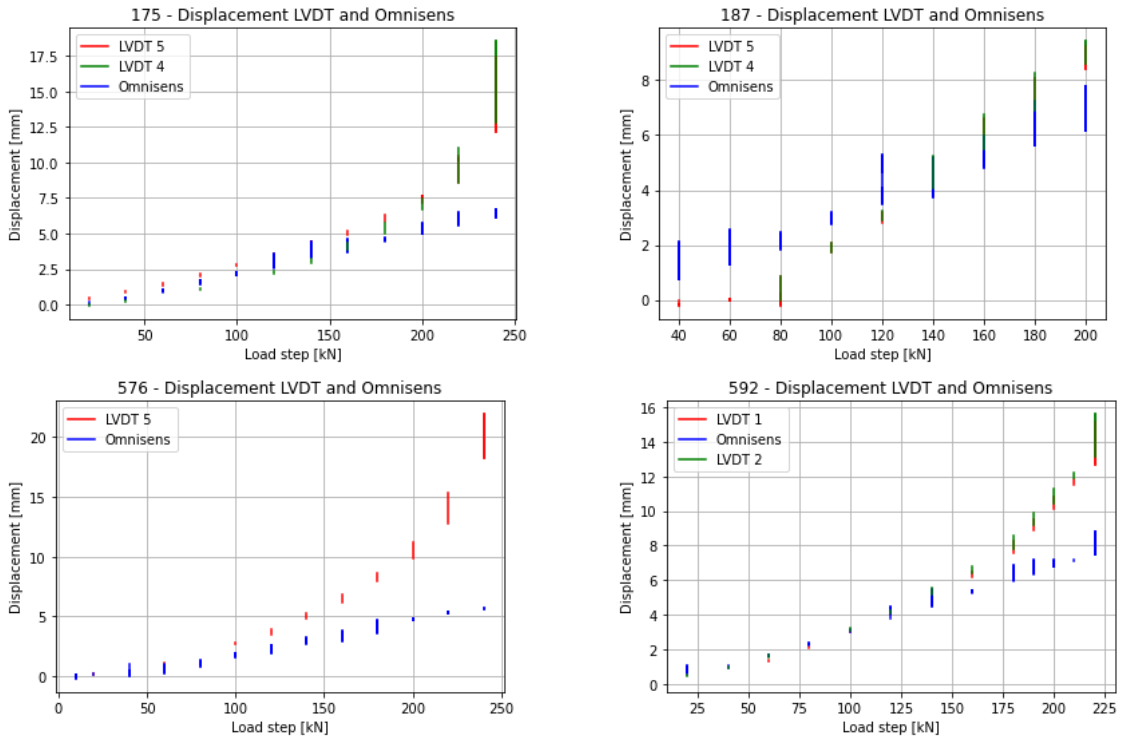

Figure 4.20: Comparison displacement LVDT and Omnisens

Figure 4.20 shows graphs of the four piles, containing the displacement measured by the LVDT combined with the displacement found after integrating the strain readings in the pile. For Pile 175 (top left) and Pile 592 (bottom right), this behaviour is observed: the Omnisens reading deviates from the LVDT reading after a particular load step. This might indicate that the load is mobilised through the entire pile, and now the pile toe starts displacing. In Pile 187, the

LVDT shows no displacement until 80 kN, which is unlikely to have happened. And in Pile 576, the Omnisens reading already starts deviating from the LVDT reading after 50 kN. Table 4.8 shows, however, that the average difference between the LVDT and Omnisens data is still a few millimetres.

Load step	175 [mm]	187 [mm]	576 [mm]	592 [mm]
1	0.386	1.04	0.146	
2	0.418	1.463	0.038	0.382
3	0.45	1.832	0.332	0.346
4	0.537	1.024	0.466	0.315
5	0.649	1.109	0.822	0.235
6	0.768	0.303	0.869	0.043
7	0.867	0.607	1.532	0.263
8	1.136	1.349	1.967	0.583
9	1.659	2.492	3.113	1.048
10	2.348		4.206	1.886
11	3.703		5.92	2.624
12	8.652		9.123	3.624
13			14.674	4.503
14				6.398

Table 4.8: Average difference LVDT and Integrated Strains per load step

4.5.3 Combined Mobilisation Curves

The combined mobilisation curves will be presented and discussed in this section. The mobilisation curves are based on two different scenarios: based on the relative strains, when the strains at the start of the tensile load test are zeroed out. And based on absolute strains, minus the strains already measured in the pile during the reference measurements. Since it was not possible to compose a mobilisation curve based on automated functions, it was chosen to make a manual fit of the mobilisation curve. Most curves show a smooth increase of mobilisation, then when the full mobilisation is reached a sharp angle is made. This shape is not in accordance with the curves in *NEN 9997-1 + C2* (2017), but it is thought that this manual fit best represents the average shaft friction at the location of full mobilisation.

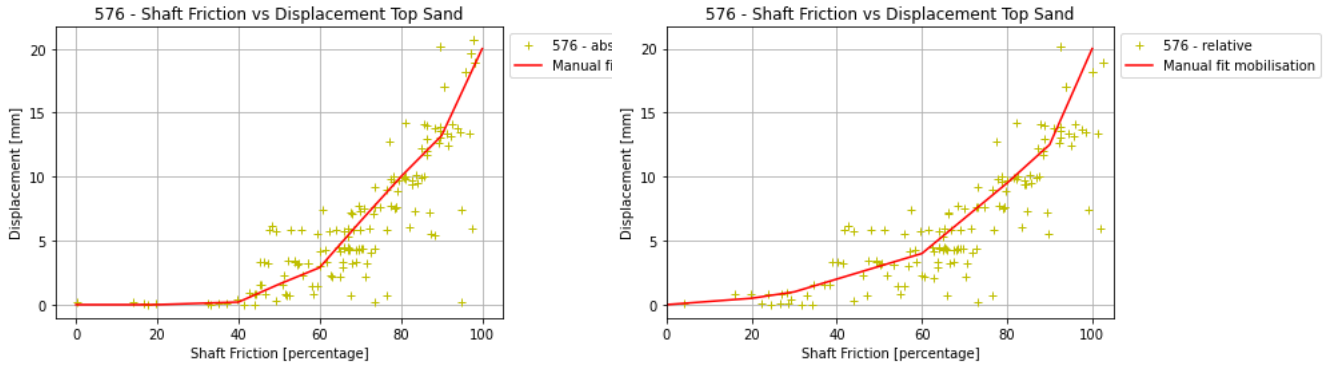

Figure 4.21: Mobilisation Curve Top Sand - Absolute (left) and Relative (right)

Since it was found in the analysis that only pile 576 mobilised shaft friction in the top sand layer, only the data from pile 576 is included for the mobilisation curve of top sand. The left plot of Figure 4.21 shows a stiffer response halfway the mobilisation of shaft friction compared to the right plot - which is based on relative strains -, but the total mobilisation is reached around the same displacement: 20 mm. So twice as much displacement is needed for total mobilisation than is mentioned in *NEN 9997-1 + C2* (2017).

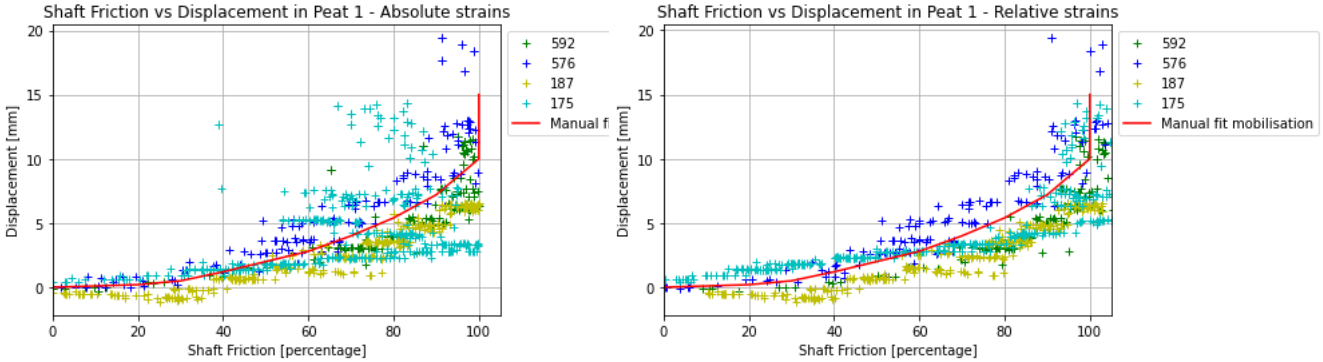

Figure 4.22: Mobilisation Curve Peat 1

Figure 4.22 shows the combined mobilisation curve for Peat 1. According to *NEN 9997-1 + C2* (2017), the maximum shaft friction is expected at a displacement of 10 mm. Both mobilisation curves - with absolute and relative strains - seem to reach full mobilisation around a displacement of 10 mm. The same manual fit was applied to both the left and right plots, which seems to fit. Pile 175 deviates the most from the other piles in the left plot: much scatter is observed.

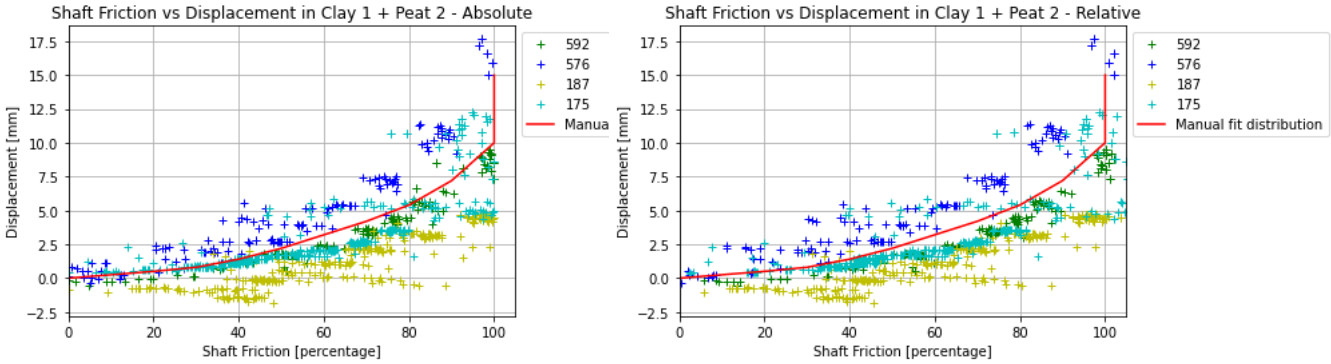

Figure 4.23: Mobilisation Curve Clay 1 + Peat 2

Figure 4.23 shows the combined mobilisation curves of the Clay 1 and Peat 2 layer. In this layer, it was manually fitted that the maximum shaft friction would occur at a displacement of 10 mm, following *NEN 9997-1 + C2* (2017). In both plots, pile 187 shows a negative displacement at specific points caused by the zero displacements of the LVDT at the beginning of the test. Since the displacement was zero according to the LVDT - this zero displacement is not expected when a tensile force is applied -, and the summation of strain readings did show a displacement, resulting in a negative displacement.

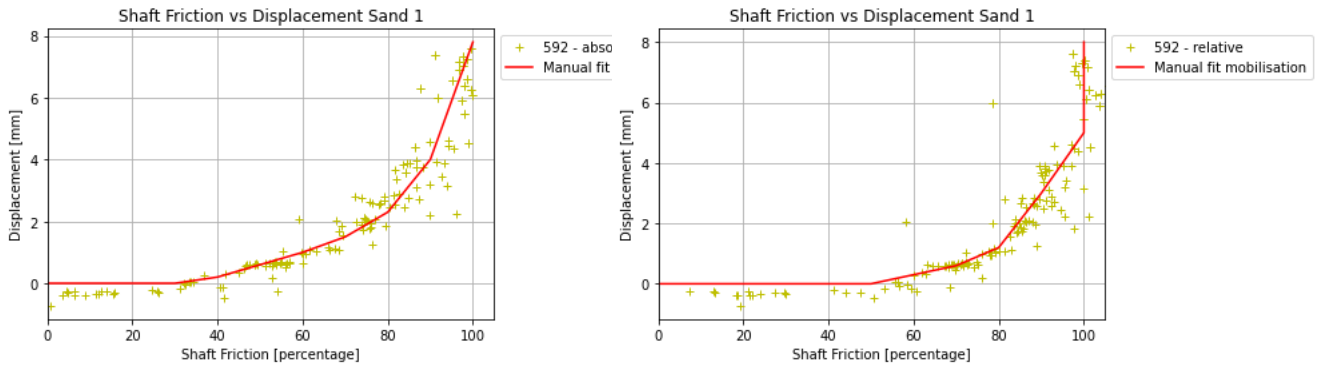

Figure 4.24: Mobilisation Curve Sand 1 - Absolute (left) and Relative (right)

Figure 4.24 shows the mobilisation curve derived from pile 592 in Sand 1. The left plot with absolute strains shows a stiffer response than the right plot: full mobilisation is reached at 8 mm displacement, whereas full mobilisation is already reached at 5 mm in the right plot. Both plots show a softer response than is mentioned by *NEN 9997-1 + C2* (2017), since less than 10 mm displacement is needed for total mobilisation.

4.5.4 Including Pile Test History

Section 3.1.5 discussed the pile history of the piles included in the analysis. In this subsection it will be explained how the results of the mobilisation curves should be interpreted when including this pile history.

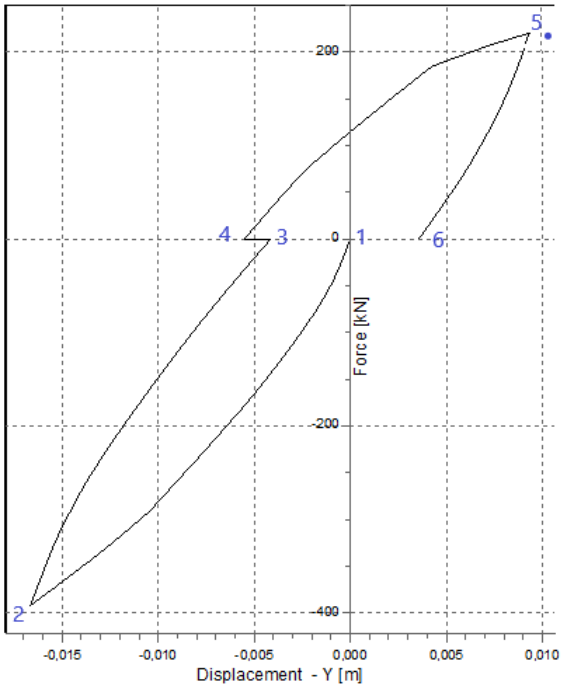

Figure 4.25: Pile Head displacement from D Pile Group

Figure 4.25 shows the pile head displacement from the simulation in D Pile Group. Negative shaft friction is mobilised during the compression load test since the sign of compression load is negative too. Unloading and reloading steps were applied during the compression load test, but

only the last step is included for simplicity. Hysteresis occurs after the compression load test - when the compressive load is removed, so the pile head displacement does not move completely back to the origin. It is also expected that additional displacement has taken place due to soil settlement in the year between the compression load test and tensile load test. This means that it is not correct to start the mobilisation curves of the tensile load test in the origin. According to Figure 4.25, the mobilisation curves of the tensile load test should have started at location 4.

4.6 Comparison Influence of Tapering

A comparison is made between the alpha factors derived from the compression load test and tensile load test to answer the research question on the influence of tapering on the soil stresses around the pile. The relative strain readings are used, so excluding residual loads. Peat 2 was not considered individually. During the analysis of the tensile load tests, this layer was too thin to be certain measurements done in this layer are based on the peat layer properties only. The values of α_s were retrieved from Honardar (2020). Pile 187 was not analysed by Honardar (2020), so no conclusions can be drawn on the influence of tapering for this pile.

4.6.1 Alpha Factors from Absolute strains

This section shows the alpha factors calculated when residual loads are included. The top sand layer is not included, since the layer was pre-drilled, and thus disturbed.

592	$q_c[kPa]$	$\tau_{max,fiber}$ [kPa]	$\alpha_{t,fiber}$	$\tau_{max,TU}$ [kPa]	$\alpha_{t,TU}$	α_s
Peat 1	779.67	49.5	0.063	56	0.072	0.056
Clay 1 + Peat 2	690.12	41	0.059	32.5	0.047	0.087
Sand 1	7509.41	8	0.001	6	0.001	0.018

Table 4.9: Absolute Alpha factors soil layers pile 592

576	$q_c[kPa]$	$\tau_{max,fiber}$ [kPa]	$\alpha_{t,fiber}$	$\tau_{max,TU}$ [kPa]	$\alpha_{t,TU}$	α_s
Peat 1	809.81	40	0.049	29	0.036	0.022
Clay 1 + Peat 2	691.5	32	0.046	19	0.027	0.046

Table 4.10: Absolute Alpha factors soil layers pile 576

187	$q_c[kPa]$	$\tau_{max,fiber}$ [kPa]	$\alpha_{t,fiber}$	$\tau_{max,TU}$ [kPa]	$\alpha_{t,TU}$
Peat 1	726.85	33	0.045	54	0.074
Clay 1 + Peat 2	725.81	32.5	0.045	32	0.044

Table 4.11: Absolute Alpha factors soil layers pile 187

175	$q_c[kPa]$	$\tau_{max,fiber}$ [kPa]	$\alpha_{t,fiber}$	$\tau_{max,TU}$ [kPa]	$\alpha_{t,TU}$	α_s
Peat 1	791.47	55	0.069	35	0.044	0.055
Clay 1 + Peat 2	668.92	-8	-0.012	-6	-0.009	0.102
Sand 1	9227.56	-380	-0.041	200	0.022	0.007

Table 4.12: Absolute Alpha factors soil layers pile 175

The hypothesis is that the alpha factor of the tensile load test is smaller than the alpha factor from the compression load test, since a tapered while should experience less friction when pulled out of the soil. The α_s from the compression load test should be compared to the α_t based on the pile stiffness from strain readings.

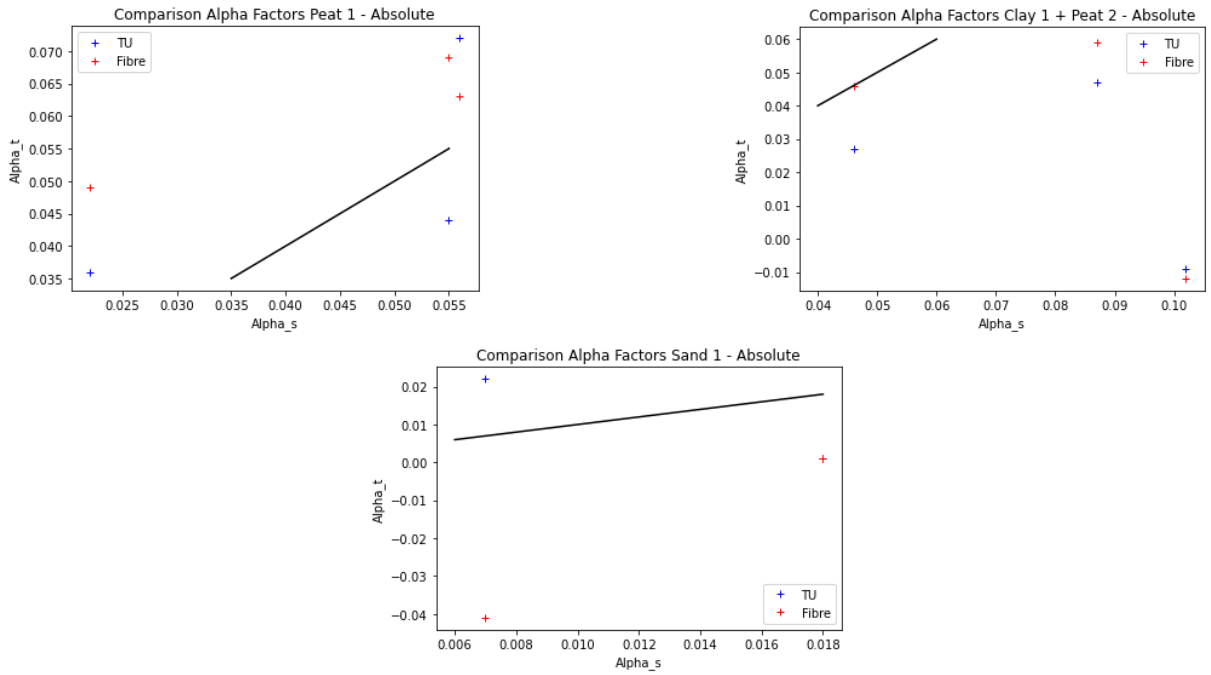

Figure 4.26: Alpha factors per soil layer - absolute strains

Figure 4.26 shows a comparison of the alpha factors per soil layer, based on absolute strains. When the measurement is below the black line, it confirms the hypothesis: α_t is smaller than α_s. Looking only at the α_t based on the tests at TU Delft, five of the eight cases confirm the hypothesis, which is 62.5 %.

4.6.2 Alpha Factors from Relative strains

Using the formula given in section 3.8.1, the following results were found. The average cone resistance was determined by first combining the three cone penetration tests performed around the pile, then calculating the average cone resistance in the specific soil layer.

592	$q_c[kPa]$	$\tau_{max,fiber}$ [kPa]	$\alpha_{t,fiber}$	$\tau_{max,TU}$ [kPa]	$\alpha_{t,TU}$	α_s
Peat 1	779.67	30.5	0.039	47	0.06	0.075
Clay 1 + Peat 2	690.12	33	0.048	28.8	0.042	0.095
Sand 1	7509.41	80	0.011	58	0.008	0.013

Table 4.13: Relative Alpha factors soil layers pile 592

576	$q_c[kPa]$	$\tau_{max,fiber}$ [kPa]	$\alpha_{t,fiber}$	$\tau_{max,TU}$ [kPa]	$\alpha_{t,TU}$	α_s
Peat 1	809.81	27	0.033	25	0.031	0.032
Clay 1 + Peat 2	691.5	23.5	0.034	20.7	0.03	0.056

Table 4.14: Relative Alpha factors soil layers pile 576

187	$q_c[kPa]$	$\tau_{max,fiber}$ [kPa]	$\alpha_{t,fiber}$	$\tau_{max,TU}$ [kPa]	$\alpha_{t,TU}$
Peat 1	726.85	33	0.045	70	0.096
Clay 1 + Peat 2	725.81	19	0.026	19	0.026

Table 4.15: Relative Alpha factors soil layers pile 187

175	$q_c[kPa]$	$\tau_{max,fiber}$ [kPa]	$\alpha_{t,fiber}$	$\tau_{max,TU}$ [kPa]	$\alpha_{t,TU}$	α_s
Peat 1	791.47	32	0.04	56.5	0.071	0.079
Clay 1 + Peat 2	668.92	27	0.04	30	0.045	0.077
Sand 1	9227.56	205	0.022	175	0.019	0.003

Table 4.16: Relative Alpha factors soil layers pile 175

Following the hypothesis that a tapered pile would experience less resistance when pulled out compared to when it is driven into the soil, the α_t from the tensile load test is expected to be smaller than the α_s from the compression load test. Since Honardar (2020) did not have access to the test results from the timber laboratory, the α_s should be compared to the α_t based on the calculated pile stiffness from strain readings.

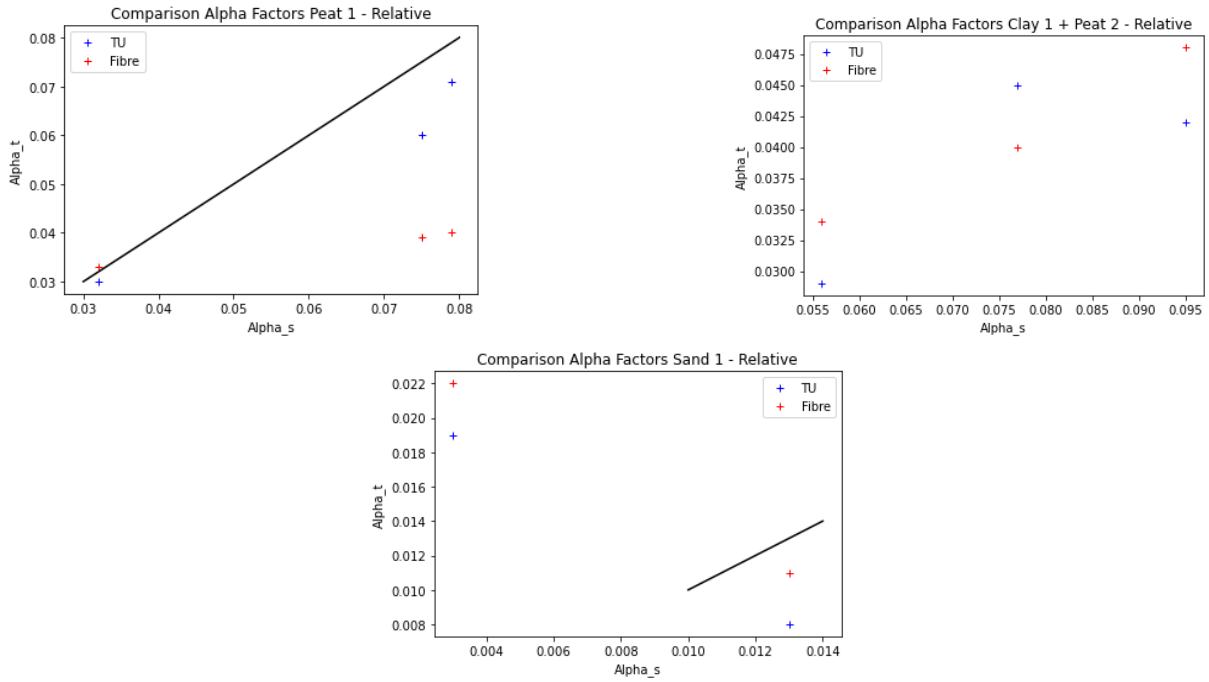

Figure 4.27: Alpha factors per soil layer - relative strains

Figure 4.27 shows a comparison of the alpha factors per soil layer, based on relative strains. When the measurement is below the black line, it confirms the hypothesis: α_t is smaller than α_s. Looking only at the α_t based on the tests at TU Delft, seven of the eight cases confirm the hypothesis, which is 87.5 %. In the plot in the right top, no line was plotted: all α_t were already significantly smaller than α_s, so it was impossible to plot the line.

Comparing the α_t based on relative strains with the α_t based on absolute strains, when absolute strains are used the factor decreases on average 14 per cent. However, there is a wide range: the biggest decrease is 120 %, and the biggest increase is 68 %. The α_t based on the TU Delft

test was used. It is thus impossible to draw conclusions on the influence of including absolute strains on the reduction of α_t.

4.7 Comparison Negative Skin Friction based on Test and NEN norms

It was mentioned in section 2.2 that according to the NEN 9997-1 norm, the influence of negative skin friction on the bearing capacity of the pile could be calculated using the formula mentioned in the same section. In this section, a comparison is made between the calculated negative skin friction utilising this formula and the negative skin friction found based on the test data.

4.7.1 Negative Skin Friction according to NEN 9997-1

$$F_{nk,k} = O_{s,gem} * \int_{j=1} d_j * K_{0,j,k} * tan(\delta_{j,k}) * \frac{\sigma'_{j-1,k} + \sigma'_{j,k}}{2} \tag{4.1}$$

The term $K_{0,j,k} * \tan(\delta_{j,k})$ in the formula is now based on the internal friction angle of the soil instead of the interaction between the pile shaft and soil. And according to NEN 9997-1, this term should be at least 0.25. It was found that when the original values of the soil layers are used, all soil layers got a value smaller than 0.25.

Parameter	592	576	187	175
$O_{topsand}$	0.679 m	0.56 m	0.799 m	0.838 m
O_{p1}	0.639 m	0.523 m	0.726 m	0.73 m
O_{c1p2}	0.557 m	0.485 m	0.622 m	0.621 m
GWT	-1.22 mNAP	-1.22 mNAP	-1.22 mNAP	-1.22 mNAP

Table 4.17: Average circumferences per soil layer and location groundwater table

Parameter	Symbol	Top Sand	Peat 1	Clay 1	Peat 2
Cone resistance	q_c [MPa]	7.99	0.67	0.47	1.03
Volumetric weight	γ [kN/m^3]	17.5	12	17	14
Soil Thickness	d [m]	4.80	1.90	4.66	0.38
Internal Friction Angle	$\phi[^\circ]$	30.0	15.0	17.5	15.0
Earth Pressure Coefficient	K_0 [-]	0.5	0.741	0.699	0.741
Pile-Soil Interaction	$\tan(\delta_{j,k})$	0.414	0.199	0.233	0.199

Table 4.18: Input parameters calculation NSF according to NEN 9997-1, Piles 592 and 576

Table 4.17 shows the average circumference for every pile in every soil layer. The circumference in every soil layer was determined by using the circumference halfway the soil layer. The location of the groundwater table was retrieved from Dinoloket.nl, by looking at the most recent groundwater table measured at 'Park Somerlust' in Overamstel Amsterdam. The reference is BRO-ID GMW000000032513. The values of Table 4.18 were retrieved from Table 2b of NEN 9997-1, using the average cone resistance found for each soil layer.

F_{nk}	Pile 592	Pile 576	Pile 187	Pile 175
Top Sand	34.51	28.46	39.1	40.49
Peat 1	29.06	23.79	32.86	32.09
Clay 1 + Peat 2	104.91	91.35	118.49	118.39
Total [kN]	168.48	143.6	190.45	190.97

Table 4.19: Contribution Negative Skin Friction per Soil Layer (*NEN 9997-1 + C2* 2017)

F_{nk}	Pile 592	Pile 576	Pile 187	Pile 175
Top Sand	28.57	23.56	32.38	33.53
Peat 1	17.14	14.03	19.38	18.93
Clay 1 + Peat 2	59.0	105.24	76.52	76.46
Total [kN]	113.47	96.59	128.28	128.92

Table 4.20: Contribution Negative Skin Friction per Soil Layer, excluding 0.25 (*NEN 9997-1 + C2* 2017)

$F_{nk,k}$, the characteristic value of the negative skin friction is equal to $F_{nk,d}$, the design value, in this case, since it was mentioned in NEN 9997-1 that a correlation factor of 1.0 should be applied for the formula used. Table 4.19 shows the calculated negative skin friction according to the current rules, with the contribution of every soil layer. In Table 4.20 the results are shown when the requirement of a minimum of 0.25 for $K_{0,j,k} * \tan(\delta_{j,k})$ is disregarded. All piles show a smaller force from negative skin friction, especially the contribution of the soft soil layers differs from Table 4.19.

4.7.2 Negative Skin Friction according to Test Results

Since the direction of movement of the pile shaft along the soil is the same in both a tensile load test and during the development of negative skin friction, it is assumed that the maximum shaft resistance occurring during a tensile load test is comparable to the friction occurring during the development of negative skin friction. So to calculate the negative skin friction based on the test results, the maximum shaft friction is translated into a force per soil layer. Then only the soil layers experiencing negative skin friction are added together. The maximum shaft friction based on relative strains is used in the calculation.

$$F_{nk,i} = \tau_{max,i} * d_i * O_i \tag{4.2}$$

Where $F_{nk,i}$ is the force created by negative skin friction of soil layer i. $\tau_{max,i}$ is the maximum shaft friction experienced in this soil layer, retrieved from the mobilisation curve created for that soil layer. d_i is the thickness of soil layer i and O_i is the circumference of the pile halfway soil layer i. The forces of the three individual soil layers are then added to find the total force that can be expected from negative skin friction.

Parameter	Symbol	Top Sand	Peat 1	Clay 1 + Peat 2
Shaft friction	τ_{max} [kPa]	5.5	47	28.8
Soil Thickness	d [m]	4.82	1.90	5.04
Circumference	O [m]	0.679	0.639	0.557

Table 4.21: Input parameters Pile 592

Parameter	Symbol	Top Sand	Peat 1	Clay 1 + Peat 2
Shaft friction	τ_{max} [kPa]	17.5	25	20.7
Soil Thickness	d [m]	4.82	1.90	5.04
Circumference	O [m]	0.56	0.523	0.485

Table 4.22: Input parameters Pile 576

Parameter	Symbol	Top Sand	Peat 1	Clay 1 + Peat 2
Shaft friction	τ_{max} [kPa]	0	70	19
Soil Thickness	d [m]	4.73	1.92	5.12
Circumference	O [m]	0.799	0.726	0.622

Table 4.23: Input parameters Pile 187

Parameter	Symbol	Top Sand	Peat 1	Clay 1 + Peat 2
Shaft friction	τ_{max} [kPa]	-2	56.5	30
Soil Thickness	d [m]	4.70	1.88	5.15
Circumference	O [m]	0.838	0.73	0.621

Table 4.24: Input parameters Pile 175

Tables 4.24, 4.23, 4.22 and 4.21 show the input parameters for all four piles. Clay 1 and Peat 2 were considered as one soil layer, since during the analysis it was shown that the peat layer was too thin to consider separately.

F_{nk}	Pile 592	Pile 576	Pile 187	Pile 175
Top Sand	18	47.24	0	-7.88
Peat 1	57.06	24.84	97.57	77.54
Clay 1 + Peat 2	80.85	50.6	60.51	95.95
Total [kN]	155.91	122.68	158.08	165.61
NEN incl. 0.25	168.48	143.6	190.45	190.97
NEN excl. 0.25	113.47	96.59	128.28	128.92

Table 4.25: Contribution Negative Skin Friction per Soil Layer based on Test Data

Table 4.25 shows the total negative skin friction to be expected according to the test data, with the contribution of each soil layer. The total values of all four piles are in between the current NEN norm - including the 0.25 requirement - and the same formula of the NEN norm, but excluding the 0.25 requirement. Based on the test results, this might implicate that the requirement of 0.25 is too conservative. To match the value from the NEN code with the test data a factor in the range of 0.21 to 0.23 is needed: 0.22 on average.

This comparison of calculations shows that the maximum shaft frictions found based on the test results give a good approximation of the negative skin friction to be expected according to *NEN 9997-1 + C2* (2017).

4.8 Simulations of Negative Skin Friction

This section will discuss the results of the simulation in D Pile Group. In section 3.9 it is explained what steps are taken during the simulation and what input data is used.

4.8.1 Simulation Pile Test History

First the entire pile test history of pile 592 was simulated. The development of displacement against force applied could be verified for the tensile load test. Figure 4.28 shows the displacement against the pile force. The different numbers in the figure will be discussed:

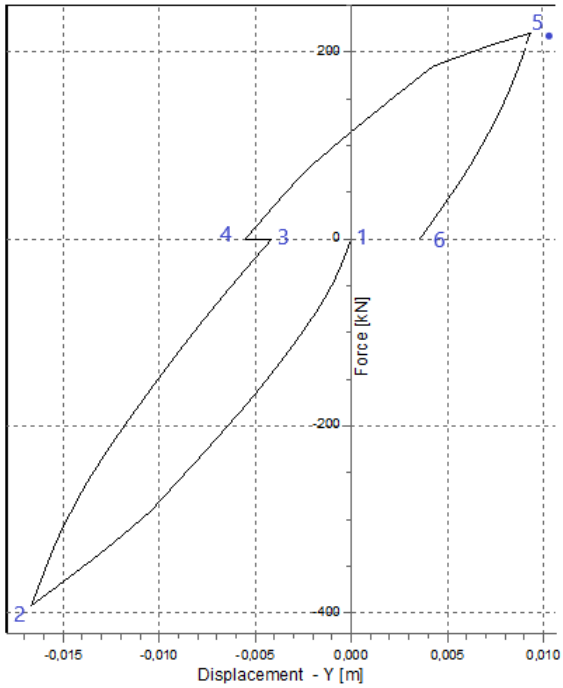

Figure 4.28: D Pile Group: Pile Head displacement Pile 592

1. The start of the compression load test at the origin (0,0).
2. The end of the compression load test: a maximum force of -392 kN (negative, since it is compression) is reached, with a pile displacement of 1 cm downward. The compression load is now removed from the pile head.
3. All compressive load on the pile head is removed. The pile showed a stiffer response to the load than during the compression load test. This is caused by hysteresis in the pile. There is a permanent deformation left in the pile. From this point, the soil displacement starts to develop.
4. After one year, a displacement of 1.3 mm was measured due to soil displacement. Now the tensile load test starts.
5. The maximum tensile load is reached, the test has produced an upward displacement of 14.8 mm. The tensile load is now removed.
6. All tensile load is removed, the pile has moved 5.8 mm downwards after removing the load.

The end bearing capacity that was found by Honardar (2020) - 218 kN including residual loads - turned out to be insufficient: when 392 kN compressive load was applied, the system failed. An

iteration was performed to find the required end bearing. The displacement between locations 4 and 5 in Figure 4.28 was verified until it matched the displacement measured by the LVDT in the tensile load test best. At an end bearing capacity of 251 kN, the displacement simulated between locations 4 and 5 was 14.82 mm. The LVDT showed a displacement of 16.13 mm during the tensile load test: this value is marked in the figure with a blue dot next to location 5. The difference between the end bearing value found by Honardar (2020) and the value needed in D Pile Group can be caused by the difference in pile geometry. However, it is chosen to continue with the end bearing value of 251 kN for the simulation of negative skin friction.

4.8.2 Simulation Development Negative Skin Friction

It was simulated how negative skin friction would develop around the pile in practical conditions when the same pile and soil input data were applied. A workload of 50 per cent of the total bearing capacity was used, so for pile 592, this was 196 kN. The load was kept on the pile head for the entire simulation. A soil displacement of 1 cm at ground level was applied, and no settlement at the top of the bearing sand layer. The factor of the soil displacement was increased until the pile failed.

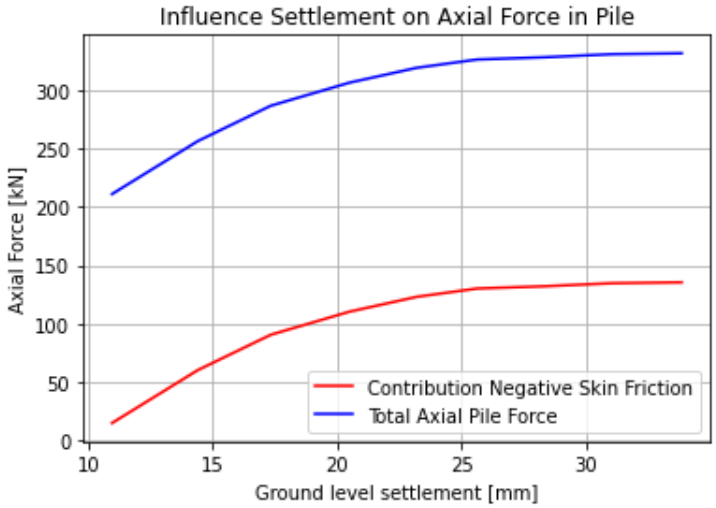

Figure 4.29: Influence Settlement on Axial Force

Figure 4.29 shows the development of axial force under the influence of soil settlement. After a certain settlement, the maximum axial force is reached: around 331 kN. Honardar (2020) showed a maximum capacity of 392 kN. The difference might be caused by the difference in pile geometry used: Honardar (2020) used a variable pile cross-section. At the maximum axial force, the negative skin friction reaches a maximum of 135 kN: this is calculated by subtracting the workload (196 kN) from the maximum axial force. So the maximum contribution of negative skin friction to the total bearing capacity of this pile turned out to be about 40 %. Comparing this value to the negative skin friction based on the NEN norms and the test data in the previous section, the result is 33 kN smaller than the current NEN code (168.48 kN) and 20 kN smaller than the test data (155.91 kN). The 20 kN difference with the test data is an inaccuracy. When comparing the proportion of negative skin friction to the axial load on the pile head, the maximum negative skin friction is 69 % of the axial load.

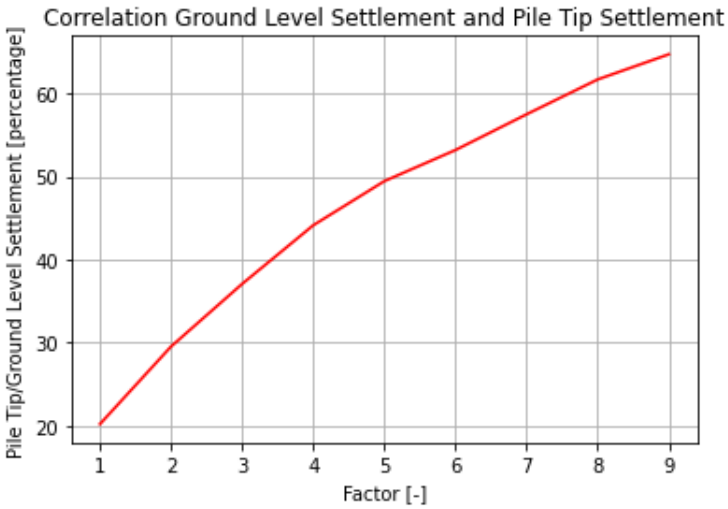

Figure 4.30: Correlation Ground Level and Pile Tip settlement

Figure 4.30 shows the ratio between the pile tip settlement and the ground level settlement under different factors. At the maximum factor - 9 - the pile tip settlement was 64.7 % of the ground level settlement: the highest ratio during the simulation.

These simulations tried to verify the pile test history and then apply the verified input data to simulate the situation of a bridge foundation pile. The simulation was only done for pile 592, since this pile showed the best results in the previous steps of the analysis. And this pile was more than a metre in the bearing sand layer. The simulations showed a smaller negative skin friction than was calculated with the current NEN code, thus also confirming that the code is conservative. The pile failed at 90 mm soil surface displacement, so it takes quite some time for all negative skin friction to be mobilised.

5. Discussion

This chapter will explain all the discussion points of the thesis. A distinction is made between discussing the test data, the test results and the comparison to the NEN norms.

5.1 Evaluation of Test Data

This section evaluates the different components of the test data.

5.1.1 Pile Geometry

The circumference measurements along the timber piles showed no continuous decreasing taper: at specific locations, the circumference was bigger than the measured circumference above. The presence of branches could have increased the local cross-section. This means that the strength can locally differ from the rest of the pile. Unfortunately, it was not possible to measure in such detail.

Piles 175 and 187 were manually debarked, piles 576 and 592 were mechanically debarked. The mechanically debarked piles have a smoother contact area with the soil, so less friction was expected. The resulting shaft friction in the soil layers shows no significant difference between the manually and mechanically debarked piles.

5.1.2 Symmetry in Wood

It was assumed that the strain readings should show symmetry to find the location of the fibre loop: if one half of the fibre experienced tension, this must be compensated with compression on the other half. This bending behaviour is encountered in all slender materials that are axially loaded. A remark for timber is that it is an organic material and thus that it might deviate from this general rule.

Another remark to this symmetry assumption is that it is now assumed that two measurement points are precisely at the same level on both sides of the pile. This is possible, but there is a slight chance this might happen.

5.1.3 Moving Average of Strain Readings

The Omnisens device measures strain throughout one metre, then moves the stretch 25 centimetres further and calculates an average strain over the next one-metre stretch. The value of a strain reading is thus derived from four of these stretches that overlap on the 25 centimetres where this measurement point is located. Especially in the part of the pile right below ground level since the strain reading is partly based on a pile section above ground. Therefore, to determine the shaft friction in the top sand layer, the first metre below ground level was not taken into account.

5.1.4 Strain Development in Measurement Locations

During the analysis, some soils showed development of shaft friction that is physiologically not possible for a timber pile during a tensile load test. The test increases the tension on the pile, which means that a positive strain is mobilised during every load step. So the shaft friction mobilised during the test should increase the harder is pulled on the pile head. Some soil layers either showed a decrease in shaft friction during the test, or an order of magnitude of friction

was found that significantly deviated from the other soil layers. The strain development of single measurements was studied in more detail to find a possible explanation for this abnormal behaviour: a possible explanation is that the pile toe started to displace during the load test.

5.2 Discussion on Reliability of Results

This section discusses the reliability of results acquired after analysing the test data.

5.2.1 Absolute or Relative strains

Mobilisation curves were derived both based on absolute and relative strains. Because of the pile test history, using the absolute strains resembles reality better, since it is expected there are still strains present in the pile.

However, in the comparison of the negative skin friction based on the NEN and the test data, the results from relative strains were used. It was found that the relative strains best approached the NEN values. In the simulation the mobilisation curves based on relative strains were used. This also led to a negative skin friction close to the NEN code. So also in the simulation the relative strains were proven best.

When deriving the alpha factors, both absolute and relative strains were compared. 14 % average reduction of α_t was found when absolute strains were included. But this was based on a wide range: -120 till +68. The relative strains confirmed the influence of tapering to be 87.5 % compared to 62.5 % when absolute strains were used. Based on the comparison with the NEN code, the relative strains were proven best. So assuming that in the comparison of the alpha factors the relative strain is then also best, 87.5 % of the alpha factors confirmed the influence of tapering.

5.2.2 Translation Tensile Load Test to Negative Skin Friction

This thesis focused on the analysis of tensile load tests. The load is increased under an axially applied tensile load until the pile is pulled out of the soil. Once the pile starts coming out of the soil, geotechnical failure occurs. The maximum shear friction that is mobilised is comparable to the shear friction mobilised when the consolidated soil moves downwards along the pile. The pile is loaded in tension during the tensile load test instead of compression.

5.2.3 Creep Effect

It was mentioned that because of the pile test history and the piles being installed more than a year before the tensile load test, creep will have developed in the pile. This creep causes a strain, measured at the beginning of the tensile load test. During the analysis, it was shown that no significant development of creep during the load test was observed, but this does not mean that there was no creep present at the start of the test.

5.2.4 Difference in Displacement LVDT and Omnisens

Integrating the strain readings inside the pile up to ground level gave a different displacement than the displacement measured by the LVDT. It had been verified whether there was a mistake in the summation of the strain readings. For example, a measurement point was excluded. After verification, it was found that there was still a slight difference of 1 mm between the LVDT and Omnisens data. It is not clear what has caused this difference.

5.2.5 Proximity Performance Compression and Tensile Load Test

It was critiqued by Daatselaar (2019) that the compression and tensile load tests in the Dapperbuurt tests were performed too close to each other in time, which might have affected the results of the tensile load tests. The same can be said for piles 187 and 576: they were tested in the extended compression load test with an axial load of 80 per cent of the maximum capacity,

which could have influenced the behaviour of the pile during the tensile load test. Especially in the force development, piles 187 and 576 showed a different behaviour from piles 175 and 592: a negative force was measured in the entire pile at the start of the test, and at the end of the test still, the lower part experienced a compressive force.

5.2.6 Derivation Mobilisation Curves

The mobilisation curves of both sand layers could only be derived based on one pile. This raises questions about whether these curves can be applied in general to other timber piles. The top sand layer was pre-drilled, and most piles were too shallow in the first sand layer. This might have increased the variability in results between the piles.

5.2.7 Simulations

In the simulation of D Pile Group, it was not possible to apply a variable pile stiffness and pile geometry. This difference to the actual piles tested can have caused uncertainty in the resulting values of the simulation. Also - to match the measured curve - a different end bearing capacity was used then was calculated by Honardar (2020).

5.3 Comparison to Norms

The comparison of the calculated negative skin friction based on *NEN 9997-1 + C2* (2017) and the test results showed two exciting observations.

First, the negative skin friction calculated according to the current rules gave similar results to the test data values. The test data was slightly smaller than the NEN values but still larger than those found when the 0.25 requirement was disregarded. So the NEN is not too conservative. The uncertainty of the test results was not calculated, so the uncertainty could have caused the deviation with the NEN.

When looking at the contribution of each single soil layer to the total sum of negative skin friction, the contribution per soil layer differs between the NEN calculations and the test results calculation.

6. Conclusion and Recommendations

This chapter will explain the conclusions that were drawn during the analysis. The answers to the research questions will be discussed, followed by recommendations for further research.

6.1 Conclusion

Part of the research was to validate the applicability of the method using fibre optic sensors to timber piles. The pile displacements found by integrating the strains measured inside the pile came very close to the displacement measured by the LVDT. On average less than 1 mm of difference was found between the two types of measurement equipment. This proves that fibre optic sensors are an excellent method to measure displacements in timber piles. The averaging of strain readings filtered out the bending effect and variability of the timber piles.

The analysis of the four piles showed that the two piles containing two fibres instead of only one had the best results. During the calculation of the E modulus based on the strain readings, these piles had the highest root mean square value: between 0.97 and 0.98. The two piles with one fibre measurement had scores between 0.93 and 0.94. Also, the two piles with two fibres showed a smoother result in the force distribution. And during the calculation of the relative settlement with the integral of the strain readings, the piles with two fibres had the smallest deviation between the displacement of the LVDT and the strain readings. It is thus advised that for future tests on timber foundation piles using fibre optic sensors, at least two full loop fibres should be working.

Mobilisation curves were derived for each soil layer, then the mobilisation curves of all four piles were combined. According to the NEN 9997-1, the maximum shaft friction is expected to be mobilised at a displacement of 10 mm for driven piles. The combined mobilisation curves confirm this value: after 10 mm displacement, the maximum shaft friction was mobilised. Some curves showed an even softer response: 20 mm of displacement was needed.

The calculation of expected negative skin friction based on NEN 9997-1 and the calculated negative skin friction based on the maximum shaft frictions mobilised during the tensile load test confirmed that the tensile load test was a good method to quantify the negative skin friction to be expected. Based on the comparison, it was shown that using 0.25 for the $K_{0,j,k} * \tan(\delta_{j,k})$ term overestimates the negative skin friction. From the test data, an average factor of 0.22 was found, with a range of 0.21 to 0.23.

The literature mentioned that a lower modulus of elasticity is expected in the pile tip since this part of the pile mainly consists of young timber. The compression load tests in the timber laboratory of TU Delft confirmed this since a reduction of 2 to 7 GPa stiffness was observed between the pile head and pile tip for the piles tested. The tests in the timber laboratory also showed that using an E modulus based on strain readings in the top of the pile creates uncertainty in the further analysis of the pile, especially for the lower parts. Thus in the further study, the measured E moduli were applied.

Using the measured pile stiffness instead of the calculated stiffness for calculating alpha factors changed the alpha values significantly. In some cases, the value increased; in others, the value decreased. It is thus essential to use the measured pile stiffness if available since it will otherwise result in a false representation of the pile.

The pile test history has made the interpretation of the test results complex. Drawing conclusions

on negative skin friction based on four piles tested in tension is feasible. Still, two piles were tested in compression at 80 per cent of their maximum bearing capacity just two months before the tensile load test. The absence of one fibre in two piles has complicated the interpretation and imposed uncertainties.

6.2 Evaluation of Research Questions

At the start of the thesis, the main research question with sub research questions was established. This section will discuss the conclusions that can be drawn for each question.

6.2.1 Accuracy current pile design methods in determining the bearing capacity of timber piles

Both the test data and simulation results gave values of negative skin friction that were close to the value found with the current pile design method. The calculation of negative skin friction in the current pile design methods is thus accurate; only the 0.25 requirement could overestimate the expected negative skin friction. Based on the test data an average factor of 0.22 was calculated, with a range of 0.21 to 0.23.

6.2.2 Influence tapering on soil stresses around pile

Based on the comparison of alpha factors found during the compression and tensile loads tests, it cannot be concluded whether tapering influences the shaft friction. The assumption was that during a tensile load test, a tapered pile would experience less friction, and thus a smaller alpha factor would be found compared to the alpha factor derived from the compression load test. The results confirmed a smaller alpha factor from the tensile load test for six of the eight comparisons based on relative strains and only three of the eight comparisons based on absolute strains. This would imply an influence of the tapering. Still, since not all soil layers confirmed this, more tensile load tests should be performed first before it can be stated that tapering influences the shaft friction mobilised around a timber pile.

6.2.3 Influence of variation in E-modulus over the length of the pile on the interpretation of measurement data

Before the results of the timber laboratory were available, the piles were assigned a constant E modulus, which was based on the strain readings of a section in the pile. The timber laboratory test results showed an average reduction of 32 % in stiffness in the bottom part compared to the top part. This means that by analysing the test data based on the calculated E modulus, especially in the lower part of the pile, a stiffer response is assumed than is the case. And this means that consequently, the calculated shaft friction along the pile is overestimated.

Using one single value for the stiffness of the pile, thus, in the end, will result in a more significant negative skin friction than is expected to occur.

6.3 Recommendations

It was mentioned in the literature that most of the bridges included in the research 'Programma Bruggen en Kademuren' were reinforced over the years, meaning foundation piles are relatively close to one another. Since it was also discussed in the literature that this group effect might have a beneficial influence on the total negative skin friction experienced by one single pile, it is worth further investigating what effect the group effect might have on the bridges in Amsterdam. It is also worth exploring if negative skin friction develops differently around a slanted foundation pile.

Preliminary research of Gemeente Amsterdam showed that bridges built after 1880 have timber foundation piles that are driven deeper into the load-bearing sand layer than was up until now assumed by Gemeente Amsterdam. This has a positive effect on the bearing capacity of the pile since the tip resistance will increase, and more shaft resistance can be developed in the bearing sand layer. But also, more negative skin friction might be present. By placing the piles deeper in the bearing sand layer and testing again, a better mobilisation curve for this load-bearing sand layer can be created. Based on the current tensile load test on four piles, it was only possible to develop a mobilisation curve based on the data of pile 592, since this was the only pile driven deep enough for good recording of the shaft friction in the first sand layer.

To disregard the pile test history - and the complexity it has caused on the test result interpretation -, tensile load tests should be performed on instrumented timber piles that were not tested before. Primarily extended compression load tests should not be performed shortly before the tensile load test since it was shown in the analysis that this might have caused deviations in the test results.

Bibliography

Bersan, Silvia et al. (2018). “Distributed strain measurements in a CFA pile using high spatial resolution fibre optic sensors”. In: *Engineering Structures* 160, pp. 554–565.

Borello, Daniel J et al. (2010). “Experimental and analytical investigation of bridge timber piles under eccentric loads”. In: *Engineering structures* 32.8, pp. 2237–2246.

Daatselaar, Floor van (2019). “The Geotechnical Bearing Capacity of Old Timber Piles”. In:

De Gans, W (2011). “De bodem onder Amsterdam: Een geologische stadswandeling”. In:

Fellenius, Bengt H (1984). “Negative skin friction and settlement of piles”. In: *Proceedings, 2nd International Seminar—Pile Foundations, Nanyang Technological Institute, Singapore*.

– (2002). “Determining the true distributions of load in instrumented piles”. In: *Deep Foundations 2002: An International Perspective on Theory, Design, Construction, and Performance*, pp. 1455–1470.

Honardar, Siavash (2020). “Geotechnical Bearing Capacity of Timber Piles in the City of Amsterdam: Derivation of bearing capacity prediction factors based on static load tests conducted on instrumented timber piles”. In:

Kong, Gangqiang et al. (2013). “Mathematical model and analysis of negative skin friction of pile group in consolidating soil”. In: *Mathematical Problems in Engineering* 2013.

Korff, Mandy (2013). *Response of piled buildings to the construction of deep excavations*. Vol. 13. IOS Press.

Leung, CF (2009). “Negative skin friction on piles”. In: *Indian Geotechnical Conference*, pp. 827–836.

NEN 9997-1 + C2 (2017). Normcommissie 351 006 ’Geotechniek’.

NPR 7201 (2017). Normcommissie 351 006 ’Geotechniek’.

Pagella, Giorgio (2021). *Determination of geometry and stiffness of 6 wooden foundation piles (Container 235) equipped with optic fibers*. Tech. rep. TU Delft.

Programmaplan Bruggen en Kademuren (2020). Gemeente Amsterdam.

Richtlijn Houten Paalfunderingen onder gebouwen (2016). F30/SBRCURnet.

Ruifu, Shen (2008). “Negative skin friction on single piles and pile groups”. In:

Spruit, Rodriaan (2020). *Feitenrapportage proefbelastingen op houten palen*. Tech. rep. Ingenieursbureau Gemeente Rotterdam.

Appendices

A. Soil Investigation

Around every pile, three Cone Penetration Tests were performed. These three tests were averaged to find the soil properties and soil boundary layers. This section shows the CPT information that is used for the further analysis of the test data.

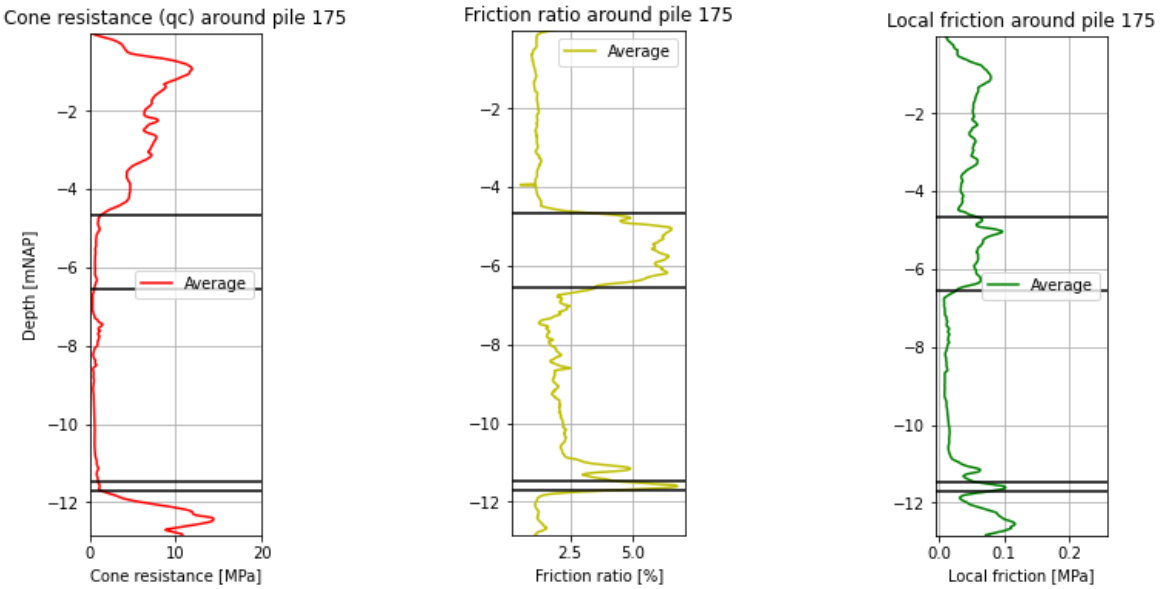

Figure A.1: Parameters from CPT of pile 175

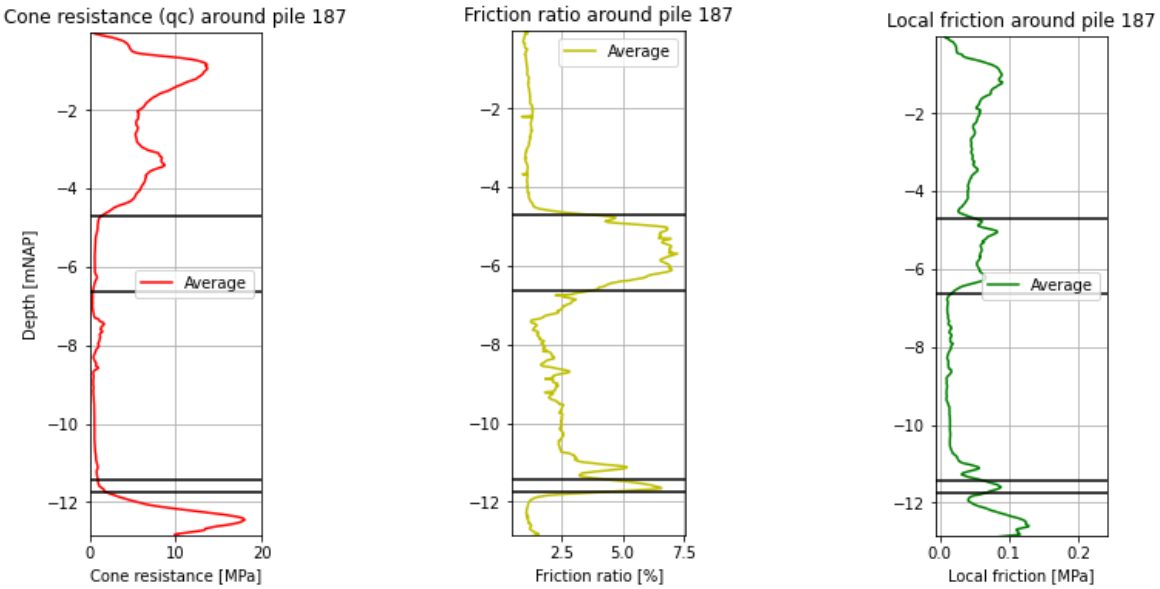

Figure A.2: Parameters from CPT of pile 187

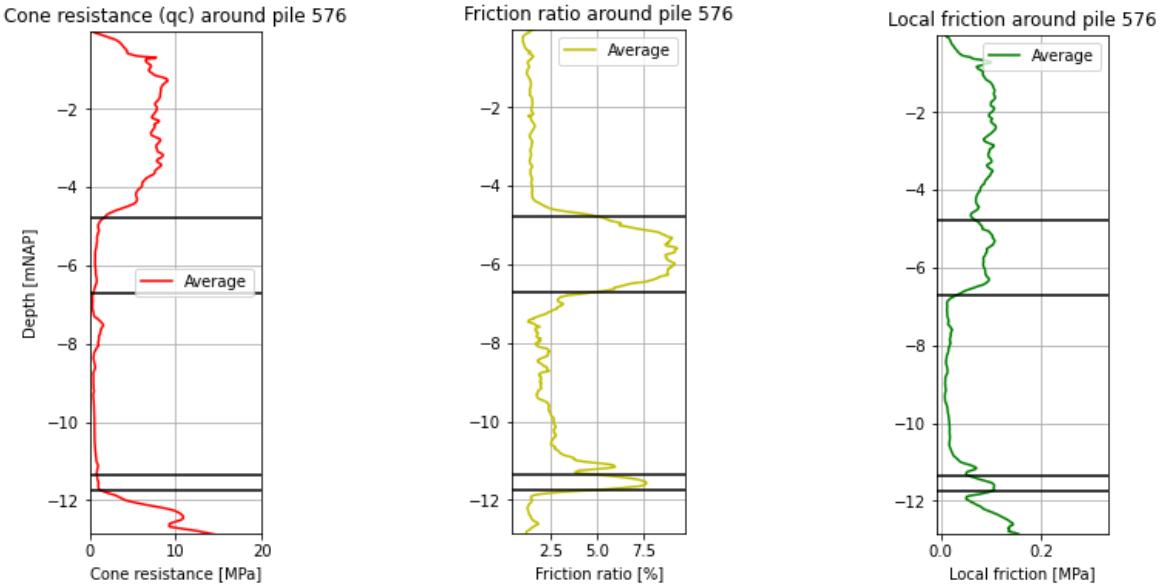

Figure A.3: Parameters from CPT of pile 576

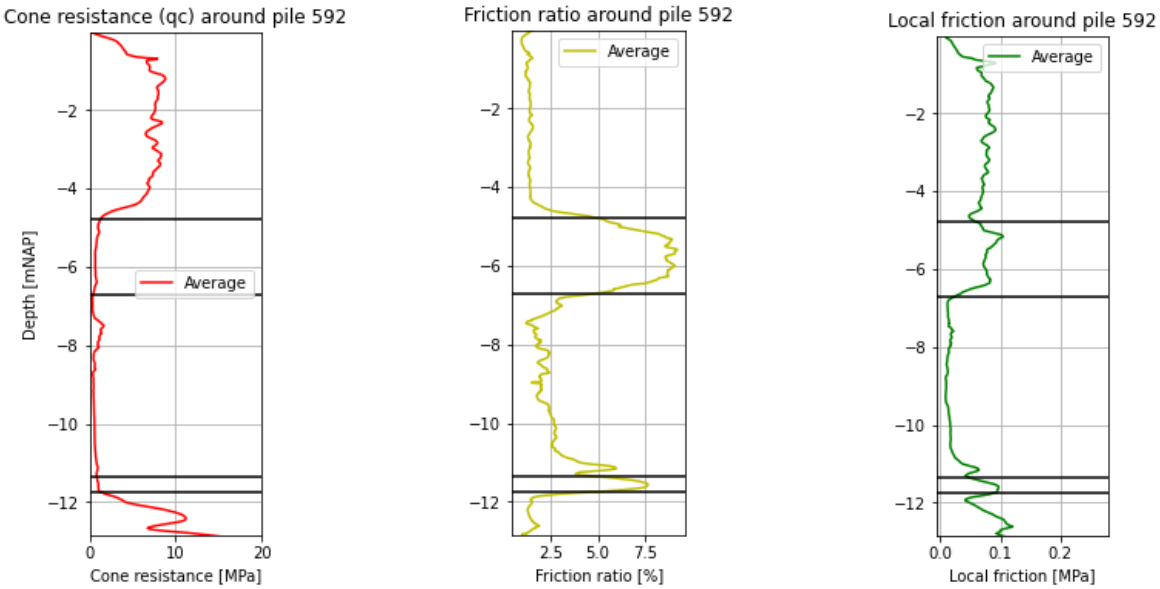

Figure A.4: Parameters from CPT of pile 592

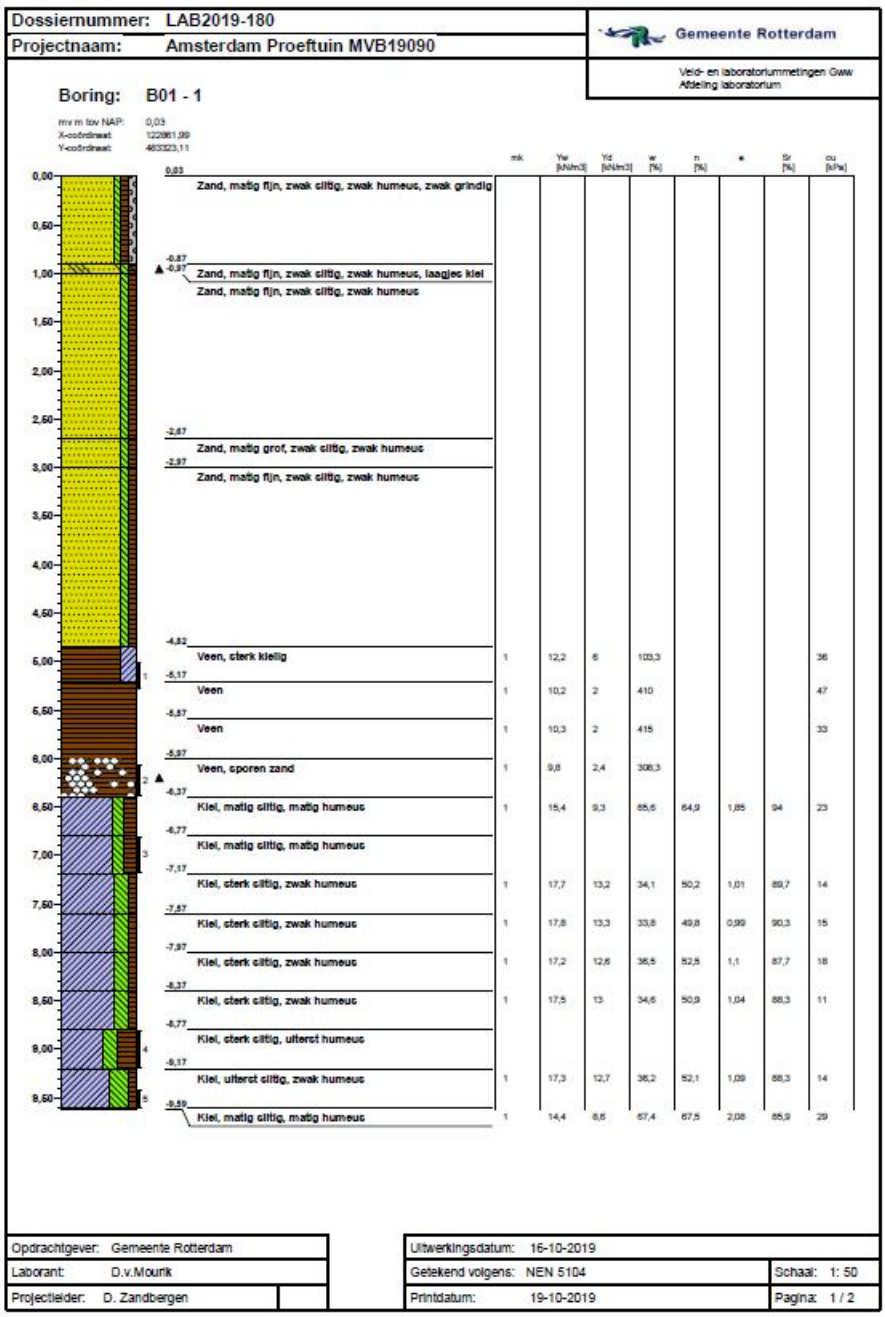

Figure A.5: Boring Overamstel site - part 1

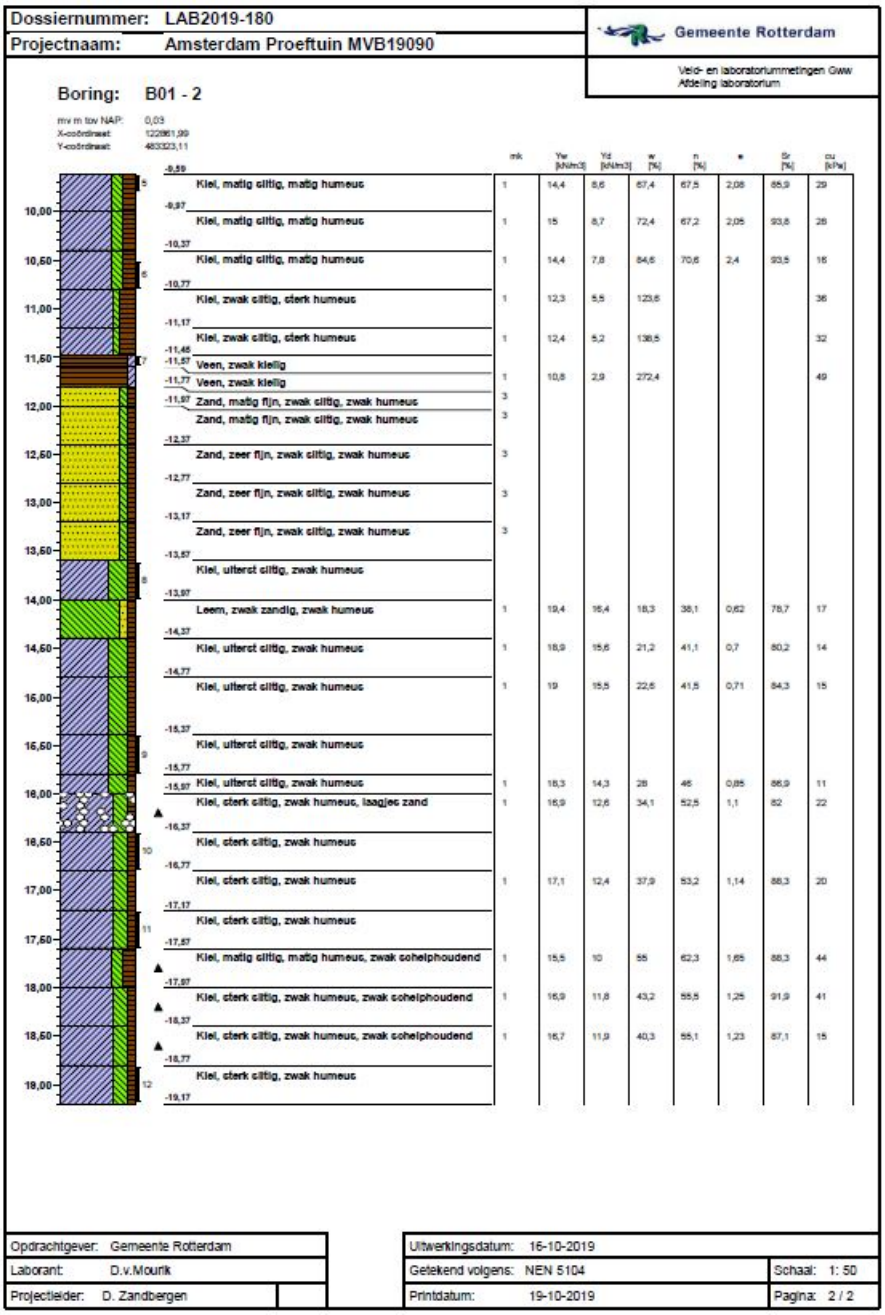

Figure A.6: Boring Overamstel site - part 2

A.1 Schematization Piles

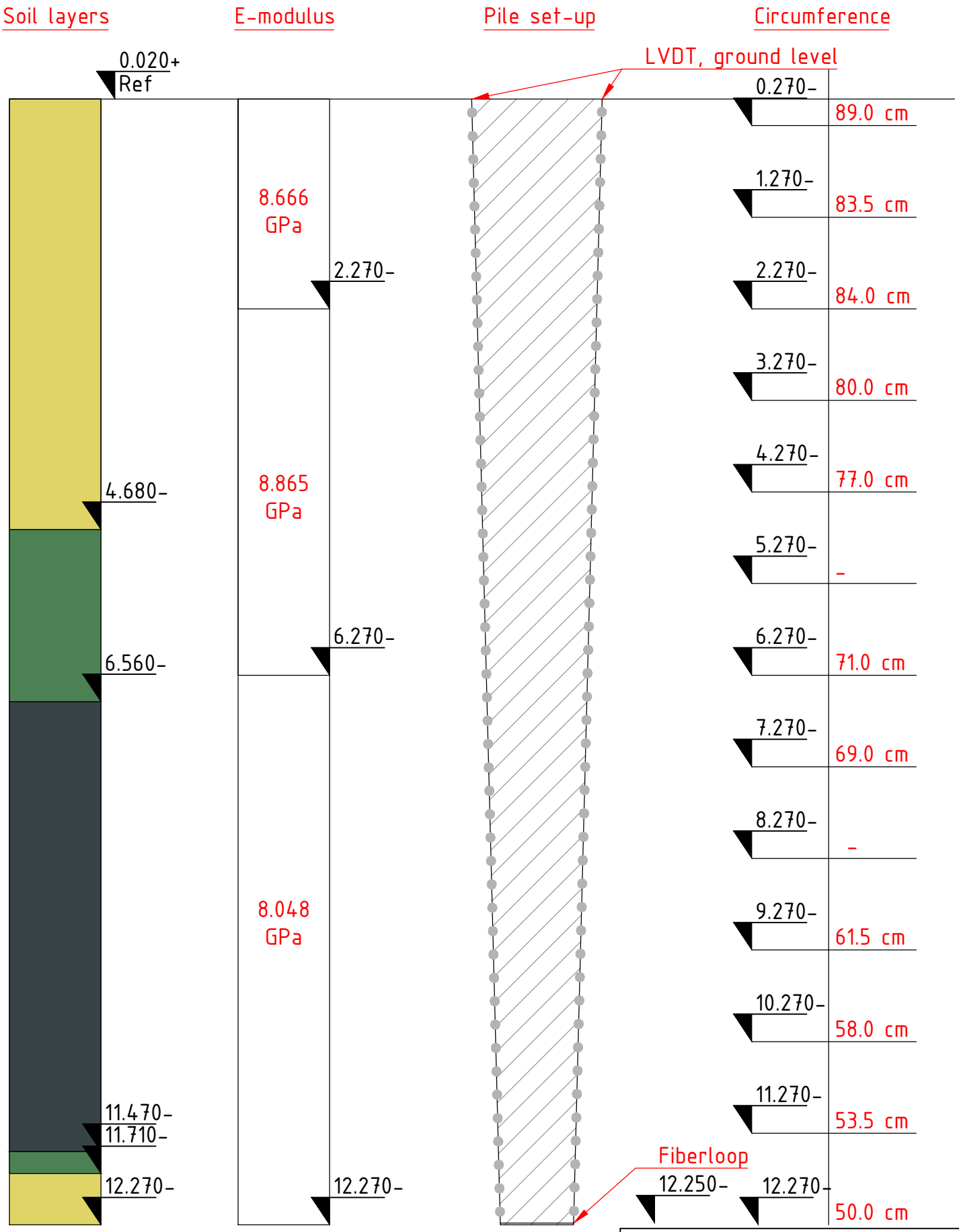

Title: Schematization Pile Analysis	
Pile nr	175
Fibre	North-South

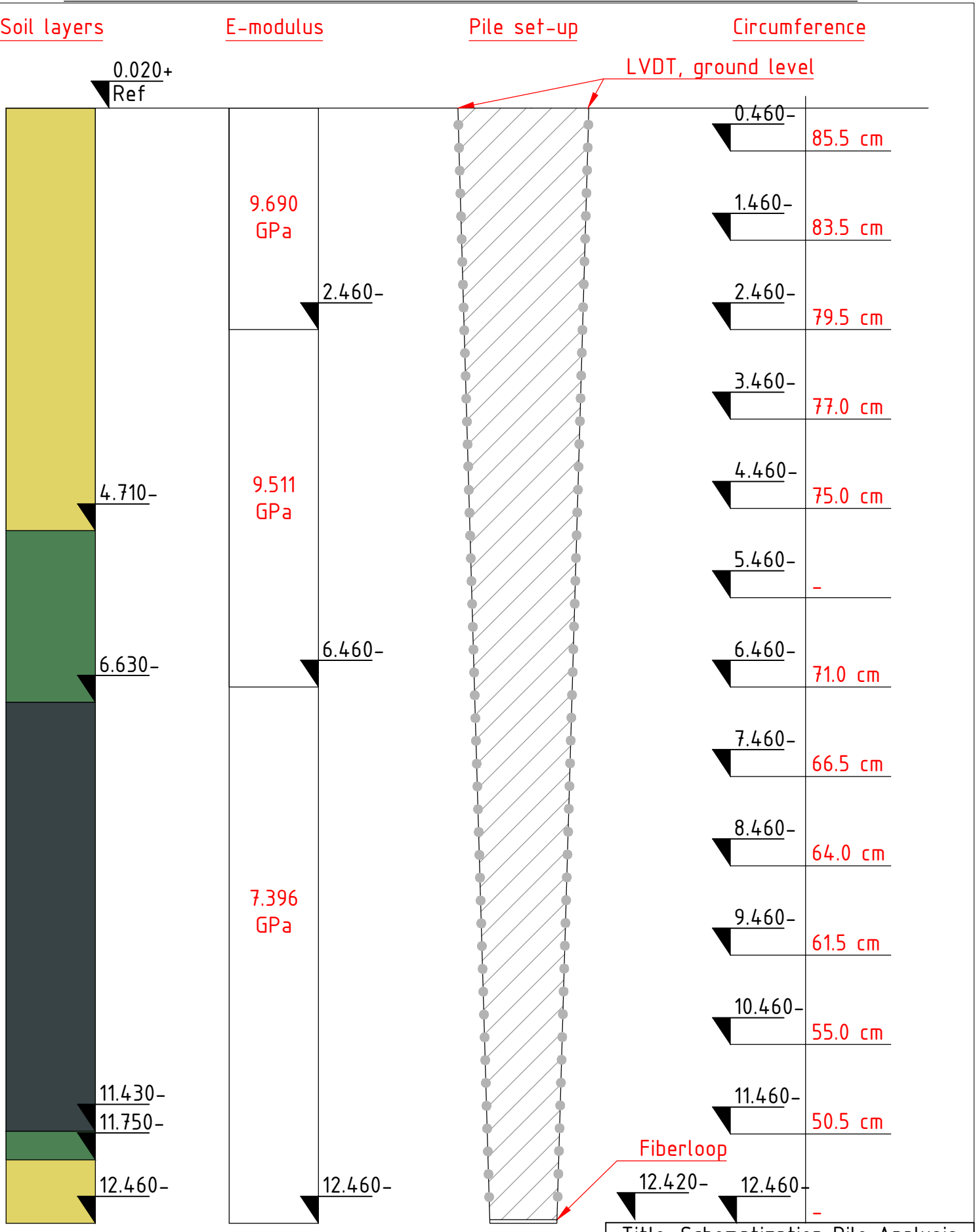

Title: Schematization Pile Analysis	
Pile nr	187
Fibre	East-West

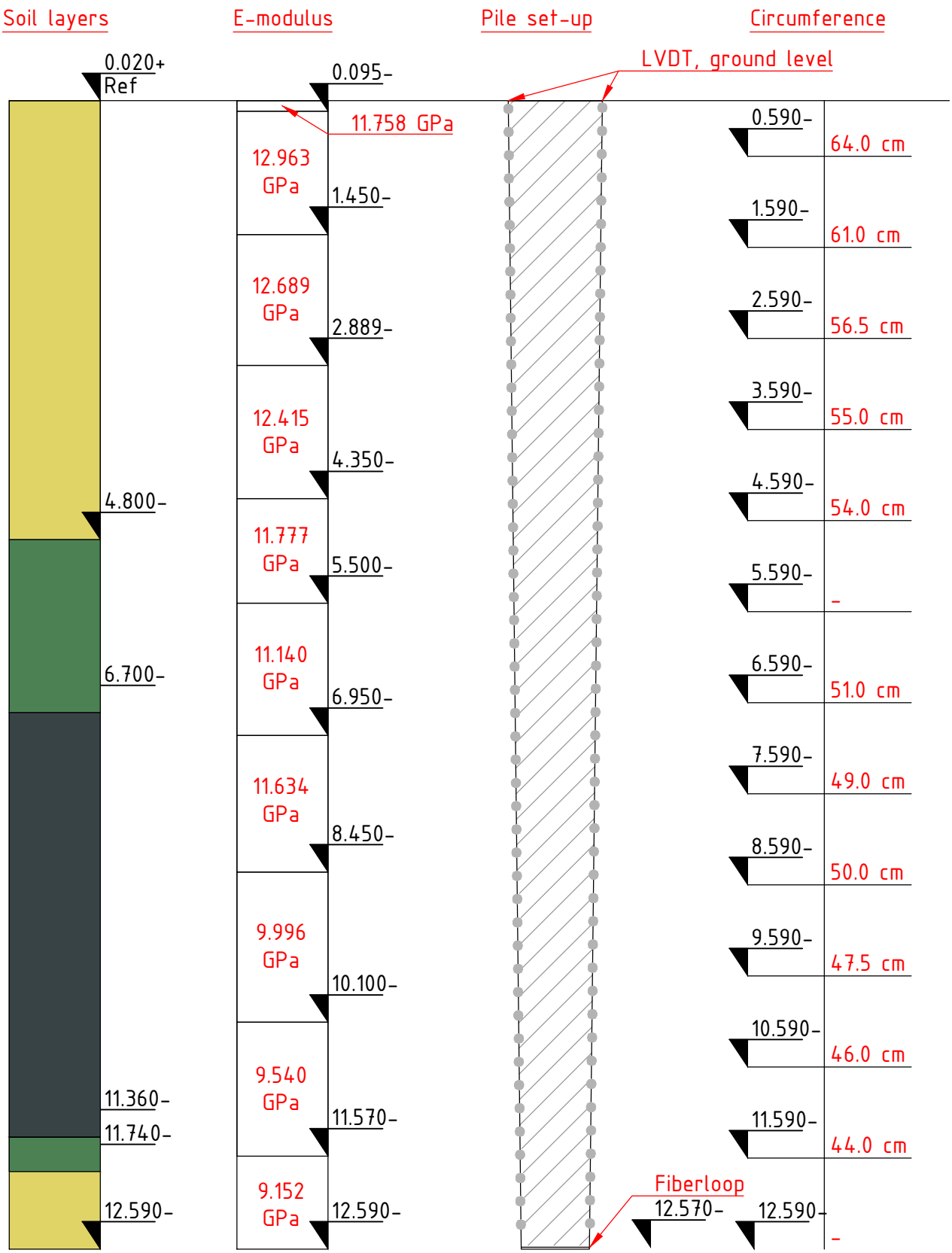

Title: Schematization Pile Analysis	
Pile nr	576
Fibre	North-South

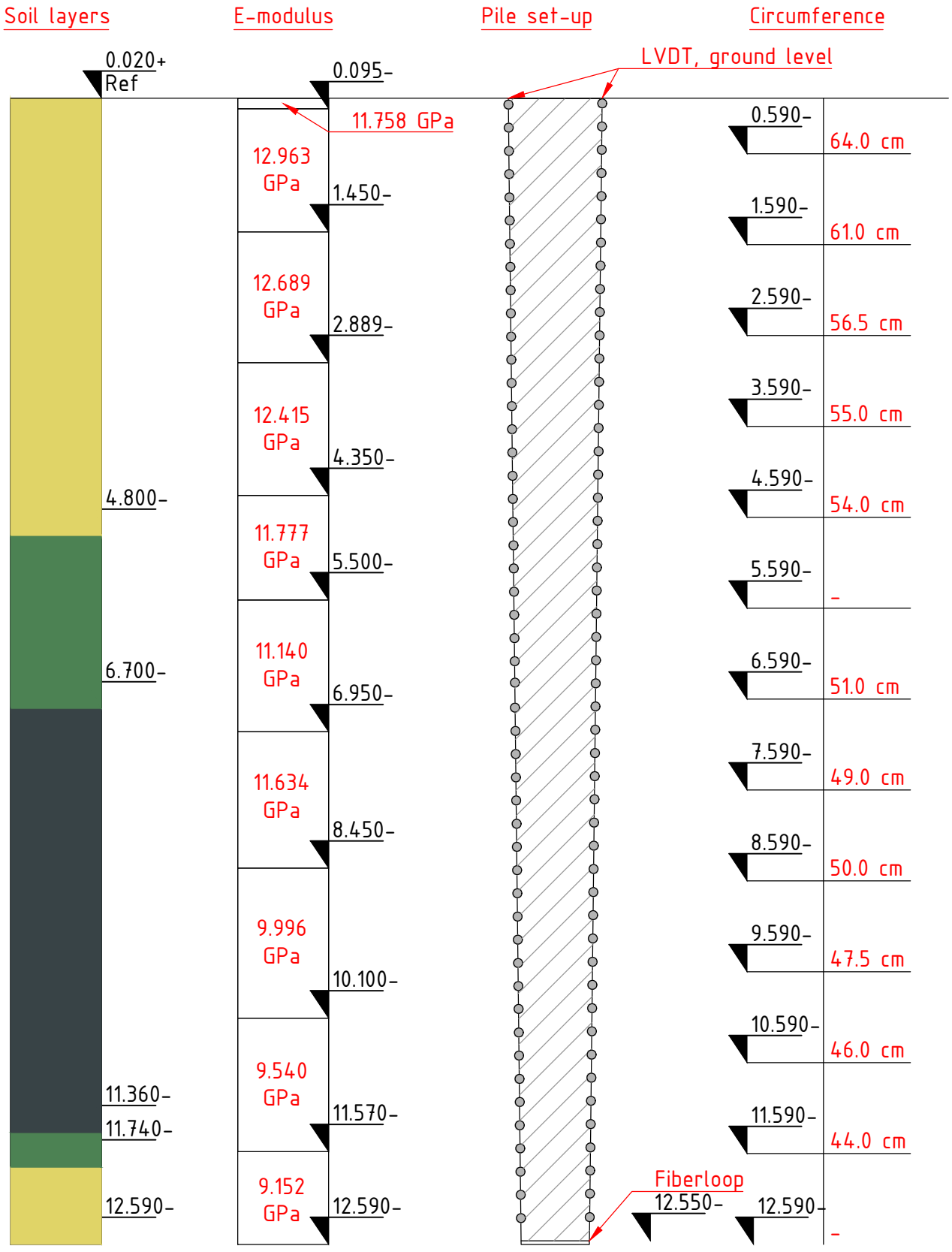

Title: Schematization Pile Analysis	
Pile nr	576
Fibre	East-West

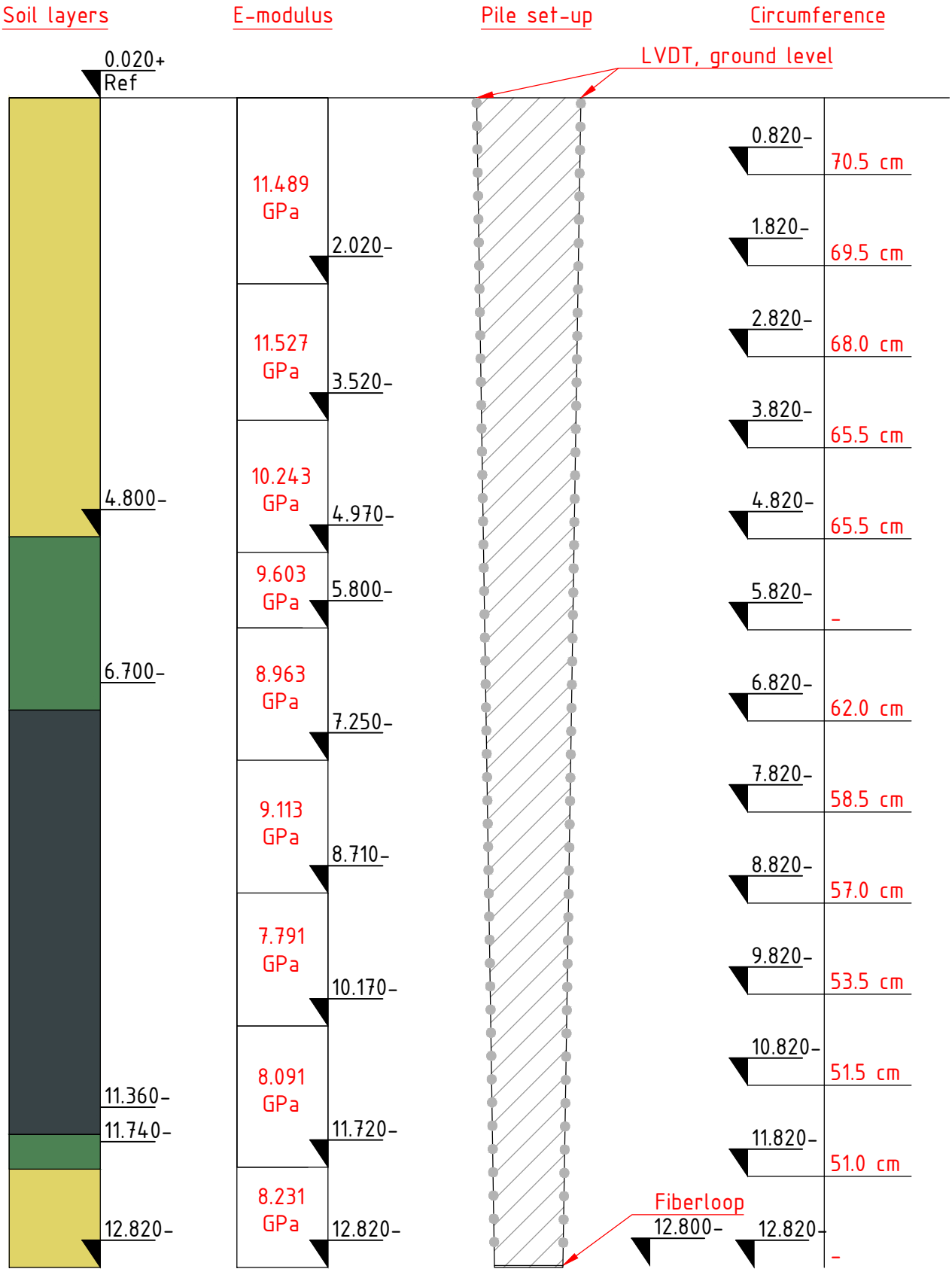

Title: Schematization Pile Analysis	
Pile nr	592
Fibre	North-South

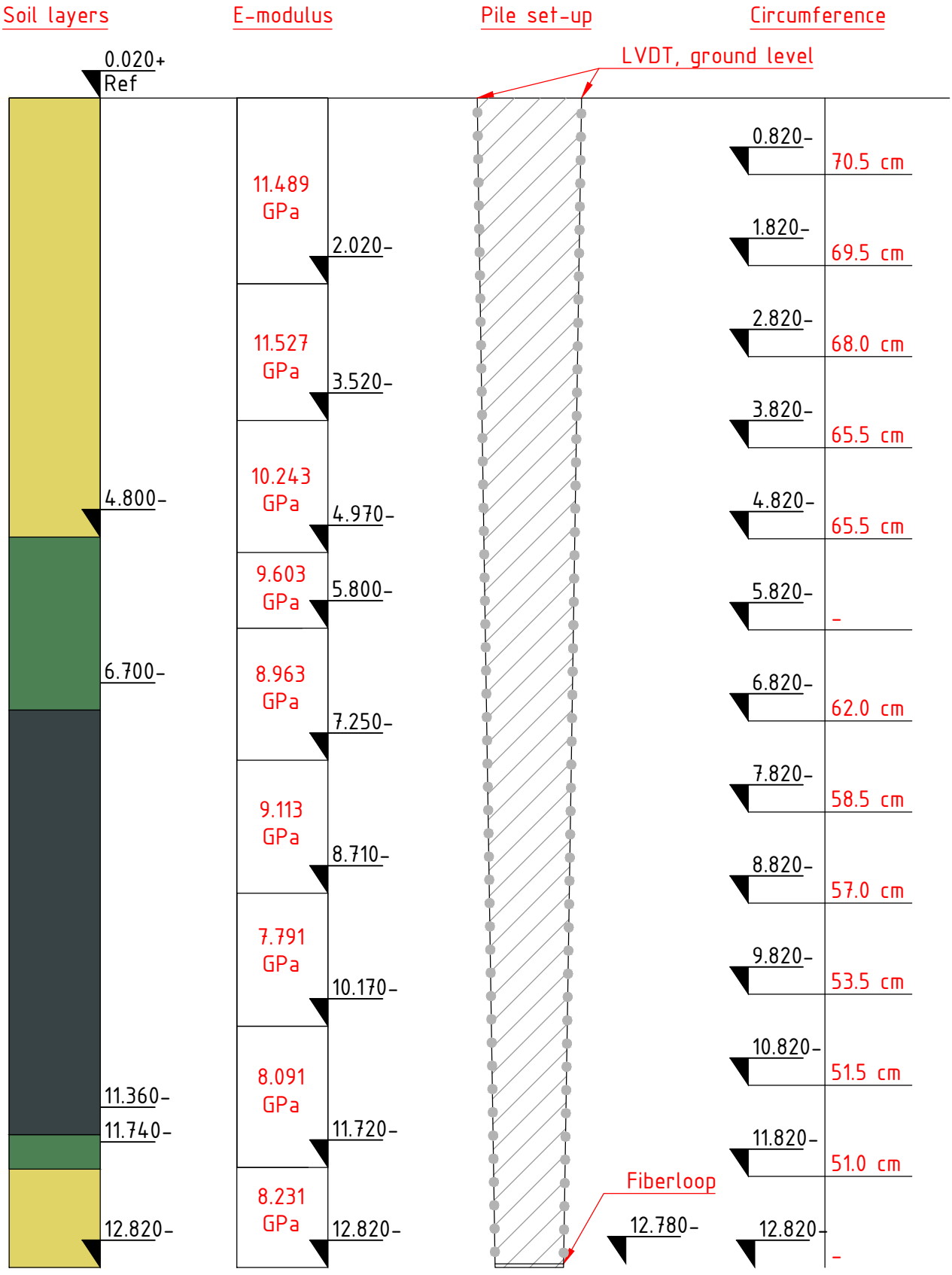

Title: Schematization Pile Analysis	
Pile nr	592
Fibre	East-West

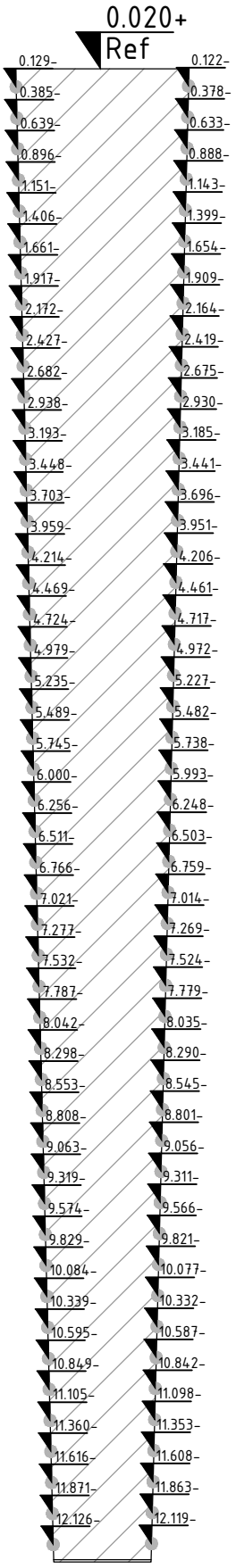

Title: Location Measurement Points	
Pile nr	175
Fibre	North-South

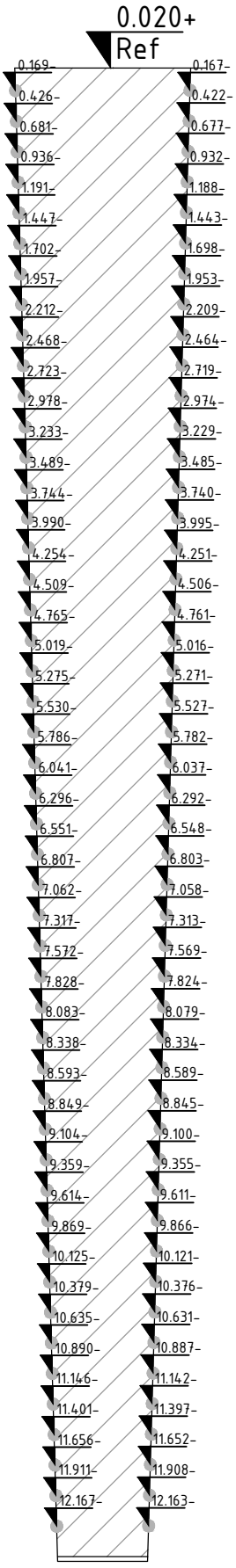

Title: Location Measurement Points	
Pile nr	187
Fibre	East-West

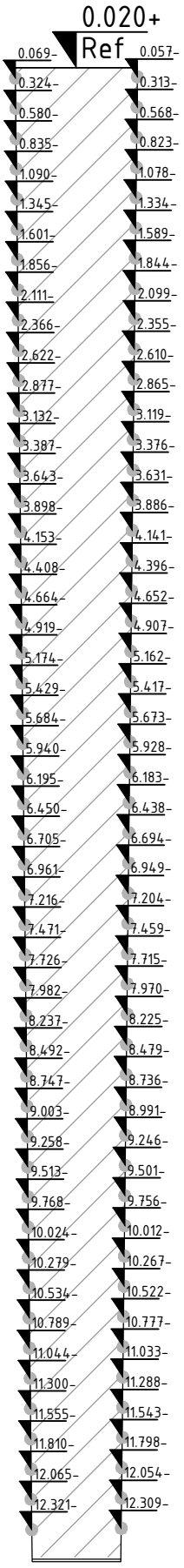

Title: Location Measurement Points	
Pile nr	576
Fibre	North-South

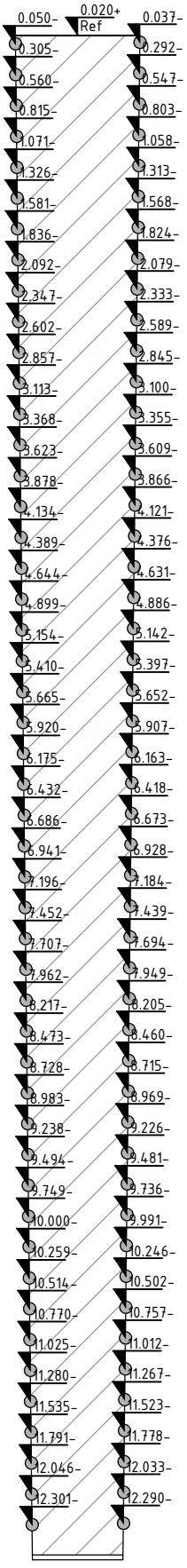

Title: Location Measurement Points	
Pile nr	576
Fibre	East-West

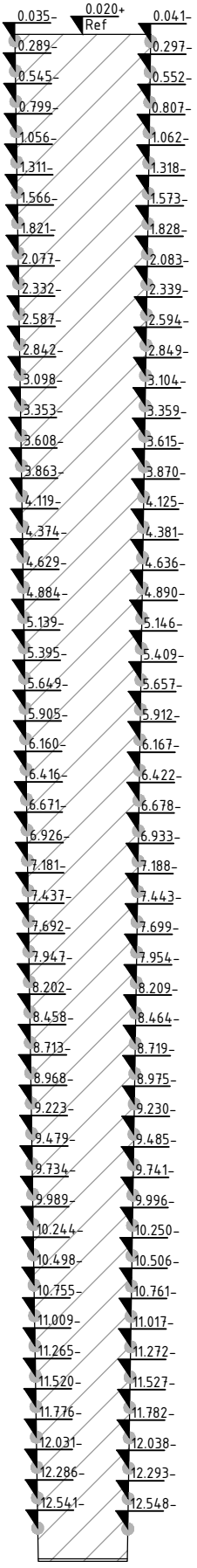

Title: Location Measurement Points	
Pile nr	592
Fibre	North-South

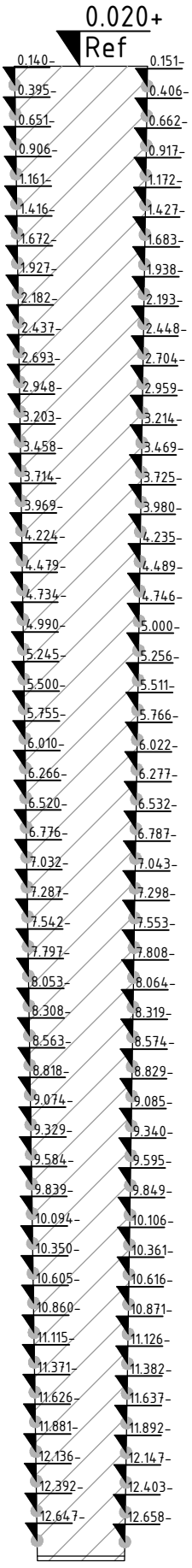

Title: Location Measurement Points	
Pile nr	592
Fibre	East-West

B. Reference measurements

This section shows the strain distributions from the reference measurements. These reference measurements were used to subtract the strain already present in the pile from the absolute strain readings.

In pile 175 the location of the loop was calibrated on the first reference test on July 16. The average strain of the test on July 17 was subtracted from the absolute strain readings of the tensile load test. The loop location was assumed to be at the same location as during the test on July 16.

In pile 187 the loop location is calibrated based on the test of July 15: the average strain of the test on July 12 is subtracted from the absolute test strain readings.

In both fibers of pile 576 the loop location is calibrated on the test of July 15: the average strains of the test on July 12 are then subtracted from the absolute test strain readings.

The loop location of both fibers of pile 592 are calibrated on the test on July 1st. Then the average strain of the test on July 15 was subtracted from the absolute test strain readings.

B.1 Pile 175

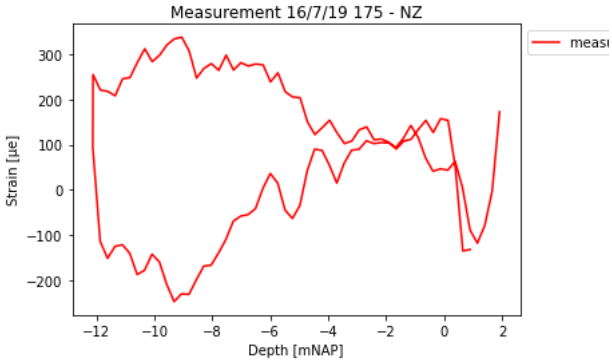

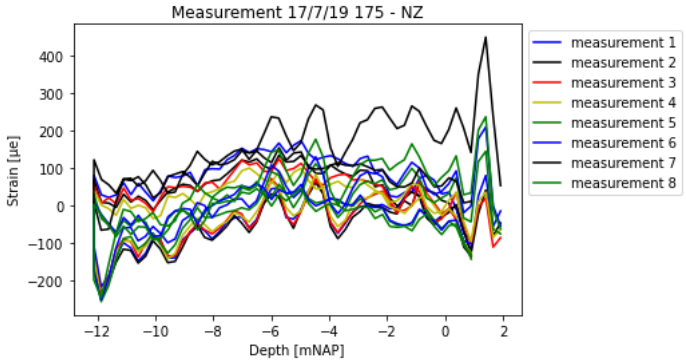

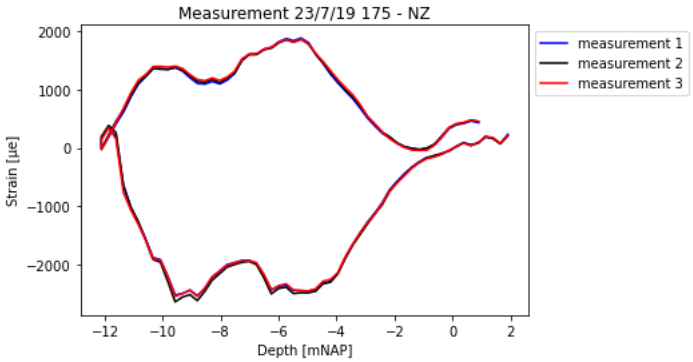

B.2 Pile 187

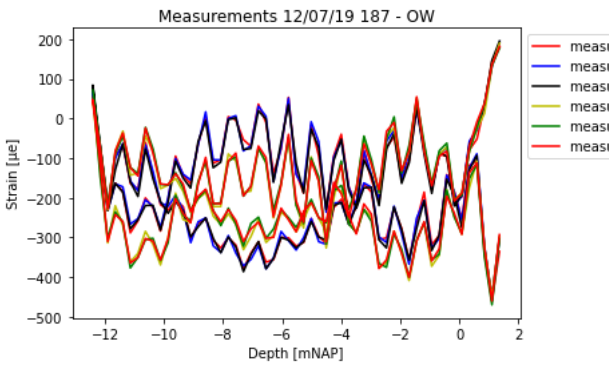

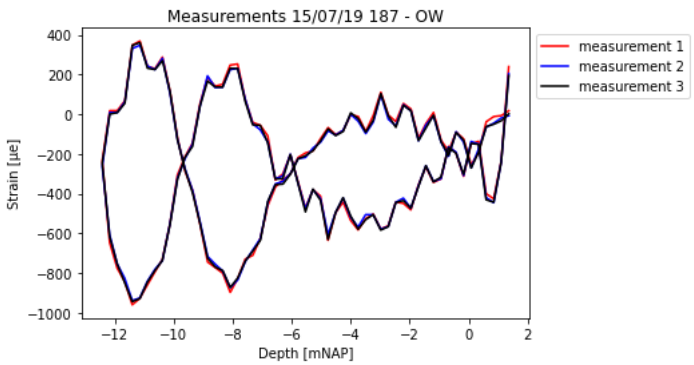

B.3 Pile 576

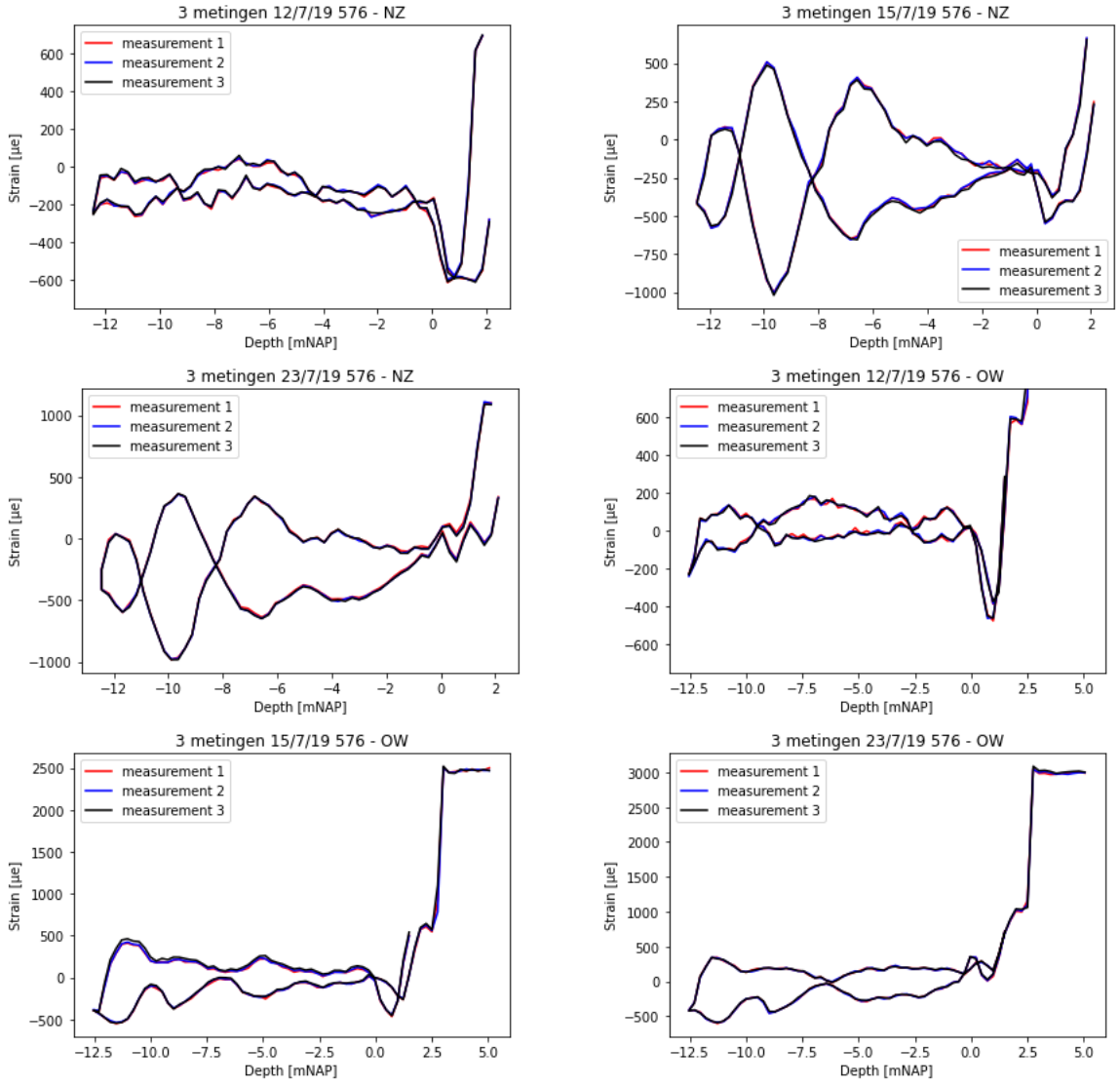
3 metingen 12/7/19 576 - NZ
3 metingen 15/7/19 576 - NZ
3 metingen 23/7/19 576 - NZ
3 metingen 12/7/19 576 - OW
3 metingen 15/7/19 576 - OW
3 metingen 23/7/19 576 - OW
measurement 1
measurement 2
measurement 3
Strain [µε]
Depth [mNAP]

B.4 Pile 592

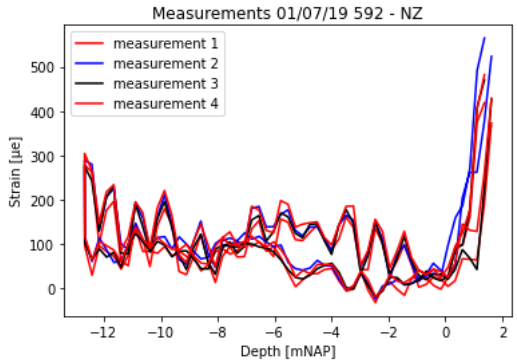
Measurements 01/07/19 592 - NZ
measurement 1
measurement 2
measurement 3
measurement 4
Strain [µe]
Depth [mNAP]

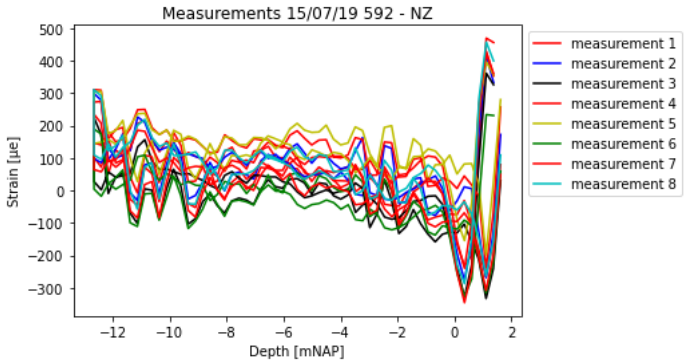
Measurements 15/07/19 592 - NZ
measurement 1
measurement 2
measurement 3
measurement 4
measurement 5
measurement 6
measurement 7
measurement 8
Strain [µe]
Depth [mNAP]

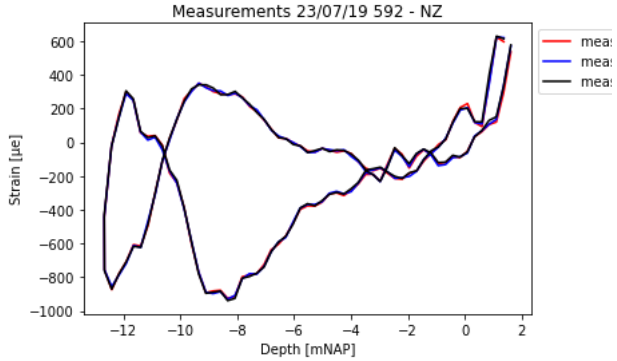
Measurements 23/07/19 592 - NZ
Strain [µe]
Depth [mNAP]

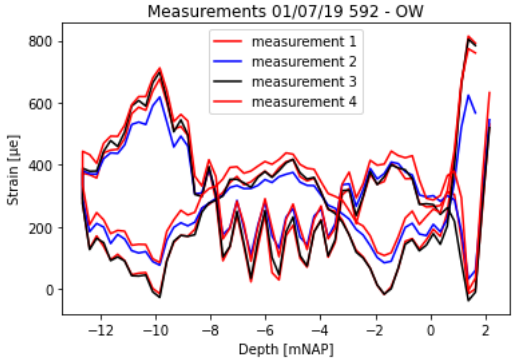
Measurements 01/07/19 592 - OW
measurement 1
measurement 2
measurement 3
measurement 4
Strain [µe]
Depth [mNAP]

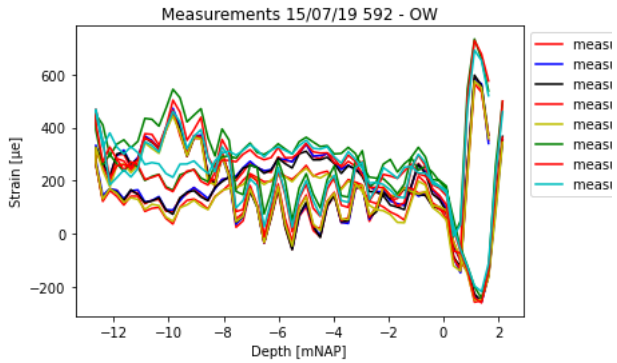
Measurements 15/07/19 592 - OW
Strain [µe]
Depth [mNAP]

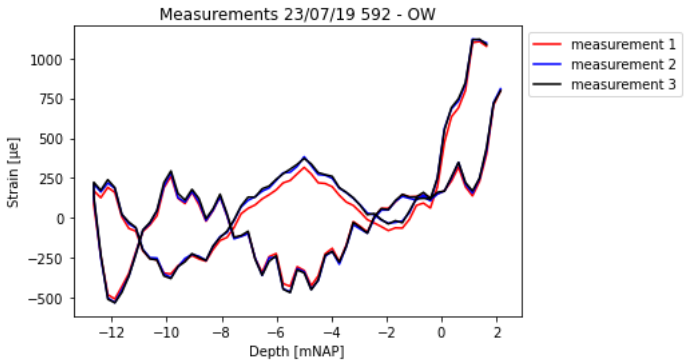
Measurements 23/07/19 592 - OW
measurement 1
measurement 2
measurement 3
Strain [µe]
Depth [mNAP]

C. Comparison Force Development with different E modulus

This section illustrates the difference in force distribution through the pile when the calculated E modulus is used, and when the results from the timber laboratory are used.

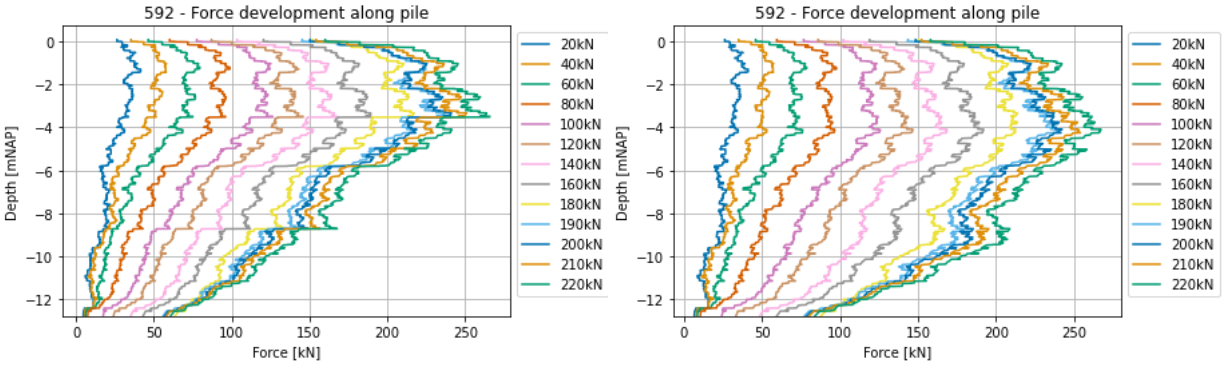

Figure C.1: 576 - Comparison in Force developments

Figure C.1 shows the difference in force distribution through pile 592 when a variable E modulus - found in the timber laboratory - is used (left), and when a calculated E modulus is assigned to the entire pile (right). The biggest difference is the response in the soft layers: the derived shaft friction was first overestimated.

D. Mobilisation Curves per Pile

D.1 Pile 175 - Absolute Strains

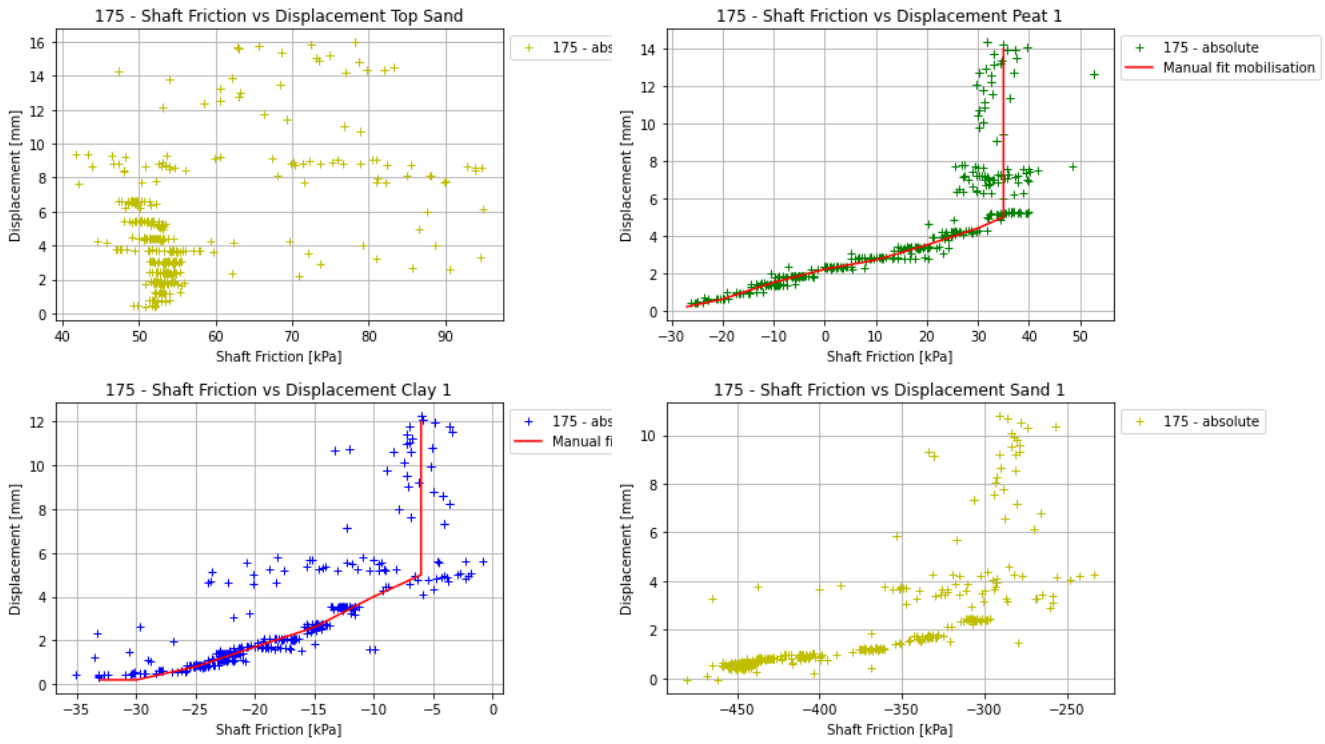

D.2 Pile 175 - Relative Strains

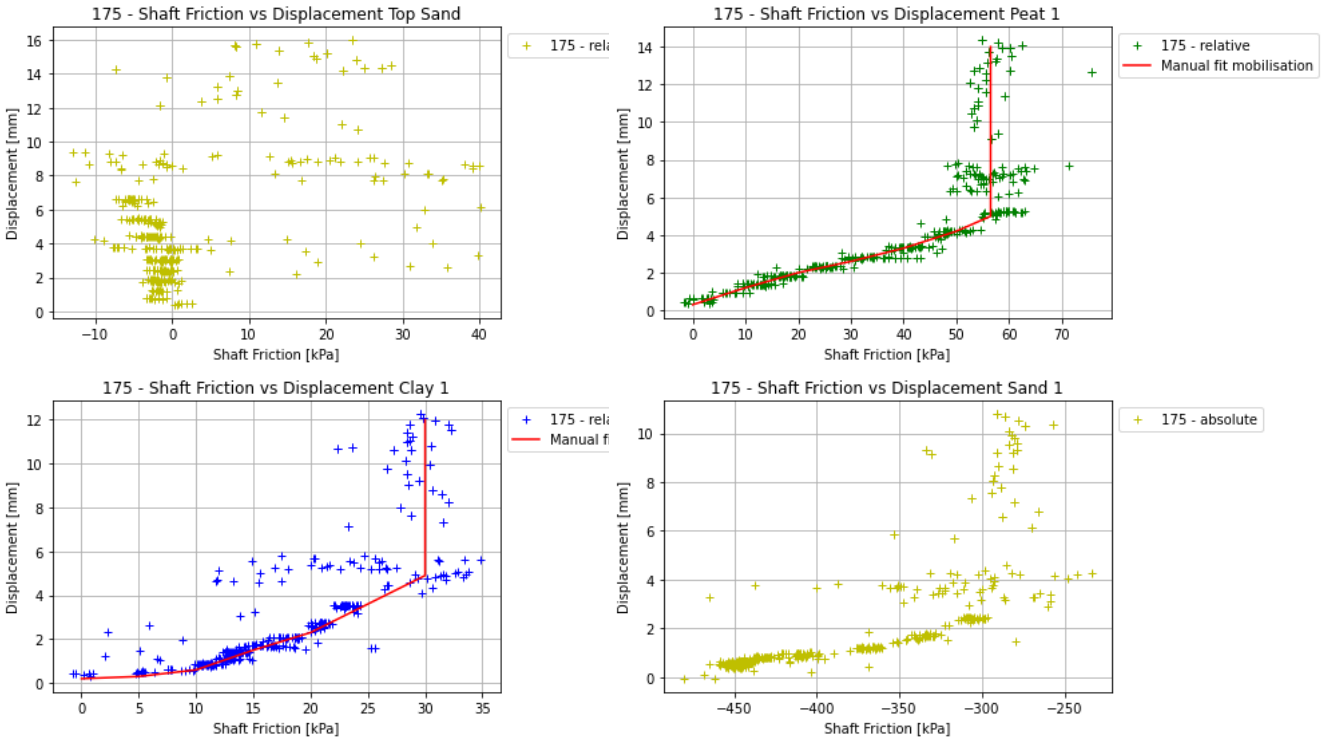

D.3 Pile 187 - Absolute Strains

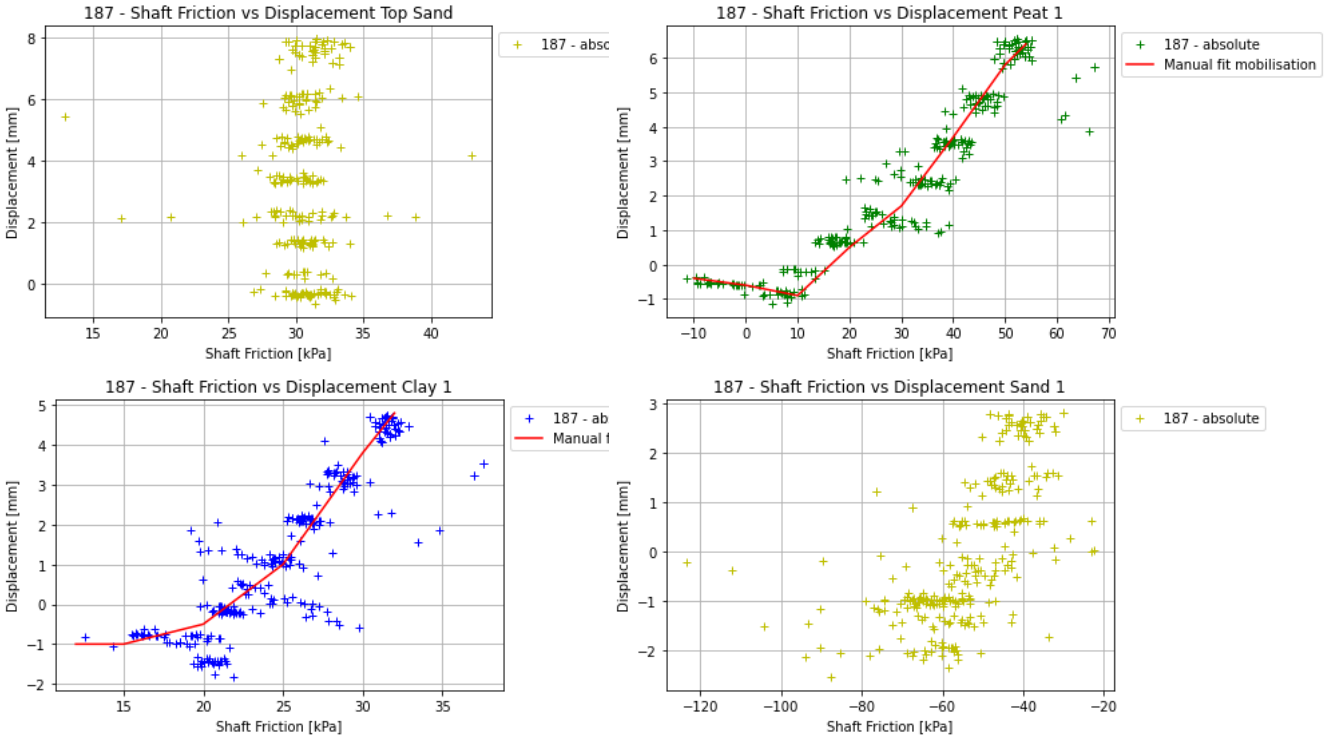

D.4 Pile 187 - Relative Strains

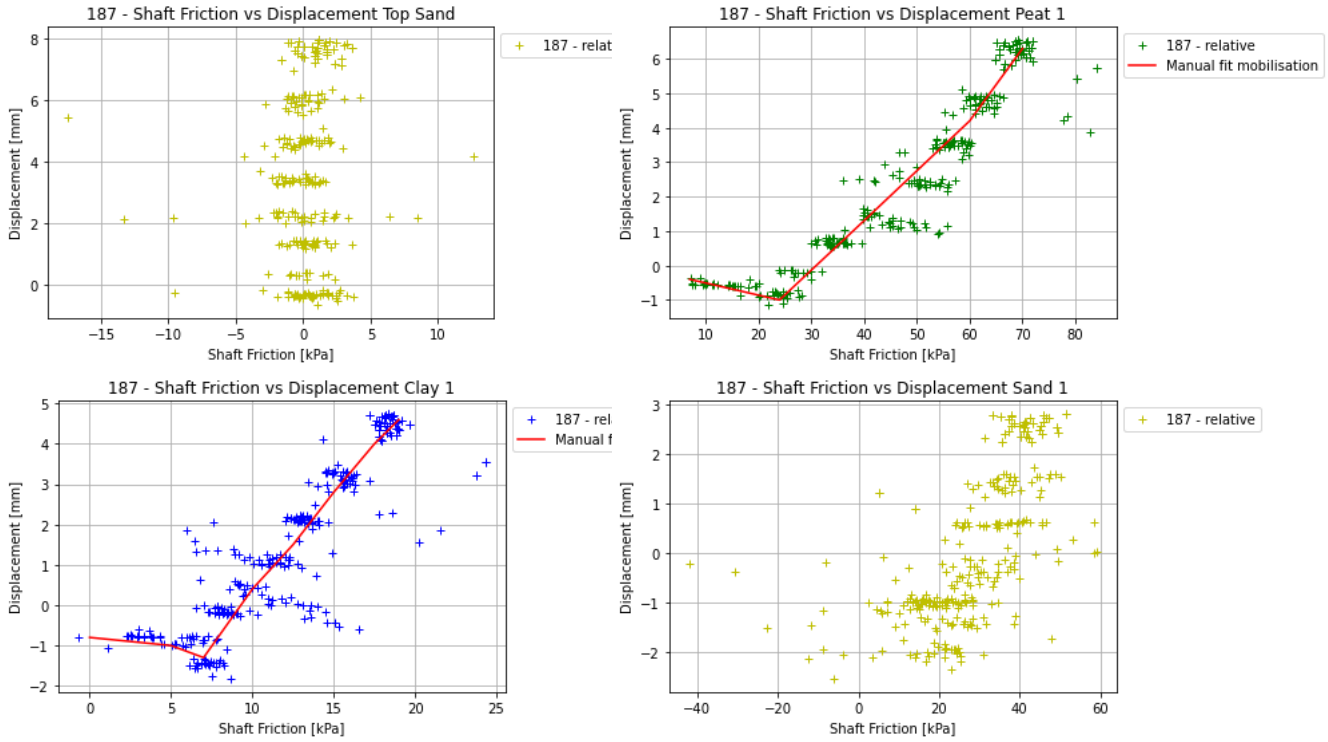

D.5 Pile 576 - Absolute Strains

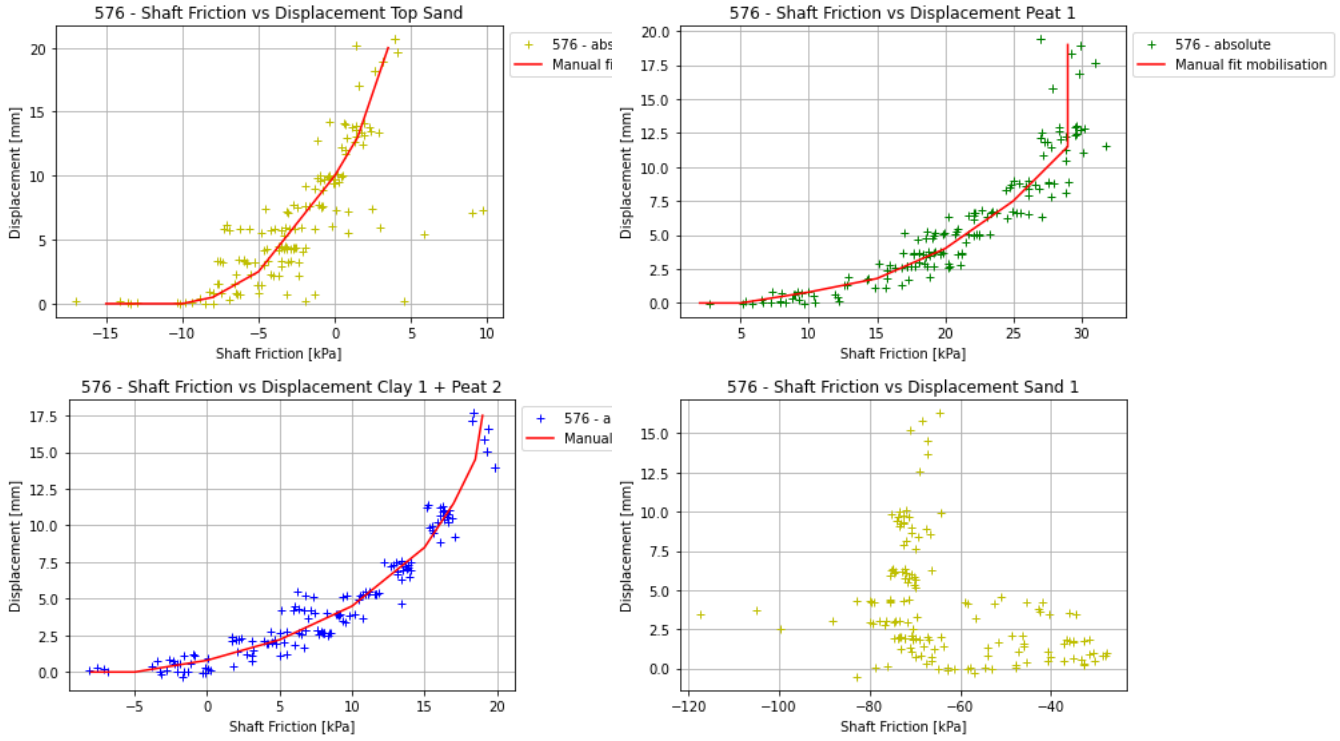

D.6 Pile 576 - Relative

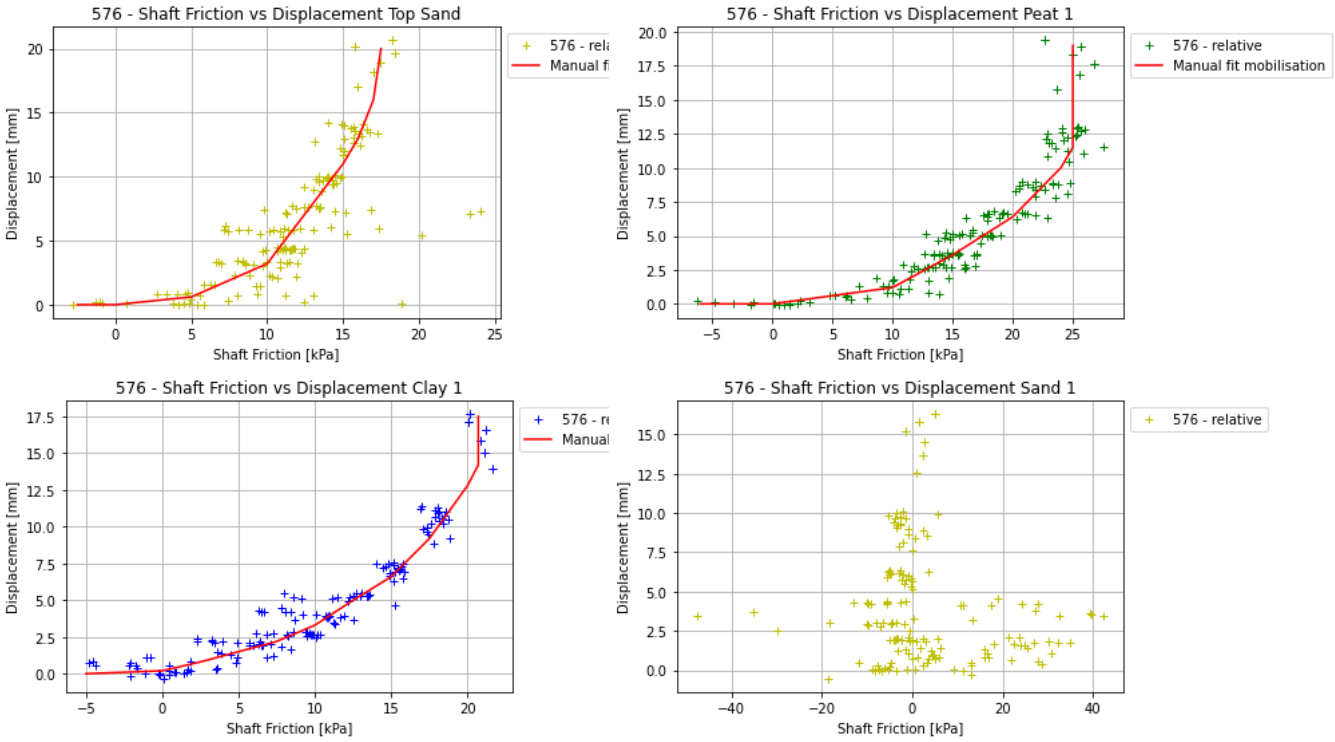

D.7 Pile 592 - Absolute Strains

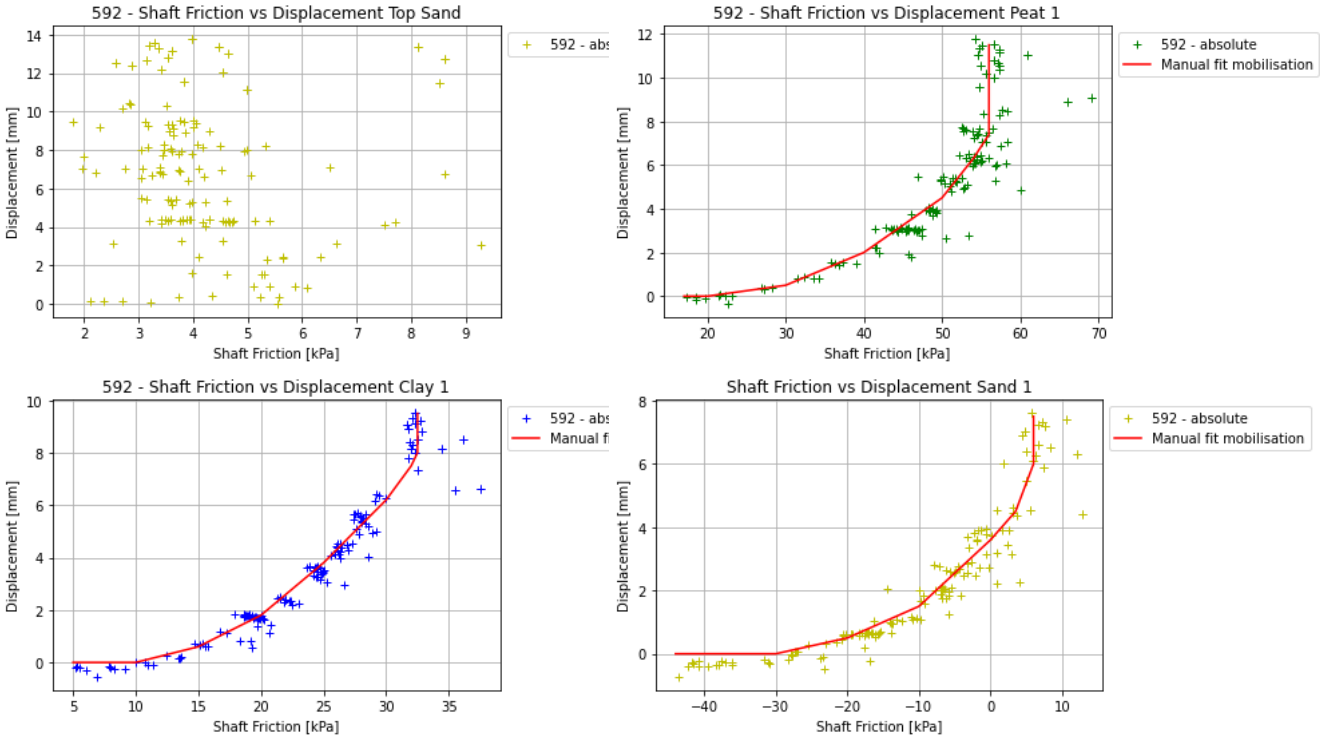

D.8 Pile 592 - Relative Strains

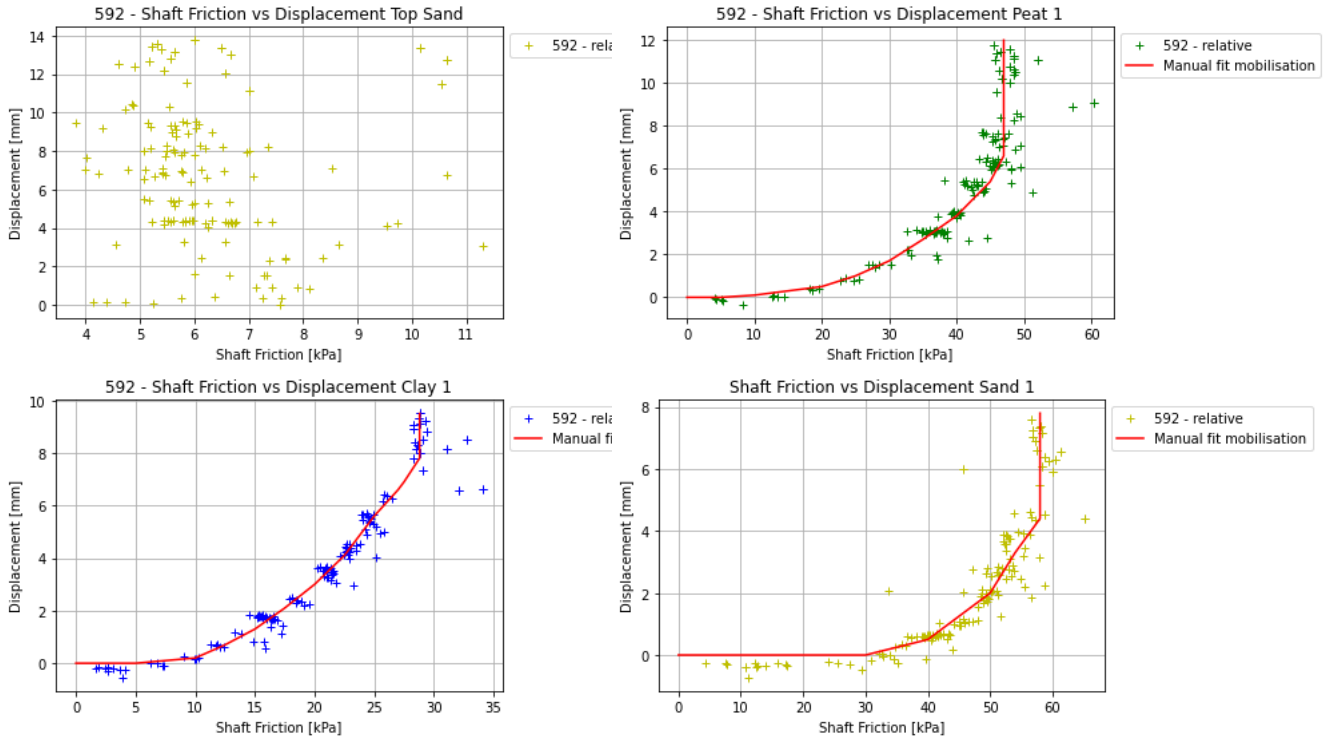

E. Check on Raw Omnisens Test Data

This section will discuss the checks that are done on the raw Omnisens data.

E.1 Strain Development in One Measurement Point

Since the graphs showing the average strain in the pile, and the shaft friction mobilisation showed some striking behaviour around the pile tip, it was decided to look into the strain development during the load steps of several measurement points around the pile tip.

E.1.1 Pile 175

North	South
-11.616 m	-11.608 m
-11.871 m	-11.863 m
-12.126 m	-12.119 m
Loop	-12.25 m

Table E.1: Location Measurement Points around Loop

Table E.1 shows the locations of the six measurement points closest to the loop of the fibre. According to Table 3.1, from the CPT averaging it was found that the sand layer starts at -11.71 mNAP around pile 175. So the two lowest measurement points on both sides of the fibre are located in the sand layer, only -11.871 and -11.863 m are rather close to the boundary. So there is a possibility that the peat layer on top of the sand layer has had an influence on the strain reading for these points.

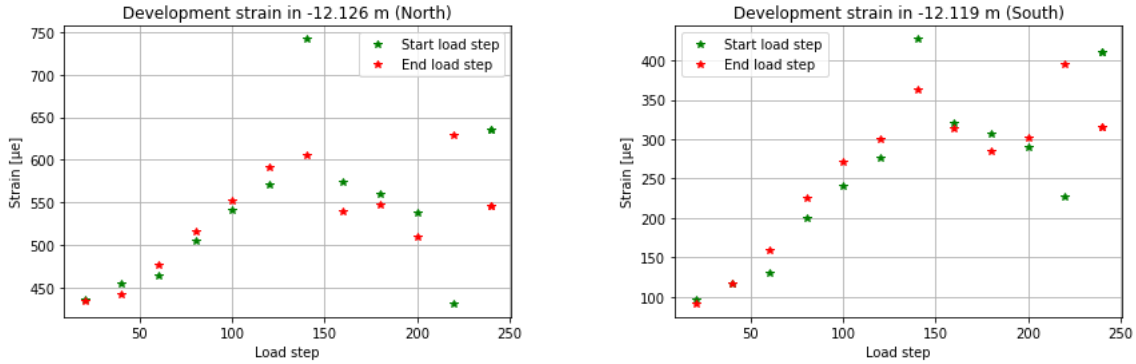

Figure E.1: Pile 175 - Strain Development in Two Measurement Points Closest to Loop

Figure E.1 shows the strain development in the two lowest measurement points. It shows that both points have a steady increase in strain, until around 140 kN. Then there seems to be scatter in the readings, even within one load step: the green dots show the strain at the beginning of the test, the red dots the strain at the end. In some load steps there is a big difference, which is not what is expected when the strain keeps increasing during the tensile load test. An explanation for this scatter might be that the pile is starting to be pulled out of the soil: the pile tip is only 56 centimeters deep into the sand layer, which is not deep.

E.1.2 Pile 187

East	West
-11.77 m	-11.792 m
-12.026 m	-12.048 m
-12.282 m	-12.303 m
Loop	-12.42 m

Table E.2: Location Measurement Points around Loop

Table E.2 shows the six measurement points closest to the loop for the East-West fibre. This is the only fibre that could be measured during the test. According to Table 3.1, around pile 187 the second sand layer starts at -11.75 mNAP. The two upper points - -11.77 and -11.792 m - would be in the sand layer, but because of the averaging over a longer distance, these points will also measure in the peat layer on top.

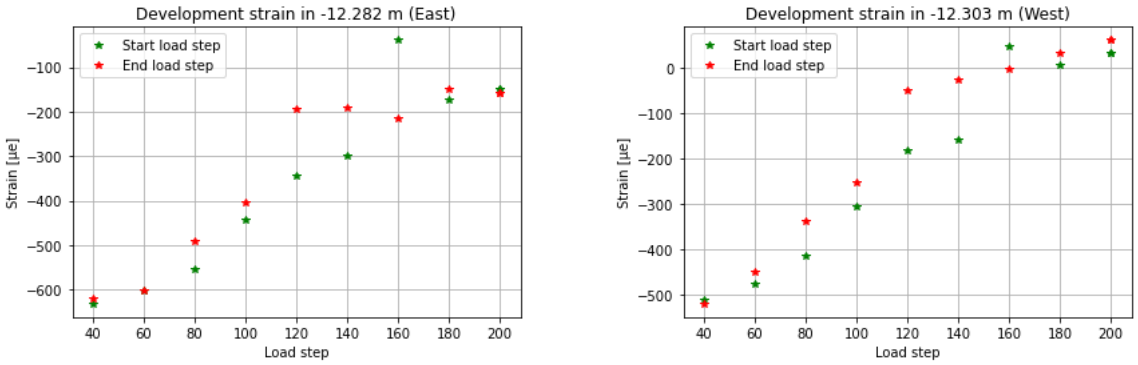

Figure E.2: Pile 187 - Strain Development in Two Measurement Points Closest to Loop

Figure E.2 shows the strain development in the two points closest to the loop. From 120 kN on the strain readings start to show scatter, but it is still possible to draw a trend line in this part. The deviation can be caused by a mistake in the measurement device, or the pile starts to loose contact from that load step on.

E.1.3 Pile 576

North	South
-11.82 m	-11.788 m
-12.075 m	-12.044 m
-12.33 m	-12.299 m
	-12.554 m

Table E.3: Location Measurement Points around Loop North-South

According to Table 3.1, the second sand layer starts at -11.74 mNAP, so all measurement points mentioned in Table E.3 are located in the sand layer. Only the two upper points on both sides might have been influenced by the peat layer on top.

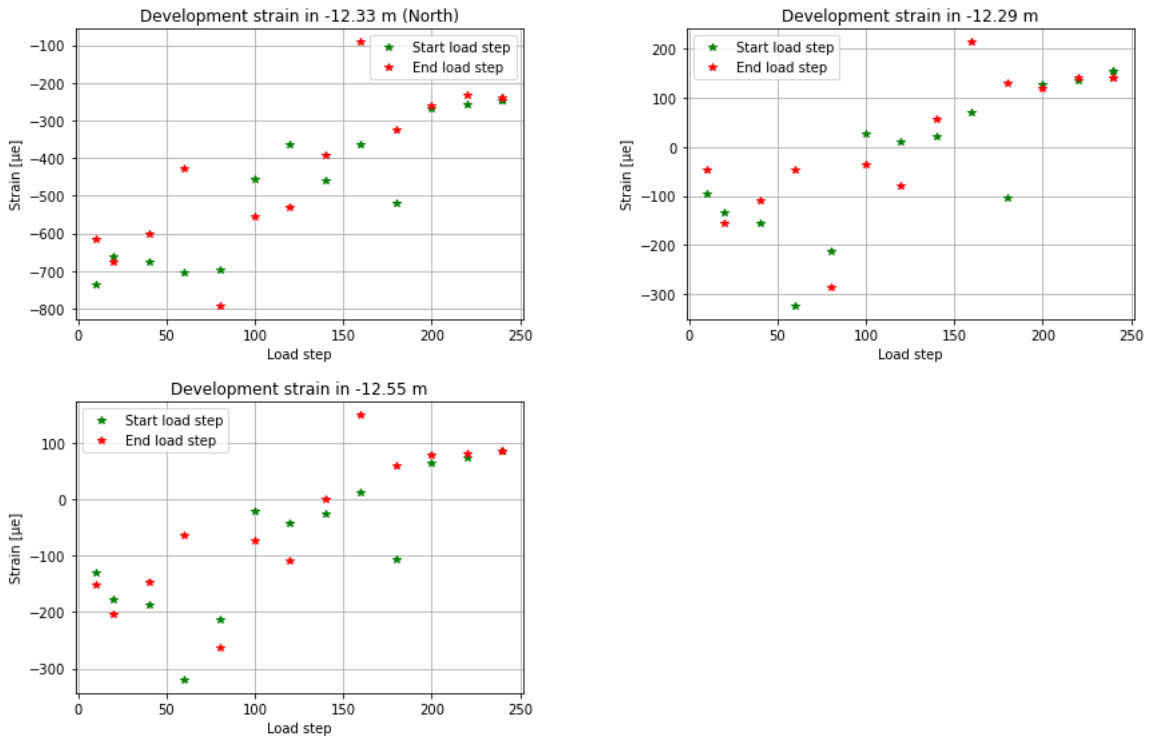

Figure E.3: Pile 576 - Strain Development in Three Measurement Points Closest to Loop of North-South

Figure E.3 shows the strain development in the three measurements closest to the loop (-12.57 mNAP). From the start of the test on there is a lot more scatter compared to the two previous piles. In some load steps there is a lot of difference between the strain at the beginning and end of the load step, but in other load steps there is almost no difference. So it is hard to say whether creep is happening during some of the load steps. The difference in time one load step was executed might have an influence on the difference in strain reading.

East	West
-11.80 m	-11.768 m
-12.06 m	-12.02 m
-12.31 m	-12.278 m
	-12.53 m

Table E.4: Location Measurement Points around Loop East-West

The two measurement points closest to the loop in Table E.4 are completely in the sand. The two measurements above on both sides are in the sand too, but might be influenced by the peat layer, that starts at -11.74 mNAP.

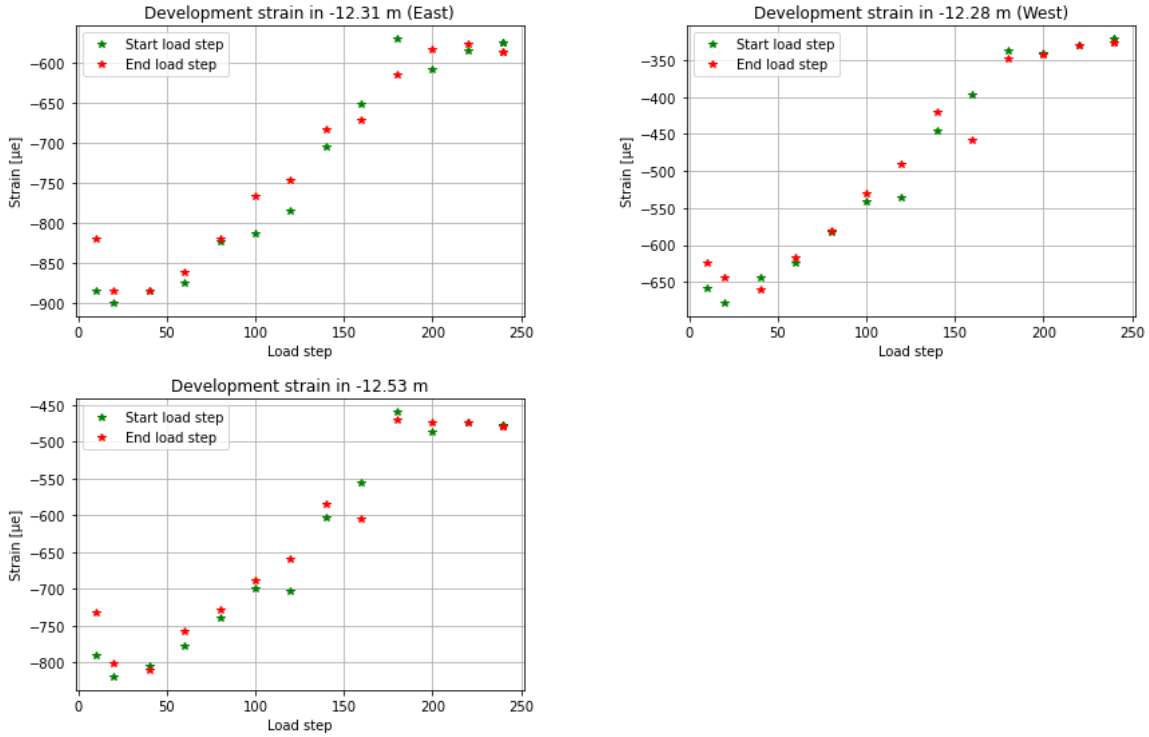

Figure E.4: Pile 576 - Strain Development in Three Measurement Points Closest to Loop of East-West

The three plots in Figure **??** show a smooth development of strain during the test, different from the plots in Figure E.3 of the North-South fibre.

E.1.4 Pile 592

North	South
-12.031 m	-12.038 m
-12.286 m	-12.292 m
-12.541 m	-12.548 m
-12.797 m	

Table E.5: Location Measurement Points around Loop North-South

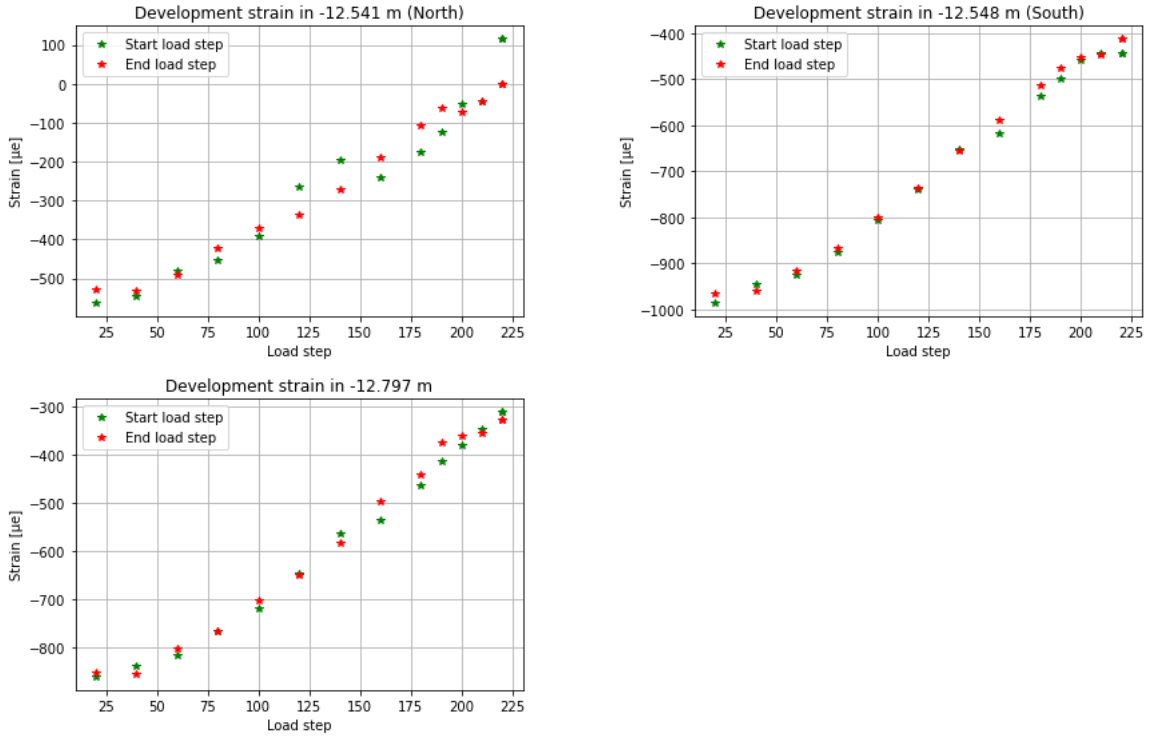

Figure E.5: Pile 592 - Strain Development in Three Measurement Points Closest to Loop of North-South Fibre

East	West
-12.136 m	-12.147 m
-12.392 m	-12.403 m
-12.647 m	-12.657 m

Table E.6: Location Measurement Points around Loop East-West

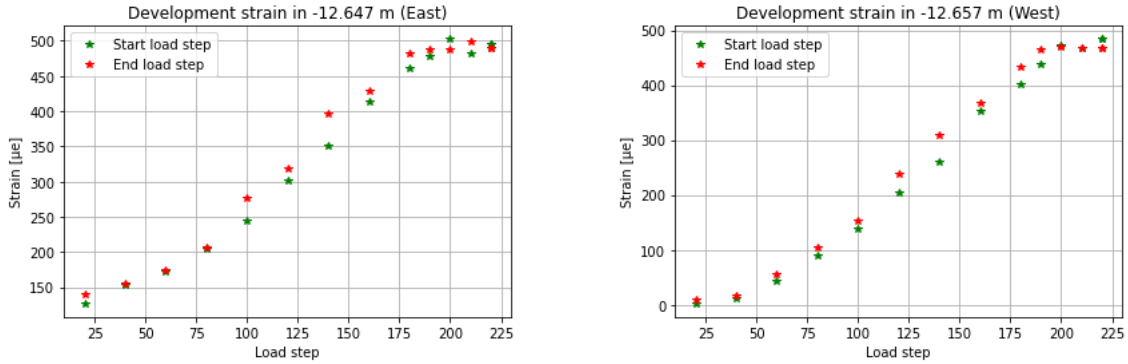

Figure E.6: Pile 592 - Strain Development in Two Measurement Points Closest to Loop of East-West fibre

E.2 All Strain Readings per Load Step

This subsection shows the strain readings of one load step for all load steps of the piles analysed. These figures show the fluctuation in strains measured during one load step. Sometimes there is an offset in a single strain reading compared to the other readings, which can be explained by the configuration of the Omnisens. For most of the analysis, the average strain of every load step was used. Only to create the mobilisation curves of the shaft friction, the original strain readings are used.

E.2.1 Pile 175

The figures of pile 175 that are shown below also show strain readings above 0 mNAP, which is above ground level. In the further analysis, only the strains measured below ground level are used. Of the measurements done above ground level, it is hard to determine what measurement has solely measured within the pile. Only load step 5 till 8 are presented, to illustrate fluctuations in strain readings within one load step.

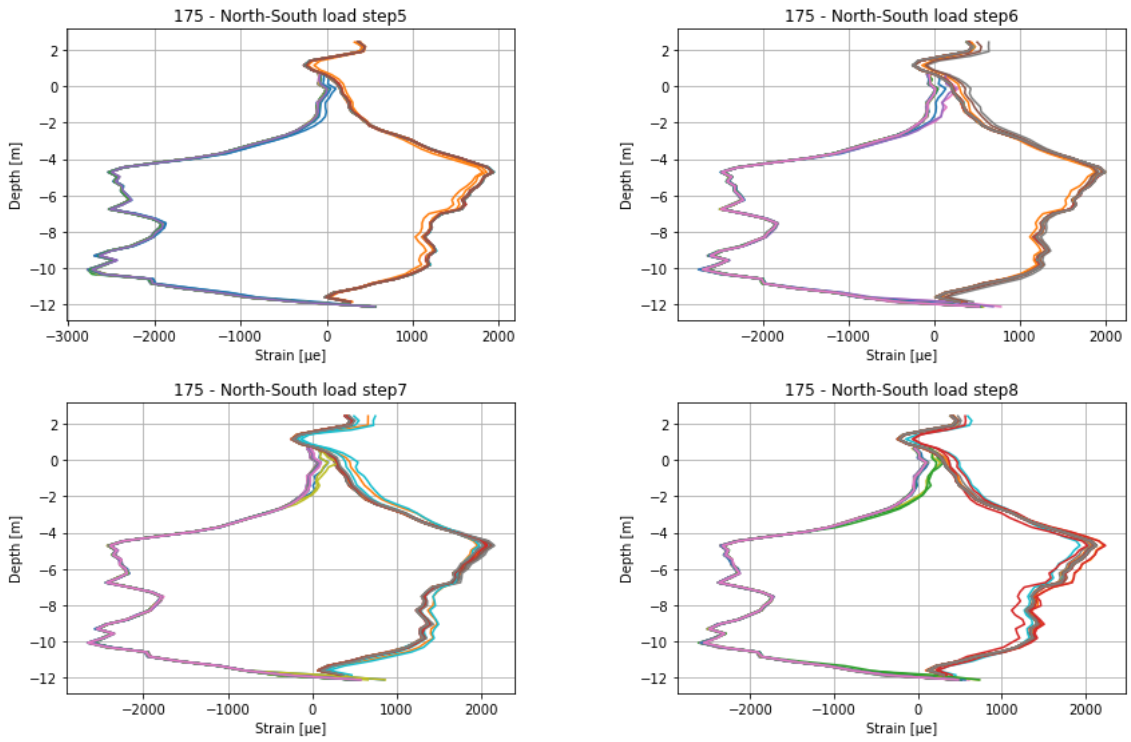

Figure E.7: Pile 175 - Strain readings load step 5 till 8

E.2.2 Pile 187

Similar to pile 175, the strain readings that can be observed above 0 mNAP in the figures below, are not used in the further analysis. Only load step 5 till 8 are presented, to illustrate fluctuations in strain readings within one load step.

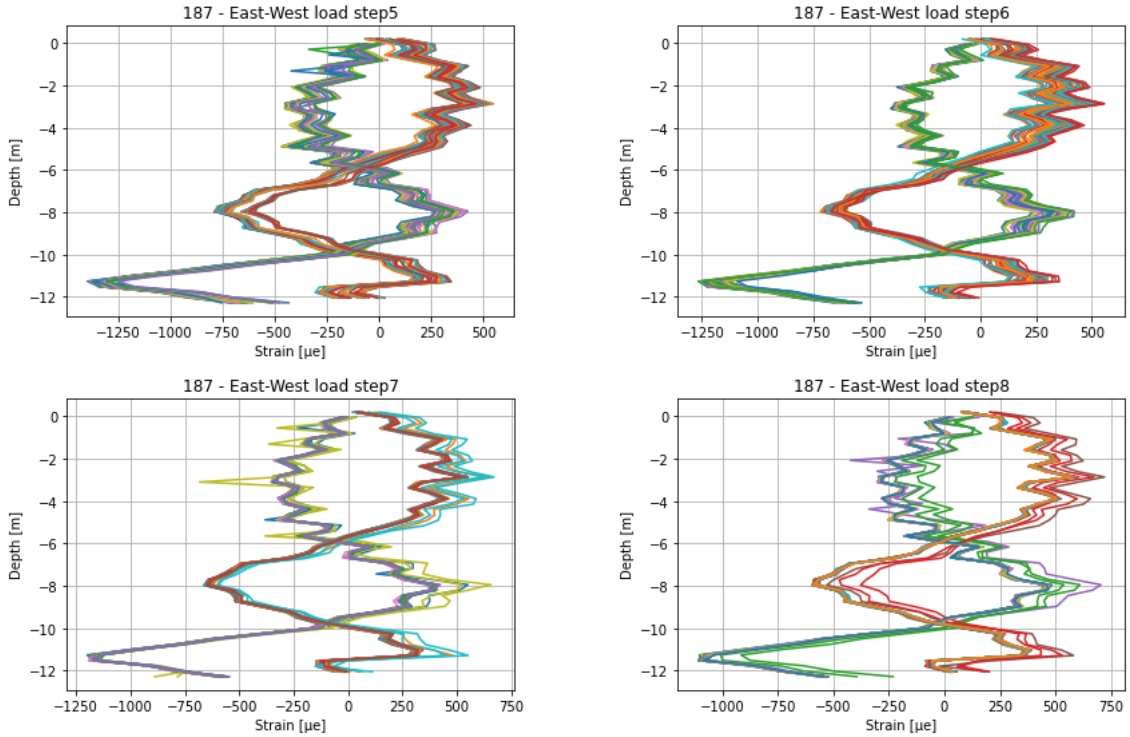

Figure E.8: Pile 187 - Strain readings load step 5 till 8

E.2.3 Pile 576

The strain readings measured above 0 mNAP are not used in the further analysis. The shape of the North-South fiber differs from the East-West fiber, which is caused by the difference in bending effects occurring in the pile.

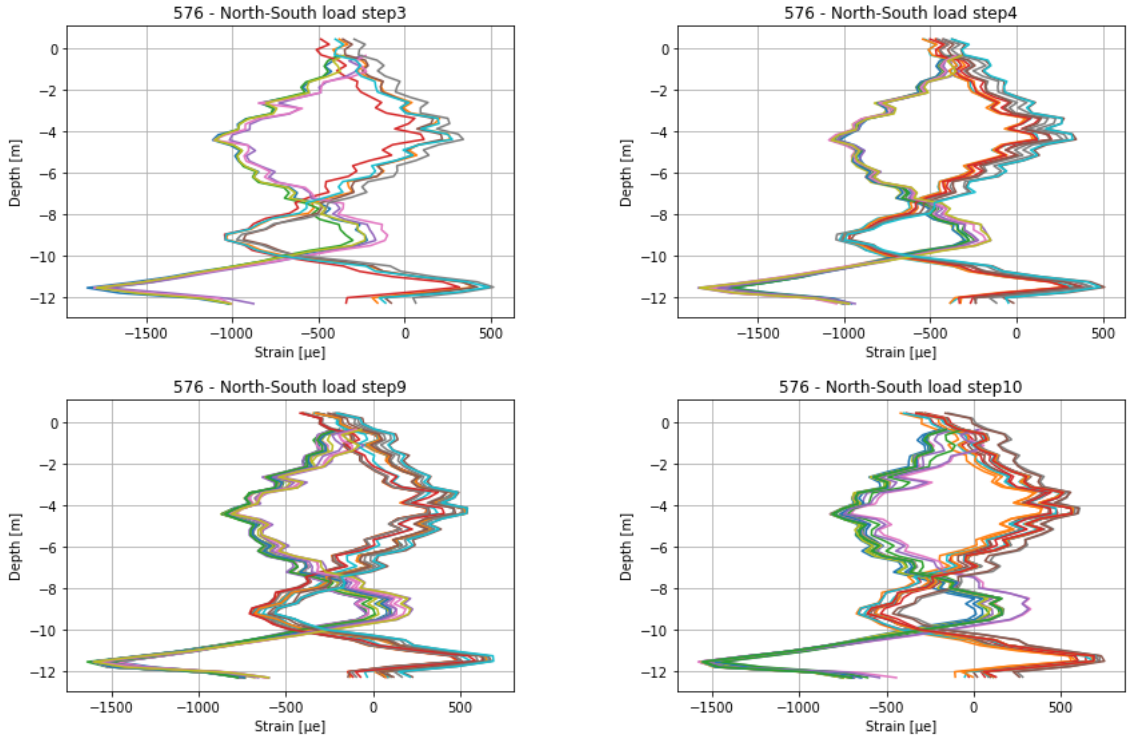

Figure E.9: Pile 576 - North-South fiber - Strain readings of load step 3, 4, 9 and 10

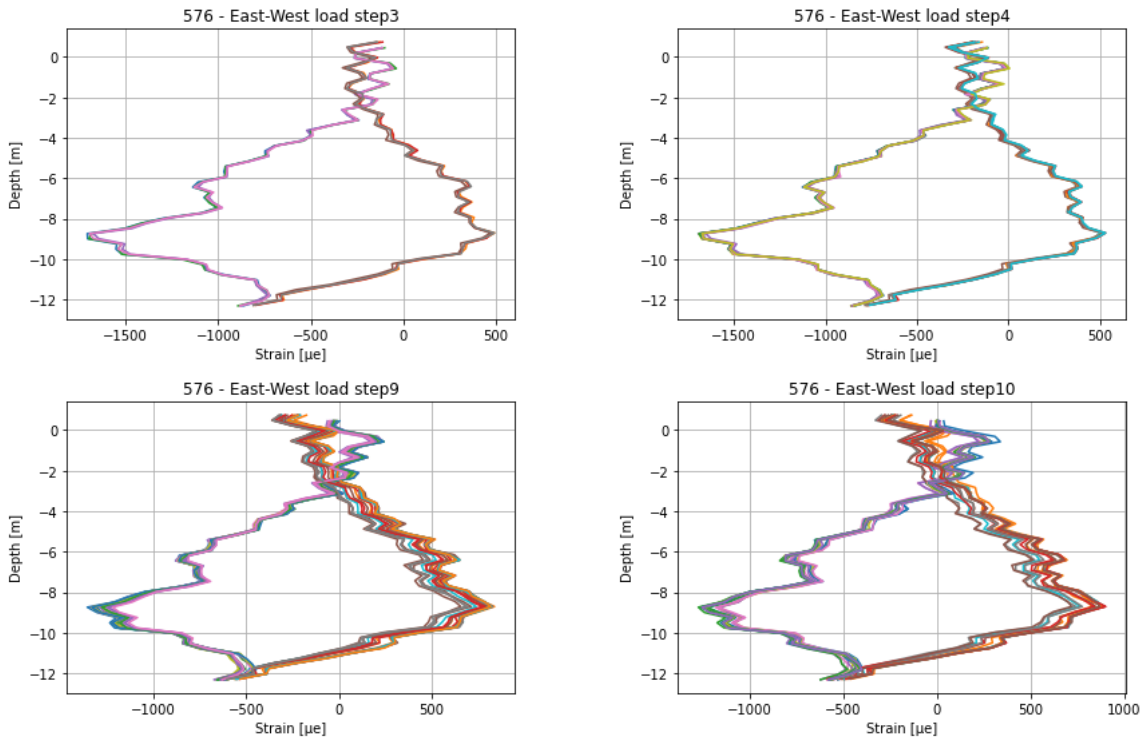

Figure E.10: Pile 576 - East-West fiber - Strain readings of load step 3, 4, 9 and 10

E.2.4 Pile 592

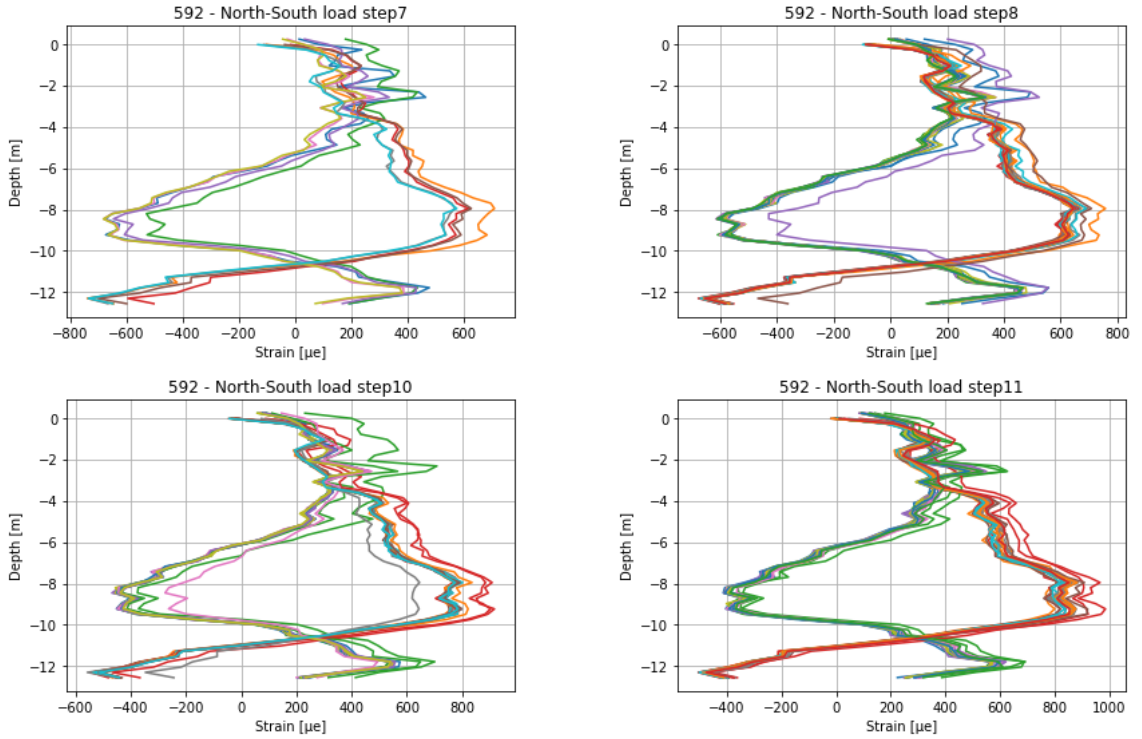

Figure E.11: Pile 592 - North-South fiber - Strain readings of load step 7, 8, 10 and 11

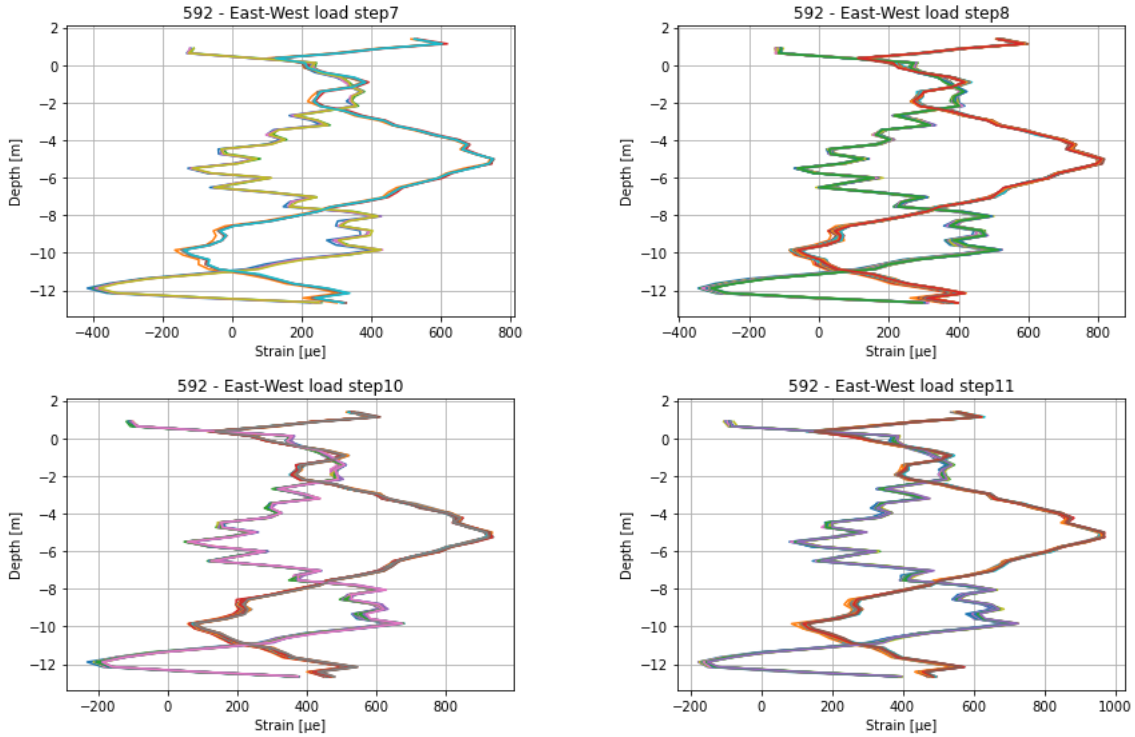

Figure E.12: Pile 592 - East-West fiber - Strain readings of load step 7, 8, 10 and 11

F. Compression Tests TU Delft

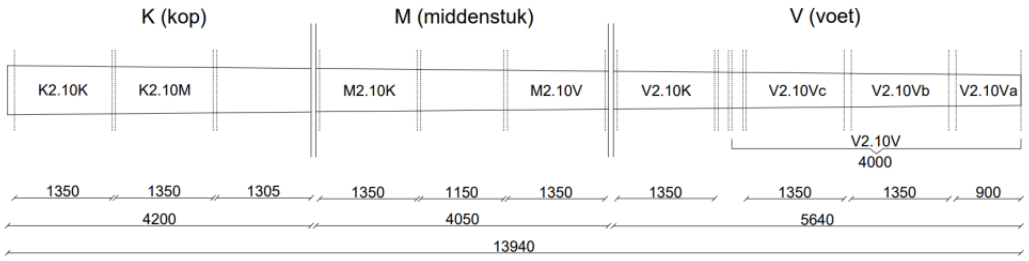

Figure F.1: Splitting of Pile 576
reprinted from Pagella (2021)

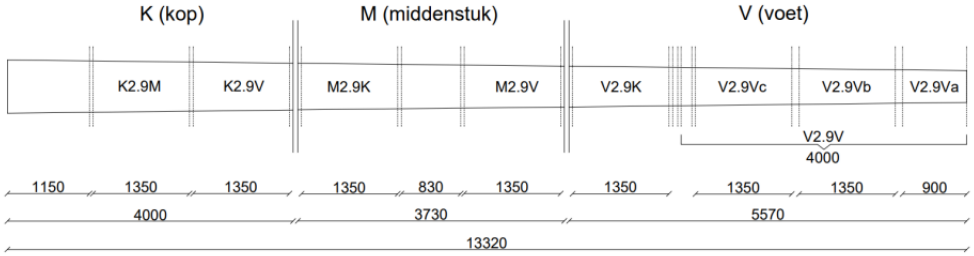

Figure F.2: Splitting of Pile 592
reprinted from Pagella (2021)

OAM P2.10 (576)						
	Length (mm)	D_avg (mm)	Density (kg/m3)	m.c. (%)	MOEdyn (Mpa)	MOEstat (Mpa)
Full pile	13940	555,0	761	-	11101	-
Head	4200	200,0	716	-	14572	-
Middle-part	4050	169,8	742	-	13516	-
Tail	5640	151,2	622	-	11191	-
K2.10K	1350	207,4	835	76	15044	11758
K2.10M	1350	200,0	804	59	13846	12963
K2.10V	-	-	-	-	-	-
M2.10K	1350	178,3	715	70	13283	12415
M2.10V	1350	161,8	746	75	12230	11140
V2.10V	4000	147,0	730	70	11580	10735
V2.10K	1350	158,1	721	73	11900	11634
V2.10Vc	900	154,9	702	74	10862	9996
V2.10Vb	900	146,4	686	70	10346	9540
V2.10Va	900	140,1	729	76	9168	9152

OAM P2.9 (592)						
	Length (mm)	D_avg (mm)	Density (kg/m3)	m.c. (%)	MOEdyn (Mpa)	MOEstat (Mpa)
Full pile	13320	616,3	807	-	10746	-
Head	4000	222,8	708	-	13567	-
Middle-part	3730	199,5	741	-	10813	-
Tail	5570	167,1	651	-	10235	-
K2.9K	-	-	-	-	-	-
K2.9M	1350	220,2	821	79	11816	11489
K2.9V	1330	212,2	710	80	11291	11527
M2.9K	1350	205,8	703	86	10339	10243
M2.9V	1350	195,8	724	98	9288	8963
V2.9V	4000	160,7	770	94	9281	9873
V2.9K	1350	184,1	696	94	9271	9113
V2.9Vc	1350	177,7	693	88	8508	7791
V2.9Vb	1350	163,9	716	82	8471	8091
V2.9Va	900	148,5	737	83	9139	8231

Figure F.3: Overview test results pile 576 (left) and 592 (right)
reprinted from Pagella (2021)

G. Pictures from Test Set-Up and Piles in Overamstel

Figure G.1: Construction of Fiber Loop in Pile Tip

Figure G.2: Predrilling of Top Sand Layer

Figure G.3: Driving Timber Piles in the soil

Figure G.4: Manually debarked (dark) and mechanically debarked (light) piles

Figure G.5: Preparation Pile Head for Tensile Load Test

Figure G.6: Side view Tensile Load Test Set-Up

Figure G.7: Top view Tensile Load Test Set-Up

Figure G.8: Full Test Set-Up before Tensile Load Test

H. Deltares Pile Group Simulations

The first report is the simulation of 592REL, where the pile test history was simulated. The second report shows the results of the simulation of negative skin friction. The factor of soil displacement was altered between 1 and 9, but only the results of factor 9 - when the maximum negative skin friction occurred - are included in the thesis report.

Report for D-Pile Group 20.2

Pile Analysis
Developed by Deltares

Date of report:	2-12-2021
Time of report:	14:11:55
Report with version:	20.2.1.30860
Date of calculation:	2-12-2021
Time of calculation:	14:09:20
Calculated with version:	20.2.1.30860
File name:	592REL

1 Table of Contents

2 Input Data

2.1 Topview Layout

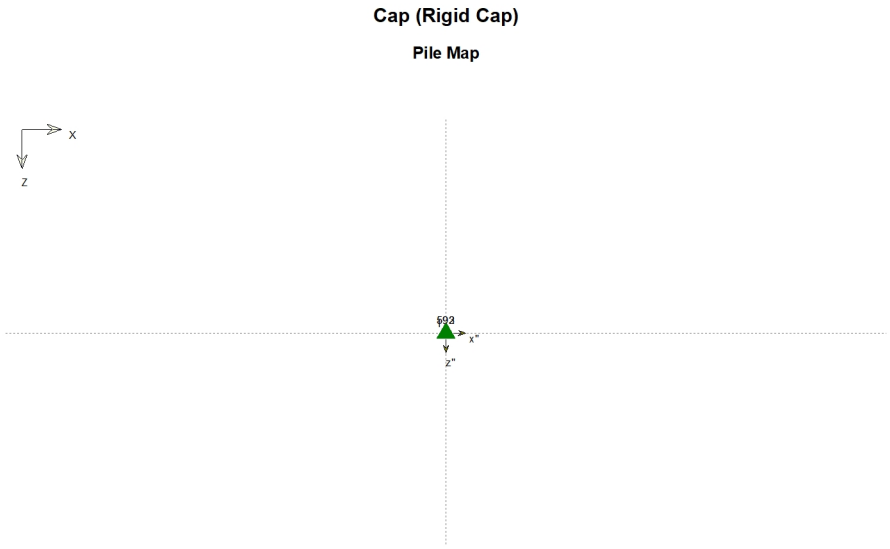

3 Calculation Results

3.1 Cap Displacements

Load step	Ux [m]	Uy [m]	Uz [m]	Theta x [rad]	Theta y [rad]	Theta z [rad]
1	0,00000	-0,00007	0,00000	0,000000	0,000000	0,000000
2	0,00000	-0,00015	0,00000	0,000000	0,000000	0,000000
3	0,00000	-0,00022	0,00000	0,000000	0,000000	0,000000
4	0,00000	-0,00029	0,00000	0,000000	0,000000	0,000000
5	0,00000	-0,00037	0,00000	0,000000	0,000000	0,000000
6	0,00000	-0,00044	0,00000	0,000000	0,000000	0,000000
7	0,00000	-0,00052	0,00000	0,000000	0,000000	0,000000
8	0,00000	-0,00060	0,00000	0,000000	0,000000	0,000000
9	0,00000	-0,00068	0,00000	0,000000	0,000000	0,000000
10	0,00000	-0,00077	0,00000	0,000000	0,000000	0,000000
11	0,00000	-0,00086	0,00000	0,000000	0,000000	0,000000
12	0,00000	-0,00096	0,00000	0,000000	0,000000	0,000000
13	0,00000	-0,00106	0,00000	0,000000	0,000000	0,000000
14	0,00000	-0,00116	0,00000	0,000000	0,000000	0,000000
15	0,00000	-0,00126	0,00000	0,000000	0,000000	0,000000
16	0,00000	-0,00137	0,00000	0,000000	0,000000	0,000000
17	0,00000	-0,00148	0,00000	0,000000	0,000000	0,000000
18	0,00000	-0,00160	0,00000	0,000000	0,000000	0,000000
19	0,00000	-0,00171	0,00000	0,000000	0,000000	0,000000
20	0,00000	-0,00184	0,00000	0,000000	0,000000	0,000000
21	0,00000	-0,00196	0,00000	0,000000	0,000000	0,000000
22	0,00000	-0,00209	0,00000	0,000000	0,000000	0,000000
23	0,00000	-0,00222	0,00000	0,000000	0,000000	0,000000
24	0,00000	-0,00236	0,00000	0,000000	0,000000	0,000000
25	0,00000	-0,00249	0,00000	0,000000	0,000000	0,000000
26	0,00000	-0,00263	0,00000	0,000000	0,000000	0,000000
27	0,00000	-0,00276	0,00000	0,000000	0,000000	0,000000
28	0,00000	-0,00290	0,00000	0,000000	0,000000	0,000000
29	0,00000	-0,00304	0,00000	0,000000	0,000000	0,000000
30	0,00000	-0,00318	0,00000	0,000000	0,000000	0,000000
31	0,00000	-0,00332	0,00000	0,000000	0,000000	0,000000
32	0,00000	-0,00346	0,00000	0,000000	0,000000	0,000000
33	0,00000	-0,00360	0,00000	0,000000	0,000000	0,000000
34	0,00000	-0,00375	0,00000	0,000000	0,000000	0,000000
35	0,00000	-0,00389	0,00000	0,000000	0,000000	0,000000
36	0,00000	-0,00404	0,00000	0,000000	0,000000	0,000000
37	0,00000	-0,00419	0,00000	0,000000	0,000000	0,000000
38	0,00000	-0,00434	0,00000	0,000000	0,000000	0,000000
39	0,00000	-0,00449	0,00000	0,000000	0,000000	0,000000
40	0,00000	-0,00465	0,00000	0,000000	0,000000	0,000000
41	0,00000	-0,00480	0,00000	0,000000	0,000000	0,000000
42	0,00000	-0,00496	0,00000	0,000000	0,000000	0,000000
43	0,00000	-0,00511	0,00000	0,000000	0,000000	0,000000
44	0,00000	-0,00527	0,00000	0,000000	0,000000	0,000000
45	0,00000	-0,00544	0,00000	0,000000	0,000000	0,000000
46	0,00000	-0,00560	0,00000	0,000000	0,000000	0,000000
47	0,00000	-0,00576	0,00000	0,000000	0,000000	0,000000
48	0,00000	-0,00593	0,00000	0,000000	0,000000	0,000000
49	0,00000	-0,00610	0,00000	0,000000	0,000000	0,000000
50	0,00000	-0,00626	0,00000	0,000000	0,000000	0,000000
51	0,00000	-0,00643	0,00000	0,000000	0,000000	0,000000
52	0,00000	-0,00660	0,00000	0,000000	0,000000	0,000000
53	0,00000	-0,00677	0,00000	0,000000	0,000000	0,000000
54	0,00000	-0,00694	0,00000	0,000000	0,000000	0,000000
55	0,00000	-0,00711	0,00000	0,000000	0,000000	0,000000
56	0,00000	-0,00728	0,00000	0,000000	0,000000	0,000000
57	0,00000	-0,00745	0,00000	0,000000	0,000000	0,000000
58	0,00000	-0,00762	0,00000	0,000000	0,000000	0,000000

Load step	Ux [m]	Uy [m]	Uz [m]	Theta x [rad]	Theta y [rad]	Theta z [rad]
59	0,00000	-0,00779	0,00000	0,000000	0,000000	0,000000
60	0,00000	-0,00796	0,00000	0,000000	0,000000	0,000000
61	0,00000	-0,00814	0,00000	0,000000	0,000000	0,000000
62	0,00000	-0,00831	0,00000	0,000000	0,000000	0,000000
63	0,00000	-0,00848	0,00000	0,000000	0,000000	0,000000
64	0,00000	-0,00865	0,00000	0,000000	0,000000	0,000000
65	0,00000	-0,00883	0,00000	0,000000	0,000000	0,000000
66	0,00000	-0,00900	0,00000	0,000000	0,000000	0,000000
67	0,00000	-0,00918	0,00000	0,000000	0,000000	0,000000
68	0,00000	-0,00935	0,00000	0,000000	0,000000	0,000000
69	0,00000	-0,00953	0,00000	0,000000	0,000000	0,000000
70	0,00000	-0,00970	0,00000	0,000000	0,000000	0,000000
71	0,00000	-0,00988	0,00000	0,000000	0,000000	0,000000
72	0,00000	-0,01005	0,00000	0,000000	0,000000	0,000000
73	0,00000	-0,01023	0,00000	0,000000	0,000000	0,000000
74	0,00000	-0,01041	0,00000	0,000000	0,000000	0,000000
75	0,00000	-0,01061	0,00000	0,000000	0,000000	0,000000
76	0,00000	-0,01083	0,00000	0,000000	0,000000	0,000000
77	0,00000	-0,01105	0,00000	0,000000	0,000000	0,000000
78	0,00000	-0,01127	0,00000	0,000000	0,000000	0,000000
79	0,00000	-0,01149	0,00000	0,000000	0,000000	0,000000
80	0,00000	-0,01171	0,00000	0,000000	0,000000	0,000000
81	0,00000	-0,01194	0,00000	0,000000	0,000000	0,000000
82	0,00000	-0,01217	0,00000	0,000000	0,000000	0,000000
83	0,00000	-0,01241	0,00000	0,000000	0,000000	0,000000
84	0,00000	-0,01264	0,00000	0,000000	0,000000	0,000000
85	0,00000	-0,01288	0,00000	0,000000	0,000000	0,000000
86	0,00000	-0,01312	0,00000	0,000000	0,000000	0,000000
87	0,00000	-0,01337	0,00000	0,000000	0,000000	0,000000
88	0,00000	-0,01361	0,00000	0,000000	0,000000	0,000000
89	0,00000	-0,01386	0,00000	0,000000	0,000000	0,000000
90	0,00000	-0,01411	0,00000	0,000000	0,000000	0,000000
91	0,00000	-0,01436	0,00000	0,000000	0,000000	0,000000
92	0,00000	-0,01461	0,00000	0,000000	0,000000	0,000000
93	0,00000	-0,01486	0,00000	0,000000	0,000000	0,000000
94	0,00000	-0,01511	0,00000	0,000000	0,000000	0,000000
95	0,00000	-0,01536	0,00000	0,000000	0,000000	0,000000
96	0,00000	-0,01562	0,00000	0,000000	0,000000	0,000000
97	0,00000	-0,01588	0,00000	0,000000	0,000000	0,000000
98	0,00000	-0,01613	0,00000	0,000000	0,000000	0,000000
99	0,00000	-0,01640	0,00000	0,000000	0,000000	0,000000
100	0,00000	-0,01666	0,00000	0,000000	0,000000	0,000000
101	0,00000	-0,01659	0,00000	0,000000	0,000000	0,000000
102	0,00000	-0,01651	0,00000	0,000000	0,000000	0,000000
103	0,00000	-0,01644	0,00000	0,000000	0,000000	0,000000
104	0,00000	-0,01637	0,00000	0,000000	0,000000	0,000000
105	0,00000	-0,01629	0,00000	0,000000	0,000000	0,000000
106	0,00000	-0,01622	0,00000	0,000000	0,000000	0,000000
107	0,00000	-0,01614	0,00000	0,000000	0,000000	0,000000
108	0,00000	-0,01607	0,00000	0,000000	0,000000	0,000000
109	0,00000	-0,01600	0,00000	0,000000	0,000000	0,000000
110	0,00000	-0,01592	0,00000	0,000000	0,000000	0,000000
111	0,00000	-0,01585	0,00000	0,000000	0,000000	0,000000
112	0,00000	-0,01577	0,00000	0,000000	0,000000	0,000000
113	0,00000	-0,01570	0,00000	0,000000	0,000000	0,000000
114	0,00000	-0,01562	0,00000	0,000000	0,000000	0,000000
115	0,00000	-0,01554	0,00000	0,000000	0,000000	0,000000
116	0,00000	-0,01546	0,00000	0,000000	0,000000	0,000000
117	0,00000	-0,01538	0,00000	0,000000	0,000000	0,000000
118	0,00000	-0,01530	0,00000	0,000000	0,000000	0,000000
119	0,00000	-0,01521	0,00000	0,000000	0,000000	0,000000
120	0,00000	-0,01512	0,00000	0,000000	0,000000	0,000000
121	0,00000	-0,01503	0,00000	0,000000	0,000000	0,000000
122	0,00000	-0,01494	0,00000	0,000000	0,000000	0,000000
123	0,00000	-0,01484	0,00000	0,000000	0,000000	0,000000

Load step	Ux [m]	Uy [m]	Uz [m]	Theta x [rad]	Theta y [rad]	Theta z [rad]
124	0,00000	-0,01475	0,00000	0,000000	0,000000	0,000000
125	0,00000	-0,01465	0,00000	0,000000	0,000000	0,000000
126	0,00000	-0,01455	0,00000	0,000000	0,000000	0,000000
127	0,00000	-0,01445	0,00000	0,000000	0,000000	0,000000
128	0,00000	-0,01434	0,00000	0,000000	0,000000	0,000000
129	0,00000	-0,01424	0,00000	0,000000	0,000000	0,000000
130	0,00000	-0,01413	0,00000	0,000000	0,000000	0,000000
131	0,00000	-0,01403	0,00000	0,000000	0,000000	0,000000
132	0,00000	-0,01392	0,00000	0,000000	0,000000	0,000000
133	0,00000	-0,01381	0,00000	0,000000	0,000000	0,000000
134	0,00000	-0,01370	0,00000	0,000000	0,000000	0,000000
135	0,00000	-0,01358	0,00000	0,000000	0,000000	0,000000
136	0,00000	-0,01347	0,00000	0,000000	0,000000	0,000000
137	0,00000	-0,01335	0,00000	0,000000	0,000000	0,000000
138	0,00000	-0,01323	0,00000	0,000000	0,000000	0,000000
139	0,00000	-0,01311	0,00000	0,000000	0,000000	0,000000
140	0,00000	-0,01299	0,00000	0,000000	0,000000	0,000000
141	0,00000	-0,01286	0,00000	0,000000	0,000000	0,000000
142	0,00000	-0,01273	0,00000	0,000000	0,000000	0,000000
143	0,00000	-0,01260	0,00000	0,000000	0,000000	0,000000
144	0,00000	-0,01247	0,00000	0,000000	0,000000	0,000000
145	0,00000	-0,01234	0,00000	0,000000	0,000000	0,000000
146	0,00000	-0,01221	0,00000	0,000000	0,000000	0,000000
147	0,00000	-0,01208	0,00000	0,000000	0,000000	0,000000
148	0,00000	-0,01194	0,00000	0,000000	0,000000	0,000000
149	0,00000	-0,01181	0,00000	0,000000	0,000000	0,000000
150	0,00000	-0,01168	0,00000	0,000000	0,000000	0,000000
151	0,00000	-0,01154	0,00000	0,000000	0,000000	0,000000
152	0,00000	-0,01141	0,00000	0,000000	0,000000	0,000000
153	0,00000	-0,01127	0,00000	0,000000	0,000000	0,000000
154	0,00000	-0,01113	0,00000	0,000000	0,000000	0,000000
155	0,00000	-0,01100	0,00000	0,000000	0,000000	0,000000
156	0,00000	-0,01086	0,00000	0,000000	0,000000	0,000000
157	0,00000	-0,01072	0,00000	0,000000	0,000000	0,000000
158	0,00000	-0,01058	0,00000	0,000000	0,000000	0,000000
159	0,00000	-0,01044	0,00000	0,000000	0,000000	0,000000
160	0,00000	-0,01030	0,00000	0,000000	0,000000	0,000000
161	0,00000	-0,01016	0,00000	0,000000	0,000000	0,000000
162	0,00000	-0,01002	0,00000	0,000000	0,000000	0,000000
163	0,00000	-0,00988	0,00000	0,000000	0,000000	0,000000
164	0,00000	-0,00974	0,00000	0,000000	0,000000	0,000000
165	0,00000	-0,00960	0,00000	0,000000	0,000000	0,000000
166	0,00000	-0,00946	0,00000	0,000000	0,000000	0,000000
167	0,00000	-0,00931	0,00000	0,000000	0,000000	0,000000
168	0,00000	-0,00917	0,00000	0,000000	0,000000	0,000000
169	0,00000	-0,00902	0,00000	0,000000	0,000000	0,000000
170	0,00000	-0,00888	0,00000	0,000000	0,000000	0,000000
171	0,00000	-0,00873	0,00000	0,000000	0,000000	0,000000
172	0,00000	-0,00858	0,00000	0,000000	0,000000	0,000000
173	0,00000	-0,00843	0,00000	0,000000	0,000000	0,000000
174	0,00000	-0,00828	0,00000	0,000000	0,000000	0,000000
175	0,00000	-0,00813	0,00000	0,000000	0,000000	0,000000
176	0,00000	-0,00798	0,00000	0,000000	0,000000	0,000000
177	0,00000	-0,00783	0,00000	0,000000	0,000000	0,000000
178	0,00000	-0,00768	0,00000	0,000000	0,000000	0,000000
179	0,00000	-0,00752	0,00000	0,000000	0,000000	0,000000
180	0,00000	-0,00737	0,00000	0,000000	0,000000	0,000000
181	0,00000	-0,00721	0,00000	0,000000	0,000000	0,000000
182	0,00000	-0,00706	0,00000	0,000000	0,000000	0,000000
183	0,00000	-0,00690	0,00000	0,000000	0,000000	0,000000
184	0,00000	-0,00675	0,00000	0,000000	0,000000	0,000000
185	0,00000	-0,00659	0,00000	0,000000	0,000000	0,000000
186	0,00000	-0,00643	0,00000	0,000000	0,000000	0,000000
187	0,00000	-0,00627	0,00000	0,000000	0,000000	0,000000
188	0,00000	-0,00611	0,00000	0,000000	0,000000	0,000000

Load step	Ux [m]	Uy [m]	Uz [m]	Theta x [rad]	Theta y [rad]	Theta z [rad]
189	0,00000	-0,00595	0,00000	0,000000	0,000000	0,000000
190	0,00000	-0,00579	0,00000	0,000000	0,000000	0,000000
191	0,00000	-0,00563	0,00000	0,000000	0,000000	0,000000
192	0,00000	-0,00546	0,00000	0,000000	0,000000	0,000000
193	0,00000	-0,00530	0,00000	0,000000	0,000000	0,000000
194	0,00000	-0,00513	0,00000	0,000000	0,000000	0,000000
195	0,00000	-0,00497	0,00000	0,000000	0,000000	0,000000
196	0,00000	-0,00480	0,00000	0,000000	0,000000	0,000000
197	0,00000	-0,00463	0,00000	0,000000	0,000000	0,000000
198	0,00000	-0,00447	0,00000	0,000000	0,000000	0,000000
199	0,00000	-0,00430	0,00000	0,000000	0,000000	0,000000
200	0,00000	-0,00413	0,00000	0,000000	0,000000	0,000000
201	0,00000	-0,00415	0,00000	0,000000	0,000000	0,000000
202	0,00000	-0,00416	0,00000	0,000000	0,000000	0,000000
203	0,00000	-0,00418	0,00000	0,000000	0,000000	0,000000
204	0,00000	-0,00419	0,00000	0,000000	0,000000	0,000000
205	0,00000	-0,00420	0,00000	0,000000	0,000000	0,000000
206	0,00000	-0,00422	0,00000	0,000000	0,000000	0,000000
207	0,00000	-0,00423	0,00000	0,000000	0,000000	0,000000
208	0,00000	-0,00425	0,00000	0,000000	0,000000	0,000000
209	0,00000	-0,00426	0,00000	0,000000	0,000000	0,000000
210	0,00000	-0,00428	0,00000	0,000000	0,000000	0,000000
211	0,00000	-0,00429	0,00000	0,000000	0,000000	0,000000
212	0,00000	-0,00431	0,00000	0,000000	0,000000	0,000000
213	0,00000	-0,00432	0,00000	0,000000	0,000000	0,000000
214	0,00000	-0,00434	0,00000	0,000000	0,000000	0,000000
215	0,00000	-0,00435	0,00000	0,000000	0,000000	0,000000
216	0,00000	-0,00437	0,00000	0,000000	0,000000	0,000000
217	0,00000	-0,00438	0,00000	0,000000	0,000000	0,000000
218	0,00000	-0,00439	0,00000	0,000000	0,000000	0,000000
219	0,00000	-0,00441	0,00000	0,000000	0,000000	0,000000
220	0,00000	-0,00442	0,00000	0,000000	0,000000	0,000000
221	0,00000	-0,00444	0,00000	0,000000	0,000000	0,000000
222	0,00000	-0,00445	0,00000	0,000000	0,000000	0,000000
223	0,00000	-0,00447	0,00000	0,000000	0,000000	0,000000
224	0,00000	-0,00448	0,00000	0,000000	0,000000	0,000000
225	0,00000	-0,00450	0,00000	0,000000	0,000000	0,000000
226	0,00000	-0,00451	0,00000	0,000000	0,000000	0,000000
227	0,00000	-0,00452	0,00000	0,000000	0,000000	0,000000
228	0,00000	-0,00454	0,00000	0,000000	0,000000	0,000000
229	0,00000	-0,00455	0,00000	0,000000	0,000000	0,000000
230	0,00000	-0,00457	0,00000	0,000000	0,000000	0,000000
231	0,00000	-0,00458	0,00000	0,000000	0,000000	0,000000
232	0,00000	-0,00460	0,00000	0,000000	0,000000	0,000000
233	0,00000	-0,00461	0,00000	0,000000	0,000000	0,000000
234	0,00000	-0,00462	0,00000	0,000000	0,000000	0,000000
235	0,00000	-0,00464	0,00000	0,000000	0,000000	0,000000
236	0,00000	-0,00465	0,00000	0,000000	0,000000	0,000000
237	0,00000	-0,00467	0,00000	0,000000	0,000000	0,000000
238	0,00000	-0,00468	0,00000	0,000000	0,000000	0,000000
239	0,00000	-0,00469	0,00000	0,000000	0,000000	0,000000
240	0,00000	-0,00471	0,00000	0,000000	0,000000	0,000000
241	0,00000	-0,00472	0,00000	0,000000	0,000000	0,000000
242	0,00000	-0,00474	0,00000	0,000000	0,000000	0,000000
243	0,00000	-0,00475	0,00000	0,000000	0,000000	0,000000
244	0,00000	-0,00476	0,00000	0,000000	0,000000	0,000000
245	0,00000	-0,00478	0,00000	0,000000	0,000000	0,000000
246	0,00000	-0,00479	0,00000	0,000000	0,000000	0,000000
247	0,00000	-0,00480	0,00000	0,000000	0,000000	0,000000
248	0,00000	-0,00482	0,00000	0,000000	0,000000	0,000000
249	0,00000	-0,00483	0,00000	0,000000	0,000000	0,000000
250	0,00000	-0,00485	0,00000	0,000000	0,000000	0,000000
251	0,00000	-0,00486	0,00000	0,000000	0,000000	0,000000
252	0,00000	-0,00487	0,00000	0,000000	0,000000	0,000000
253	0,00000	-0,00489	0,00000	0,000000	0,000000	0,000000

Load step	Ux [m]	Uy [m]	Uz [m]	Theta x [rad]	Theta y [rad]	Theta z [rad]
254	0,00000	-0,00490	0,00000	0,000000	0,000000	0,000000
255	0,00000	-0,00491	0,00000	0,000000	0,000000	0,000000
256	0,00000	-0,00493	0,00000	0,000000	0,000000	0,000000
257	0,00000	-0,00494	0,00000	0,000000	0,000000	0,000000
258	0,00000	-0,00495	0,00000	0,000000	0,000000	0,000000
259	0,00000	-0,00497	0,00000	0,000000	0,000000	0,000000
260	0,00000	-0,00498	0,00000	0,000000	0,000000	0,000000
261	0,00000	-0,00499	0,00000	0,000000	0,000000	0,000000
262	0,00000	-0,00501	0,00000	0,000000	0,000000	0,000000
263	0,00000	-0,00502	0,00000	0,000000	0,000000	0,000000
264	0,00000	-0,00503	0,00000	0,000000	0,000000	0,000000
265	0,00000	-0,00505	0,00000	0,000000	0,000000	0,000000
266	0,00000	-0,00506	0,00000	0,000000	0,000000	0,000000
267	0,00000	-0,00508	0,00000	0,000000	0,000000	0,000000
268	0,00000	-0,00509	0,00000	0,000000	0,000000	0,000000
269	0,00000	-0,00510	0,00000	0,000000	0,000000	0,000000
270	0,00000	-0,00512	0,00000	0,000000	0,000000	0,000000
271	0,00000	-0,00513	0,00000	0,000000	0,000000	0,000000
272	0,00000	-0,00514	0,00000	0,000000	0,000000	0,000000
273	0,00000	-0,00516	0,00000	0,000000	0,000000	0,000000
274	0,00000	-0,00517	0,00000	0,000000	0,000000	0,000000
275	0,00000	-0,00518	0,00000	0,000000	0,000000	0,000000
276	0,00000	-0,00519	0,00000	0,000000	0,000000	0,000000
277	0,00000	-0,00521	0,00000	0,000000	0,000000	0,000000
278	0,00000	-0,00522	0,00000	0,000000	0,000000	0,000000
279	0,00000	-0,00523	0,00000	0,000000	0,000000	0,000000
280	0,00000	-0,00525	0,00000	0,000000	0,000000	0,000000
281	0,00000	-0,00526	0,00000	0,000000	0,000000	0,000000
282	0,00000	-0,00527	0,00000	0,000000	0,000000	0,000000
283	0,00000	-0,00529	0,00000	0,000000	0,000000	0,000000
284	0,00000	-0,00530	0,00000	0,000000	0,000000	0,000000
285	0,00000	-0,00531	0,00000	0,000000	0,000000	0,000000
286	0,00000	-0,00533	0,00000	0,000000	0,000000	0,000000
287	0,00000	-0,00534	0,00000	0,000000	0,000000	0,000000
288	0,00000	-0,00535	0,00000	0,000000	0,000000	0,000000
289	0,00000	-0,00537	0,00000	0,000000	0,000000	0,000000
290	0,00000	-0,00538	0,00000	0,000000	0,000000	0,000000
291	0,00000	-0,00539	0,00000	0,000000	0,000000	0,000000
292	0,00000	-0,00540	0,00000	0,000000	0,000000	0,000000
293	0,00000	-0,00542	0,00000	0,000000	0,000000	0,000000
294	0,00000	-0,00543	0,00000	0,000000	0,000000	0,000000
295	0,00000	-0,00544	0,00000	0,000000	0,000000	0,000000
296	0,00000	-0,00546	0,00000	0,000000	0,000000	0,000000
297	0,00000	-0,00547	0,00000	0,000000	0,000000	0,000000
298	0,00000	-0,00548	0,00000	0,000000	0,000000	0,000000
299	0,00000	-0,00549	0,00000	0,000000	0,000000	0,000000
300	0,00000	-0,00551	0,00000	0,000000	0,000000	0,000000
301	0,00000	-0,00542	0,00000	0,000000	0,000000	0,000000
302	0,00000	-0,00532	0,00000	0,000000	0,000000	0,000000
303	0,00000	-0,00523	0,00000	0,000000	0,000000	0,000000
304	0,00000	-0,00514	0,00000	0,000000	0,000000	0,000000
305	0,00000	-0,00505	0,00000	0,000000	0,000000	0,000000
306	0,00000	-0,00496	0,00000	0,000000	0,000000	0,000000
307	0,00000	-0,00487	0,00000	0,000000	0,000000	0,000000
308	0,00000	-0,00477	0,00000	0,000000	0,000000	0,000000
309	0,00000	-0,00468	0,00000	0,000000	0,000000	0,000000
310	0,00000	-0,00459	0,00000	0,000000	0,000000	0,000000
311	0,00000	-0,00450	0,00000	0,000000	0,000000	0,000000
312	0,00000	-0,00440	0,00000	0,000000	0,000000	0,000000
313	0,00000	-0,00431	0,00000	0,000000	0,000000	0,000000
314	0,00000	-0,00422	0,00000	0,000000	0,000000	0,000000
315	0,00000	-0,00412	0,00000	0,000000	0,000000	0,000000
316	0,00000	-0,00403	0,00000	0,000000	0,000000	0,000000
317	0,00000	-0,00393	0,00000	0,000000	0,000000	0,000000
318	0,00000	-0,00384	0,00000	0,000000	0,000000	0,000000

Load step	Ux [m]	Uy [m]	Uz [m]	Theta x [rad]	Theta y [rad]	Theta z [rad]
319	0,00000	-0,00374	0,00000	0,000000	0,000000	0,000000
320	0,00000	-0,00365	0,00000	0,000000	0,000000	0,000000
321	0,00000	-0,00355	0,00000	0,000000	0,000000	0,000000
322	0,00000	-0,00346	0,00000	0,000000	0,000000	0,000000
323	0,00000	-0,00336	0,00000	0,000000	0,000000	0,000000
324	0,00000	-0,00327	0,00000	0,000000	0,000000	0,000000
325	0,00000	-0,00317	0,00000	0,000000	0,000000	0,000000
326	0,00000	-0,00308	0,00000	0,000000	0,000000	0,000000
327	0,00000	-0,00298	0,00000	0,000000	0,000000	0,000000
328	0,00000	-0,00288	0,00000	0,000000	0,000000	0,000000
329	0,00000	-0,00278	0,00000	0,000000	0,000000	0,000000
330	0,00000	-0,00268	0,00000	0,000000	0,000000	0,000000
331	0,00000	-0,00258	0,00000	0,000000	0,000000	0,000000
332	0,00000	-0,00248	0,00000	0,000000	0,000000	0,000000
333	0,00000	-0,00238	0,00000	0,000000	0,000000	0,000000
334	0,00000	-0,00227	0,00000	0,000000	0,000000	0,000000
335	0,00000	-0,00215	0,00000	0,000000	0,000000	0,000000
336	0,00000	-0,00203	0,00000	0,000000	0,000000	0,000000
337	0,00000	-0,00191	0,00000	0,000000	0,000000	0,000000
338	0,00000	-0,00178	0,00000	0,000000	0,000000	0,000000
339	0,00000	-0,00166	0,00000	0,000000	0,000000	0,000000
340	0,00000	-0,00153	0,00000	0,000000	0,000000	0,000000
341	0,00000	-0,00141	0,00000	0,000000	0,000000	0,000000
342	0,00000	-0,00128	0,00000	0,000000	0,000000	0,000000
343	0,00000	-0,00116	0,00000	0,000000	0,000000	0,000000
344	0,00000	-0,00103	0,00000	0,000000	0,000000	0,000000
345	0,00000	-0,00091	0,00000	0,000000	0,000000	0,000000
346	0,00000	-0,00078	0,00000	0,000000	0,000000	0,000000
347	0,00000	-0,00065	0,00000	0,000000	0,000000	0,000000
348	0,00000	-0,00052	0,00000	0,000000	0,000000	0,000000
349	0,00000	-0,00040	0,00000	0,000000	0,000000	0,000000
350	0,00000	-0,00027	0,00000	0,000000	0,000000	0,000000
351	0,00000	-0,00014	0,00000	0,000000	0,000000	0,000000
352	0,00000	-0,00001	0,00000	0,000000	0,000000	0,000000
353	0,00000	0,00012	0,00000	0,000000	0,000000	0,000000
354	0,00000	0,00025	0,00000	0,000000	0,000000	0,000000
355	0,00000	0,00038	0,00000	0,000000	0,000000	0,000000
356	0,00000	0,00051	0,00000	0,000000	0,000000	0,000000
357	0,00000	0,00064	0,00000	0,000000	0,000000	0,000000
358	0,00000	0,00077	0,00000	0,000000	0,000000	0,000000
359	0,00000	0,00090	0,00000	0,000000	0,000000	0,000000
360	0,00000	0,00103	0,00000	0,000000	0,000000	0,000000
361	0,00000	0,00116	0,00000	0,000000	0,000000	0,000000
362	0,00000	0,00130	0,00000	0,000000	0,000000	0,000000
363	0,00000	0,00143	0,00000	0,000000	0,000000	0,000000
364	0,00000	0,00156	0,00000	0,000000	0,000000	0,000000
365	0,00000	0,00169	0,00000	0,000000	0,000000	0,000000
366	0,00000	0,00183	0,00000	0,000000	0,000000	0,000000
367	0,00000	0,00196	0,00000	0,000000	0,000000	0,000000
368	0,00000	0,00209	0,00000	0,000000	0,000000	0,000000
369	0,00000	0,00223	0,00000	0,000000	0,000000	0,000000
370	0,00000	0,00236	0,00000	0,000000	0,000000	0,000000
371	0,00000	0,00250	0,00000	0,000000	0,000000	0,000000
372	0,00000	0,00263	0,00000	0,000000	0,000000	0,000000
373	0,00000	0,00277	0,00000	0,000000	0,000000	0,000000
374	0,00000	0,00290	0,00000	0,000000	0,000000	0,000000
375	0,00000	0,00304	0,00000	0,000000	0,000000	0,000000
376	0,00000	0,00317	0,00000	0,000000	0,000000	0,000000
377	0,00000	0,00331	0,00000	0,000000	0,000000	0,000000
378	0,00000	0,00345	0,00000	0,000000	0,000000	0,000000
379	0,00000	0,00358	0,00000	0,000000	0,000000	0,000000
380	0,00000	0,00372	0,00000	0,000000	0,000000	0,000000
381	0,00000	0,00386	0,00000	0,000000	0,000000	0,000000
382	0,00000	0,00399	0,00000	0,000000	0,000000	0,000000
383	0,00000	0,00413	0,00000	0,000000	0,000000	0,000000

Load step	Ux [m]	Uy [m]	Uz [m]	Theta x [rad]	Theta y [rad]	Theta z [rad]
384	0,00000	0,00431	0,00000	0,000000	0,000000	0,000000
385	0,00000	0,00458	0,00000	0,000000	0,000000	0,000000
386	0,00000	0,00485	0,00000	0,000000	0,000000	0,000000
387	0,00000	0,00514	0,00000	0,000000	0,000000	0,000000
388	0,00000	0,00543	0,00000	0,000000	0,000000	0,000000
389	0,00000	0,00572	0,00000	0,000000	0,000000	0,000000
390	0,00000	0,00601	0,00000	0,000000	0,000000	0,000000
391	0,00000	0,00631	0,00000	0,000000	0,000000	0,000000
392	0,00000	0,00661	0,00000	0,000000	0,000000	0,000000
393	0,00000	0,00692	0,00000	0,000000	0,000000	0,000000
394	0,00000	0,00723	0,00000	0,000000	0,000000	0,000000
395	0,00000	0,00756	0,00000	0,000000	0,000000	0,000000
396	0,00000	0,00790	0,00000	0,000000	0,000000	0,000000
397	0,00000	0,00824	0,00000	0,000000	0,000000	0,000000
398	0,00000	0,00860	0,00000	0,000000	0,000000	0,000000
399	0,00000	0,00898	0,00000	0,000000	0,000000	0,000000
400	0,00000	0,00938	0,00000	0,000000	0,000000	0,000000
401	0,00000	0,00936	0,00000	0,000000	0,000000	0,000000
402	0,00000	0,00934	0,00000	0,000000	0,000000	0,000000
403	0,00000	0,00932	0,00000	0,000000	0,000000	0,000000
404	0,00000	0,00930	0,00000	0,000000	0,000000	0,000000
405	0,00000	0,00928	0,00000	0,000000	0,000000	0,000000
406	0,00000	0,00926	0,00000	0,000000	0,000000	0,000000
407	0,00000	0,00924	0,00000	0,000000	0,000000	0,000000
408	0,00000	0,00922	0,00000	0,000000	0,000000	0,000000
409	0,00000	0,00920	0,00000	0,000000	0,000000	0,000000
410	0,00000	0,00918	0,00000	0,000000	0,000000	0,000000
411	0,00000	0,00916	0,00000	0,000000	0,000000	0,000000
412	0,00000	0,00914	0,00000	0,000000	0,000000	0,000000
413	0,00000	0,00912	0,00000	0,000000	0,000000	0,000000
414	0,00000	0,00910	0,00000	0,000000	0,000000	0,000000
415	0,00000	0,00908	0,00000	0,000000	0,000000	0,000000
416	0,00000	0,00905	0,00000	0,000000	0,000000	0,000000
417	0,00000	0,00903	0,00000	0,000000	0,000000	0,000000
418	0,00000	0,00901	0,00000	0,000000	0,000000	0,000000
419	0,00000	0,00899	0,00000	0,000000	0,000000	0,000000
420	0,00000	0,00897	0,00000	0,000000	0,000000	0,000000
421	0,00000	0,00895	0,00000	0,000000	0,000000	0,000000
422	0,00000	0,00893	0,00000	0,000000	0,000000	0,000000
423	0,00000	0,00891	0,00000	0,000000	0,000000	0,000000
424	0,00000	0,00889	0,00000	0,000000	0,000000	0,000000
425	0,00000	0,00887	0,00000	0,000000	0,000000	0,000000
426	0,00000	0,00885	0,00000	0,000000	0,000000	0,000000
427	0,00000	0,00883	0,00000	0,000000	0,000000	0,000000
428	0,00000	0,00881	0,00000	0,000000	0,000000	0,000000
429	0,00000	0,00879	0,00000	0,000000	0,000000	0,000000
430	0,00000	0,00877	0,00000	0,000000	0,000000	0,000000
431	0,00000	0,00875	0,00000	0,000000	0,000000	0,000000
432	0,00000	0,00872	0,00000	0,000000	0,000000	0,000000
433	0,00000	0,00870	0,00000	0,000000	0,000000	0,000000
434	0,00000	0,00868	0,00000	0,000000	0,000000	0,000000
435	0,00000	0,00866	0,00000	0,000000	0,000000	0,000000
436	0,00000	0,00864	0,00000	0,000000	0,000000	0,000000
437	0,00000	0,00862	0,00000	0,000000	0,000000	0,000000
438	0,00000	0,00860	0,00000	0,000000	0,000000	0,000000
439	0,00000	0,00858	0,00000	0,000000	0,000000	0,000000
440	0,00000	0,00856	0,00000	0,000000	0,000000	0,000000
441	0,00000	0,00854	0,00000	0,000000	0,000000	0,000000
442	0,00000	0,00852	0,00000	0,000000	0,000000	0,000000
443	0,00000	0,00850	0,00000	0,000000	0,000000	0,000000
444	0,00000	0,00847	0,00000	0,000000	0,000000	0,000000
445	0,00000	0,00845	0,00000	0,000000	0,000000	0,000000
446	0,00000	0,00843	0,00000	0,000000	0,000000	0,000000
447	0,00000	0,00841	0,00000	0,000000	0,000000	0,000000
448	0,00000	0,00839	0,00000	0,000000	0,000000	0,000000

Load step	Ux [m]	Uy [m]	Uz [m]	Theta x [rad]	Theta y [rad]	Theta z [rad]
449	0,00000	0,00837	0,00000	0,000000	0,000000	0,000000
450	0,00000	0,00834	0,00000	0,000000	0,000000	0,000000
451	0,00000	0,00832	0,00000	0,000000	0,000000	0,000000
452	0,00000	0,00830	0,00000	0,000000	0,000000	0,000000
453	0,00000	0,00828	0,00000	0,000000	0,000000	0,000000
454	0,00000	0,00826	0,00000	0,000000	0,000000	0,000000
455	0,00000	0,00823	0,00000	0,000000	0,000000	0,000000
456	0,00000	0,00821	0,00000	0,000000	0,000000	0,000000
457	0,00000	0,00819	0,00000	0,000000	0,000000	0,000000
458	0,00000	0,00817	0,00000	0,000000	0,000000	0,000000
459	0,00000	0,00815	0,00000	0,000000	0,000000	0,000000
460	0,00000	0,00812	0,00000	0,000000	0,000000	0,000000
461	0,00000	0,00810	0,00000	0,000000	0,000000	0,000000
462	0,00000	0,00808	0,00000	0,000000	0,000000	0,000000
463	0,00000	0,00805	0,00000	0,000000	0,000000	0,000000
464	0,00000	0,00803	0,00000	0,000000	0,000000	0,000000
465	0,00000	0,00801	0,00000	0,000000	0,000000	0,000000
466	0,00000	0,00798	0,00000	0,000000	0,000000	0,000000
467	0,00000	0,00796	0,00000	0,000000	0,000000	0,000000
468	0,00000	0,00793	0,00000	0,000000	0,000000	0,000000
469	0,00000	0,00791	0,00000	0,000000	0,000000	0,000000
470	0,00000	0,00788	0,00000	0,000000	0,000000	0,000000
471	0,00000	0,00786	0,00000	0,000000	0,000000	0,000000
472	0,00000	0,00783	0,00000	0,000000	0,000000	0,000000
473	0,00000	0,00781	0,00000	0,000000	0,000000	0,000000
474	0,00000	0,00778	0,00000	0,000000	0,000000	0,000000
475	0,00000	0,00775	0,00000	0,000000	0,000000	0,000000
476	0,00000	0,00773	0,00000	0,000000	0,000000	0,000000
477	0,00000	0,00770	0,00000	0,000000	0,000000	0,000000
478	0,00000	0,00768	0,00000	0,000000	0,000000	0,000000
479	0,00000	0,00765	0,00000	0,000000	0,000000	0,000000
480	0,00000	0,00762	0,00000	0,000000	0,000000	0,000000
481	0,00000	0,00760	0,00000	0,000000	0,000000	0,000000
482	0,00000	0,00757	0,00000	0,000000	0,000000	0,000000
483	0,00000	0,00754	0,00000	0,000000	0,000000	0,000000
484	0,00000	0,00751	0,00000	0,000000	0,000000	0,000000
485	0,00000	0,00749	0,00000	0,000000	0,000000	0,000000
486	0,00000	0,00746	0,00000	0,000000	0,000000	0,000000
487	0,00000	0,00743	0,00000	0,000000	0,000000	0,000000
488	0,00000	0,00740	0,00000	0,000000	0,000000	0,000000
489	0,00000	0,00738	0,00000	0,000000	0,000000	0,000000
490	0,00000	0,00735	0,00000	0,000000	0,000000	0,000000
491	0,00000	0,00732	0,00000	0,000000	0,000000	0,000000
492	0,00000	0,00729	0,00000	0,000000	0,000000	0,000000
493	0,00000	0,00726	0,00000	0,000000	0,000000	0,000000
494	0,00000	0,00724	0,00000	0,000000	0,000000	0,000000
495	0,00000	0,00721	0,00000	0,000000	0,000000	0,000000
496	0,00000	0,00718	0,00000	0,000000	0,000000	0,000000
497	0,00000	0,00715	0,00000	0,000000	0,000000	0,000000
498	0,00000	0,00712	0,00000	0,000000	0,000000	0,000000
499	0,00000	0,00709	0,00000	0,000000	0,000000	0,000000
500	0,00000	0,00706	0,00000	0,000000	0,000000	0,000000
501	0,00000	0,00703	0,00000	0,000000	0,000000	0,000000
502	0,00000	0,00700	0,00000	0,000000	0,000000	0,000000
503	0,00000	0,00698	0,00000	0,000000	0,000000	0,000000
504	0,00000	0,00695	0,00000	0,000000	0,000000	0,000000
505	0,00000	0,00692	0,00000	0,000000	0,000000	0,000000
506	0,00000	0,00689	0,00000	0,000000	0,000000	0,000000
507	0,00000	0,00686	0,00000	0,000000	0,000000	0,000000
508	0,00000	0,00683	0,00000	0,000000	0,000000	0,000000
509	0,00000	0,00680	0,00000	0,000000	0,000000	0,000000
510	0,00000	0,00677	0,00000	0,000000	0,000000	0,000000
511	0,00000	0,00674	0,00000	0,000000	0,000000	0,000000
512	0,00000	0,00671	0,00000	0,000000	0,000000	0,000000
513	0,00000	0,00668	0,00000	0,000000	0,000000	0,000000

Load step	Ux [m]	Uy [m]	Uz [m]	Theta x [rad]	Theta y [rad]	Theta z [rad]
514	0,00000	0,00665	0,00000	0,000000	0,000000	0,000000
515	0,00000	0,00661	0,00000	0,000000	0,000000	0,000000
516	0,00000	0,00658	0,00000	0,000000	0,000000	0,000000
517	0,00000	0,00655	0,00000	0,000000	0,000000	0,000000
518	0,00000	0,00652	0,00000	0,000000	0,000000	0,000000
519	0,00000	0,00649	0,00000	0,000000	0,000000	0,000000
520	0,00000	0,00646	0,00000	0,000000	0,000000	0,000000
521	0,00000	0,00643	0,00000	0,000000	0,000000	0,000000
522	0,00000	0,00640	0,00000	0,000000	0,000000	0,000000
523	0,00000	0,00637	0,00000	0,000000	0,000000	0,000000
524	0,00000	0,00633	0,00000	0,000000	0,000000	0,000000
525	0,00000	0,00630	0,00000	0,000000	0,000000	0,000000
526	0,00000	0,00627	0,00000	0,000000	0,000000	0,000000
527	0,00000	0,00624	0,00000	0,000000	0,000000	0,000000
528	0,00000	0,00620	0,00000	0,000000	0,000000	0,000000
529	0,00000	0,00617	0,00000	0,000000	0,000000	0,000000
530	0,00000	0,00614	0,00000	0,000000	0,000000	0,000000
531	0,00000	0,00610	0,00000	0,000000	0,000000	0,000000
532	0,00000	0,00607	0,00000	0,000000	0,000000	0,000000
533	0,00000	0,00604	0,00000	0,000000	0,000000	0,000000
534	0,00000	0,00600	0,00000	0,000000	0,000000	0,000000
535	0,00000	0,00597	0,00000	0,000000	0,000000	0,000000
536	0,00000	0,00594	0,00000	0,000000	0,000000	0,000000
537	0,00000	0,00590	0,00000	0,000000	0,000000	0,000000
538	0,00000	0,00587	0,00000	0,000000	0,000000	0,000000
539	0,00000	0,00583	0,00000	0,000000	0,000000	0,000000
540	0,00000	0,00580	0,00000	0,000000	0,000000	0,000000
541	0,00000	0,00577	0,00000	0,000000	0,000000	0,000000
542	0,00000	0,00573	0,00000	0,000000	0,000000	0,000000
543	0,00000	0,00570	0,00000	0,000000	0,000000	0,000000
544	0,00000	0,00566	0,00000	0,000000	0,000000	0,000000
545	0,00000	0,00563	0,00000	0,000000	0,000000	0,000000
546	0,00000	0,00559	0,00000	0,000000	0,000000	0,000000
547	0,00000	0,00556	0,00000	0,000000	0,000000	0,000000
548	0,00000	0,00552	0,00000	0,000000	0,000000	0,000000
549	0,00000	0,00548	0,00000	0,000000	0,000000	0,000000
550	0,00000	0,00545	0,00000	0,000000	0,000000	0,000000
551	0,00000	0,00541	0,00000	0,000000	0,000000	0,000000
552	0,00000	0,00538	0,00000	0,000000	0,000000	0,000000
553	0,00000	0,00534	0,00000	0,000000	0,000000	0,000000
554	0,00000	0,00530	0,00000	0,000000	0,000000	0,000000
555	0,00000	0,00527	0,00000	0,000000	0,000000	0,000000
556	0,00000	0,00523	0,00000	0,000000	0,000000	0,000000
557	0,00000	0,00519	0,00000	0,000000	0,000000	0,000000
558	0,00000	0,00515	0,00000	0,000000	0,000000	0,000000
559	0,00000	0,00512	0,00000	0,000000	0,000000	0,000000
560	0,00000	0,00508	0,00000	0,000000	0,000000	0,000000
561	0,00000	0,00504	0,00000	0,000000	0,000000	0,000000
562	0,00000	0,00501	0,00000	0,000000	0,000000	0,000000
563	0,00000	0,00497	0,00000	0,000000	0,000000	0,000000
564	0,00000	0,00493	0,00000	0,000000	0,000000	0,000000
565	0,00000	0,00489	0,00000	0,000000	0,000000	0,000000
566	0,00000	0,00486	0,00000	0,000000	0,000000	0,000000
567	0,00000	0,00482	0,00000	0,000000	0,000000	0,000000
568	0,00000	0,00478	0,00000	0,000000	0,000000	0,000000
569	0,00000	0,00475	0,00000	0,000000	0,000000	0,000000
570	0,00000	0,00471	0,00000	0,000000	0,000000	0,000000
571	0,00000	0,00467	0,00000	0,000000	0,000000	0,000000
572	0,00000	0,00463	0,00000	0,000000	0,000000	0,000000
573	0,00000	0,00460	0,00000	0,000000	0,000000	0,000000
574	0,00000	0,00456	0,00000	0,000000	0,000000	0,000000
575	0,00000	0,00452	0,00000	0,000000	0,000000	0,000000
576	0,00000	0,00448	0,00000	0,000000	0,000000	0,000000
577	0,00000	0,00445	0,00000	0,000000	0,000000	0,000000
578	0,00000	0,00441	0,00000	0,000000	0,000000	0,000000

Load step	Ux [m]	Uy [m]	Uz [m]	Theta x [rad]	Theta y [rad]	Theta z [rad]
579	0,00000	0,00437	0,00000	0,000000	0,000000	0,000000
580	0,00000	0,00433	0,00000	0,000000	0,000000	0,000000
581	0,00000	0,00429	0,00000	0,000000	0,000000	0,000000
582	0,00000	0,00426	0,00000	0,000000	0,000000	0,000000
583	0,00000	0,00422	0,00000	0,000000	0,000000	0,000000
584	0,00000	0,00418	0,00000	0,000000	0,000000	0,000000
585	0,00000	0,00414	0,00000	0,000000	0,000000	0,000000
586	0,00000	0,00410	0,00000	0,000000	0,000000	0,000000
587	0,00000	0,00407	0,00000	0,000000	0,000000	0,000000
588	0,00000	0,00403	0,00000	0,000000	0,000000	0,000000
589	0,00000	0,00399	0,00000	0,000000	0,000000	0,000000
590	0,00000	0,00395	0,00000	0,000000	0,000000	0,000000
591	0,00000	0,00391	0,00000	0,000000	0,000000	0,000000
592	0,00000	0,00387	0,00000	0,000000	0,000000	0,000000
593	0,00000	0,00384	0,00000	0,000000	0,000000	0,000000
594	0,00000	0,00380	0,00000	0,000000	0,000000	0,000000
595	0,00000	0,00376	0,00000	0,000000	0,000000	0,000000
596	0,00000	0,00372	0,00000	0,000000	0,000000	0,000000
597	0,00000	0,00368	0,00000	0,000000	0,000000	0,000000
598	0,00000	0,00364	0,00000	0,000000	0,000000	0,000000
599	0,00000	0,00361	0,00000	0,000000	0,000000	0,000000
600	0,00000	0,00357	0,00000	0,000000	0,000000	0,000000

3.2 Cap Plot in Y-direction

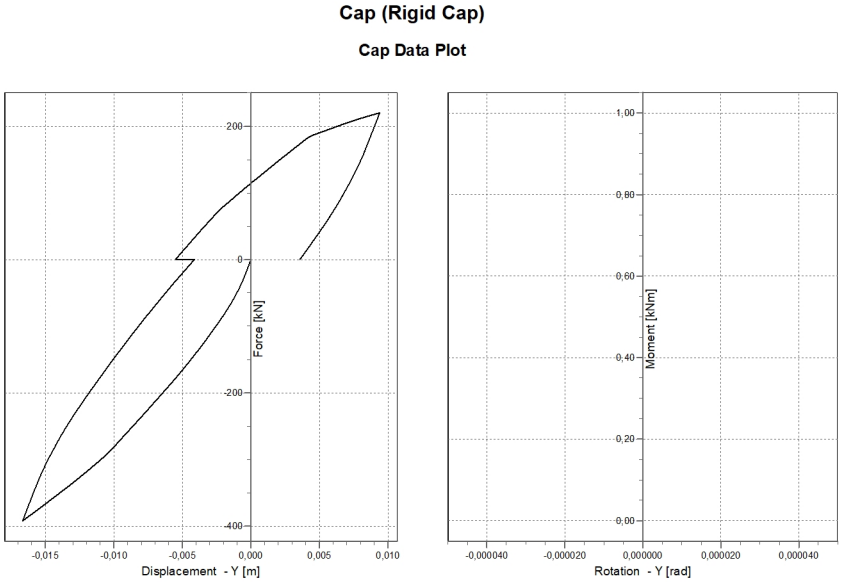

3.3 Piletop Results at Loadstep 100

3.3.1 Global Forces

Pile no.	Fx [kN]	Fy [kN]	Fz [kN]	Mxx [kNm]	Myy [kNm]	Mzz [kNm]
1	0,000	-392,000	0,000	0,000	0,000	0,000

3.3.2 Displacements

Pile no.	Global			Local		
	Ux [m]	Uy [m]	Uz [m]	Ux [m]	Uy [m]	Uz [m]
1	0,00000	-0,01666	0,00000	0,00000	-0,01666	0,00000

3.4 Piletop Results at Loadstep 200

3.4.1 Global Forces

Pile no.	Fx [kN]	Fy [kN]	Fz [kN]	Mxx [kNm]	Myy [kNm]	Mzz [kNm]
1	0,000	0,000	0,000	0,000	0,000	0,000

3.4.2 Displacements

Pile no.	Global			Local		
	Ux [m]	Uy [m]	Uz [m]	Ux [m]	Uy [m]	Uz [m]
1	0,00000	-0,00413	0,00000	0,00000	-0,00413	0,00000

3.5 Piletop Results at Loadstep 300

3.5.1 Global Forces

Pile no.	Fx [kN]	Fy [kN]	Fz [kN]	Mxx [kNm]	Myy [kNm]	Mzz [kNm]
1	0,000	0,000	0,000	0,000	0,000	0,000

3.5.2 Displacements

Pile no.	Global			Local		
	Ux [m]	Uy [m]	Uz [m]	Ux [m]	Uy [m]	Uz [m]
1	0,00000	-0,00551	0,00000	0,00000	-0,00551	0,00000

3.6 Piletop Results at Loadstep 400

3.6.1 Global Forces

Pile no.	Fx [kN]	Fy [kN]	Fz [kN]	Mxx [kNm]	Myy [kNm]	Mzz [kNm]
1	0,000	220,000	0,000	0,000	0,000	0,000

3.6.2 Displacements

Pile no.	Global			Local		
	Ux [m]	Uy [m]	Uz [m]	Ux [m]	Uy [m]	Uz [m]
1	0,00000	0,00938	0,00000	0,00000	0,00938	0,00000

3.7 Piletop Results at Loadstep 600

3.7.1 Global Forces

Pile no.	Fx [kN]	Fy [kN]	Fz [kN]	Mxx [kNm]	Myy [kNm]	Mzz [kNm]
1	0,000	0,000	0,000	0,000	0,000	0,000

3.7.2 Displacements

Pile no.	Global			Local		
	Ux [m]	Uy [m]	Uz [m]	Ux [m]	Uy [m]	Uz [m]
1	0,00000	0,00357	0,00000	0,00000	0,00357	0,00000

End of Report

Report for D-Pile Group 20.2

Pile Analysis
Developed by Deltares

Date of report:	2-12-2021
Time of report:	17:04:50
Report with version:	20.2.1.30860
Date of calculation:	2-12-2021
Time of calculation:	17:02:41
Calculated with version:	20.2.1.30860
File name:	592SIM

1 Table of Contents

2 Input Data

2.1 Topview Layout

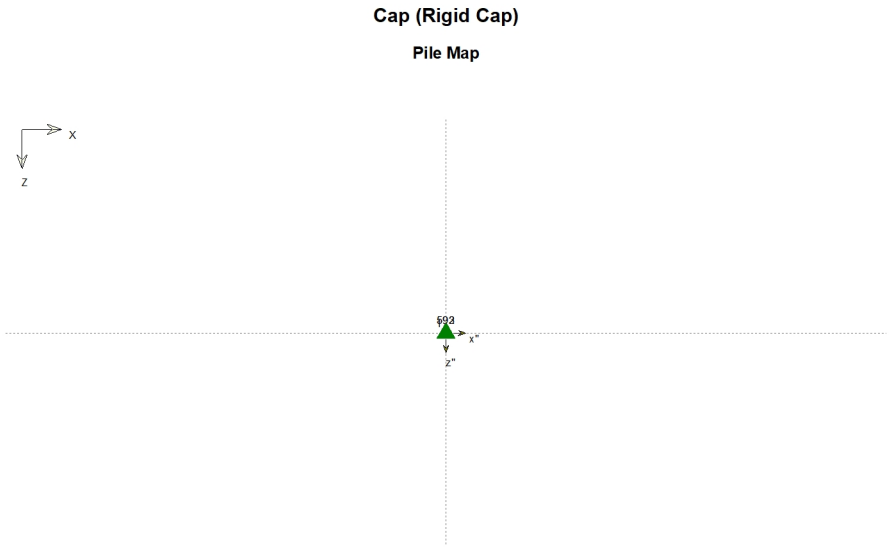

3 Calculation Results

3.1 Cap Displacements

Load step	Ux [m]	Uy [m]	Uz [m]	Theta x [rad]	Theta y [rad]	Theta z [rad]
1	0,00000	-0,00004	0,00000	0,000000	0,000000	0,000000
2	0,00000	-0,00007	0,00000	0,000000	0,000000	0,000000
3	0,00000	-0,00011	0,00000	0,000000	0,000000	0,000000
4	0,00000	-0,00015	0,00000	0,000000	0,000000	0,000000
5	0,00000	-0,00018	0,00000	0,000000	0,000000	0,000000
6	0,00000	-0,00022	0,00000	0,000000	0,000000	0,000000
7	0,00000	-0,00026	0,00000	0,000000	0,000000	0,000000
8	0,00000	-0,00029	0,00000	0,000000	0,000000	0,000000
9	0,00000	-0,00033	0,00000	0,000000	0,000000	0,000000
10	0,00000	-0,00037	0,00000	0,000000	0,000000	0,000000
11	0,00000	-0,00040	0,00000	0,000000	0,000000	0,000000
12	0,00000	-0,00044	0,00000	0,000000	0,000000	0,000000
13	0,00000	-0,00048	0,00000	0,000000	0,000000	0,000000
14	0,00000	-0,00052	0,00000	0,000000	0,000000	0,000000
15	0,00000	-0,00056	0,00000	0,000000	0,000000	0,000000
16	0,00000	-0,00060	0,00000	0,000000	0,000000	0,000000
17	0,00000	-0,00064	0,00000	0,000000	0,000000	0,000000
18	0,00000	-0,00068	0,00000	0,000000	0,000000	0,000000
19	0,00000	-0,00072	0,00000	0,000000	0,000000	0,000000
20	0,00000	-0,00077	0,00000	0,000000	0,000000	0,000000
21	0,00000	-0,00081	0,00000	0,000000	0,000000	0,000000
22	0,00000	-0,00086	0,00000	0,000000	0,000000	0,000000
23	0,00000	-0,00091	0,00000	0,000000	0,000000	0,000000
24	0,00000	-0,00096	0,00000	0,000000	0,000000	0,000000
25	0,00000	-0,00101	0,00000	0,000000	0,000000	0,000000
26	0,00000	-0,00106	0,00000	0,000000	0,000000	0,000000
27	0,00000	-0,00111	0,00000	0,000000	0,000000	0,000000
28	0,00000	-0,00116	0,00000	0,000000	0,000000	0,000000
29	0,00000	-0,00121	0,00000	0,000000	0,000000	0,000000
30	0,00000	-0,00126	0,00000	0,000000	0,000000	0,000000
31	0,00000	-0,00132	0,00000	0,000000	0,000000	0,000000
32	0,00000	-0,00137	0,00000	0,000000	0,000000	0,000000
33	0,00000	-0,00142	0,00000	0,000000	0,000000	0,000000
34	0,00000	-0,00148	0,00000	0,000000	0,000000	0,000000
35	0,00000	-0,00154	0,00000	0,000000	0,000000	0,000000
36	0,00000	-0,00160	0,00000	0,000000	0,000000	0,000000
37	0,00000	-0,00165	0,00000	0,000000	0,000000	0,000000
38	0,00000	-0,00171	0,00000	0,000000	0,000000	0,000000
39	0,00000	-0,00177	0,00000	0,000000	0,000000	0,000000
40	0,00000	-0,00184	0,00000	0,000000	0,000000	0,000000
41	0,00000	-0,00190	0,00000	0,000000	0,000000	0,000000
42	0,00000	-0,00196	0,00000	0,000000	0,000000	0,000000
43	0,00000	-0,00203	0,00000	0,000000	0,000000	0,000000
44	0,00000	-0,00209	0,00000	0,000000	0,000000	0,000000
45	0,00000	-0,00216	0,00000	0,000000	0,000000	0,000000
46	0,00000	-0,00222	0,00000	0,000000	0,000000	0,000000
47	0,00000	-0,00229	0,00000	0,000000	0,000000	0,000000
48	0,00000	-0,00236	0,00000	0,000000	0,000000	0,000000
49	0,00000	-0,00242	0,00000	0,000000	0,000000	0,000000
50	0,00000	-0,00249	0,00000	0,000000	0,000000	0,000000
51	0,00000	-0,00256	0,00000	0,000000	0,000000	0,000000
52	0,00000	-0,00263	0,00000	0,000000	0,000000	0,000000
53	0,00000	-0,00269	0,00000	0,000000	0,000000	0,000000
54	0,00000	-0,00276	0,00000	0,000000	0,000000	0,000000
55	0,00000	-0,00283	0,00000	0,000000	0,000000	0,000000
56	0,00000	-0,00290	0,00000	0,000000	0,000000	0,000000
57	0,00000	-0,00297	0,00000	0,000000	0,000000	0,000000
58	0,00000	-0,00304	0,00000	0,000000	0,000000	0,000000

Load step	Ux [m]	Uy [m]	Uz [m]	Theta x [rad]	Theta y [rad]	Theta z [rad]
59	0,00000	-0,00311	0,00000	0,000000	0,000000	0,000000
60	0,00000	-0,00318	0,00000	0,000000	0,000000	0,000000
61	0,00000	-0,00325	0,00000	0,000000	0,000000	0,000000
62	0,00000	-0,00332	0,00000	0,000000	0,000000	0,000000
63	0,00000	-0,00339	0,00000	0,000000	0,000000	0,000000
64	0,00000	-0,00346	0,00000	0,000000	0,000000	0,000000
65	0,00000	-0,00353	0,00000	0,000000	0,000000	0,000000
66	0,00000	-0,00360	0,00000	0,000000	0,000000	0,000000
67	0,00000	-0,00367	0,00000	0,000000	0,000000	0,000000
68	0,00000	-0,00375	0,00000	0,000000	0,000000	0,000000
69	0,00000	-0,00382	0,00000	0,000000	0,000000	0,000000
70	0,00000	-0,00389	0,00000	0,000000	0,000000	0,000000
71	0,00000	-0,00397	0,00000	0,000000	0,000000	0,000000
72	0,00000	-0,00404	0,00000	0,000000	0,000000	0,000000
73	0,00000	-0,00411	0,00000	0,000000	0,000000	0,000000
74	0,00000	-0,00419	0,00000	0,000000	0,000000	0,000000
75	0,00000	-0,00426	0,00000	0,000000	0,000000	0,000000
76	0,00000	-0,00434	0,00000	0,000000	0,000000	0,000000
77	0,00000	-0,00442	0,00000	0,000000	0,000000	0,000000
78	0,00000	-0,00449	0,00000	0,000000	0,000000	0,000000
79	0,00000	-0,00457	0,00000	0,000000	0,000000	0,000000
80	0,00000	-0,00465	0,00000	0,000000	0,000000	0,000000
81	0,00000	-0,00472	0,00000	0,000000	0,000000	0,000000
82	0,00000	-0,00480	0,00000	0,000000	0,000000	0,000000
83	0,00000	-0,00488	0,00000	0,000000	0,000000	0,000000
84	0,00000	-0,00496	0,00000	0,000000	0,000000	0,000000
85	0,00000	-0,00504	0,00000	0,000000	0,000000	0,000000
86	0,00000	-0,00511	0,00000	0,000000	0,000000	0,000000
87	0,00000	-0,00519	0,00000	0,000000	0,000000	0,000000
88	0,00000	-0,00527	0,00000	0,000000	0,000000	0,000000
89	0,00000	-0,00535	0,00000	0,000000	0,000000	0,000000
90	0,00000	-0,00544	0,00000	0,000000	0,000000	0,000000
91	0,00000	-0,00552	0,00000	0,000000	0,000000	0,000000
92	0,00000	-0,00560	0,00000	0,000000	0,000000	0,000000
93	0,00000	-0,00568	0,00000	0,000000	0,000000	0,000000
94	0,00000	-0,00576	0,00000	0,000000	0,000000	0,000000
95	0,00000	-0,00585	0,00000	0,000000	0,000000	0,000000
96	0,00000	-0,00593	0,00000	0,000000	0,000000	0,000000
97	0,00000	-0,00601	0,00000	0,000000	0,000000	0,000000
98	0,00000	-0,00610	0,00000	0,000000	0,000000	0,000000
99	0,00000	-0,00618	0,00000	0,000000	0,000000	0,000000
100	0,00000	-0,00626	0,00000	0,000000	0,000000	0,000000
101	0,00000	-0,00680	0,00000	0,000000	0,000000	0,000000
102	0,00000	-0,00731	0,00000	0,000000	0,000000	0,000000
103	0,00000	-0,00781	0,00000	0,000000	0,000000	0,000000
104	0,00000	-0,00827	0,00000	0,000000	0,000000	0,000000
105	0,00000	-0,00868	0,00000	0,000000	0,000000	0,000000
106	0,00000	-0,00907	0,00000	0,000000	0,000000	0,000000
107	0,00000	-0,00946	0,00000	0,000000	0,000000	0,000000
108	0,00000	-0,00984	0,00000	0,000000	0,000000	0,000000
109	0,00000	-0,01022	0,00000	0,000000	0,000000	0,000000
110	0,00000	-0,01058	0,00000	0,000000	0,000000	0,000000
111	0,00000	-0,01093	0,00000	0,000000	0,000000	0,000000
112	0,00000	-0,01128	0,00000	0,000000	0,000000	0,000000
113	0,00000	-0,01162	0,00000	0,000000	0,000000	0,000000
114	0,00000	-0,01195	0,00000	0,000000	0,000000	0,000000
115	0,00000	-0,01227	0,00000	0,000000	0,000000	0,000000
116	0,00000	-0,01258	0,00000	0,000000	0,000000	0,000000
117	0,00000	-0,01288	0,00000	0,000000	0,000000	0,000000
118	0,00000	-0,01317	0,00000	0,000000	0,000000	0,000000
119	0,00000	-0,01346	0,00000	0,000000	0,000000	0,000000
120	0,00000	-0,01375	0,00000	0,000000	0,000000	0,000000
121	0,00000	-0,01404	0,00000	0,000000	0,000000	0,000000
122	0,00000	-0,01433	0,00000	0,000000	0,000000	0,000000
123	0,00000	-0,01461	0,00000	0,000000	0,000000	0,000000

Load step	Ux [m]	Uy [m]	Uz [m]	Theta x [rad]	Theta y [rad]	Theta z [rad]
124	0,00000	-0,01490	0,00000	0,000000	0,000000	0,000000
125	0,00000	-0,01517	0,00000	0,000000	0,000000	0,000000
126	0,00000	-0,01544	0,00000	0,000000	0,000000	0,000000
127	0,00000	-0,01571	0,00000	0,000000	0,000000	0,000000
128	0,00000	-0,01598	0,00000	0,000000	0,000000	0,000000
129	0,00000	-0,01625	0,00000	0,000000	0,000000	0,000000
130	0,00000	-0,01651	0,00000	0,000000	0,000000	0,000000
131	0,00000	-0,01677	0,00000	0,000000	0,000000	0,000000
132	0,00000	-0,01703	0,00000	0,000000	0,000000	0,000000
133	0,00000	-0,01733	0,00000	0,000000	0,000000	0,000000
134	0,00000	-0,01762	0,00000	0,000000	0,000000	0,000000
135	0,00000	-0,01791	0,00000	0,000000	0,000000	0,000000
136	0,00000	-0,01820	0,00000	0,000000	0,000000	0,000000
137	0,00000	-0,01848	0,00000	0,000000	0,000000	0,000000
138	0,00000	-0,01877	0,00000	0,000000	0,000000	0,000000
139	0,00000	-0,01905	0,00000	0,000000	0,000000	0,000000
140	0,00000	-0,01934	0,00000	0,000000	0,000000	0,000000
141	0,00000	-0,01962	0,00000	0,000000	0,000000	0,000000
142	0,00000	-0,01989	0,00000	0,000000	0,000000	0,000000
143	0,00000	-0,02017	0,00000	0,000000	0,000000	0,000000
144	0,00000	-0,02044	0,00000	0,000000	0,000000	0,000000
145	0,00000	-0,02070	0,00000	0,000000	0,000000	0,000000
146	0,00000	-0,02097	0,00000	0,000000	0,000000	0,000000
147	0,00000	-0,02122	0,00000	0,000000	0,000000	0,000000
148	0,00000	-0,02148	0,00000	0,000000	0,000000	0,000000
149	0,00000	-0,02172	0,00000	0,000000	0,000000	0,000000
150	0,00000	-0,02197	0,00000	0,000000	0,000000	0,000000
151	0,00000	-0,02221	0,00000	0,000000	0,000000	0,000000
152	0,00000	-0,02245	0,00000	0,000000	0,000000	0,000000
153	0,00000	-0,02268	0,00000	0,000000	0,000000	0,000000
154	0,00000	-0,02291	0,00000	0,000000	0,000000	0,000000
155	0,00000	-0,02313	0,00000	0,000000	0,000000	0,000000
156	0,00000	-0,02336	0,00000	0,000000	0,000000	0,000000
157	0,00000	-0,02358	0,00000	0,000000	0,000000	0,000000
158	0,00000	-0,02379	0,00000	0,000000	0,000000	0,000000
159	0,00000	-0,02401	0,00000	0,000000	0,000000	0,000000
160	0,00000	-0,02422	0,00000	0,000000	0,000000	0,000000
161	0,00000	-0,02442	0,00000	0,000000	0,000000	0,000000
162	0,00000	-0,02463	0,00000	0,000000	0,000000	0,000000
163	0,00000	-0,02483	0,00000	0,000000	0,000000	0,000000
164	0,00000	-0,02502	0,00000	0,000000	0,000000	0,000000
165	0,00000	-0,02525	0,00000	0,000000	0,000000	0,000000
166	0,00000	-0,02548	0,00000	0,000000	0,000000	0,000000
167	0,00000	-0,02572	0,00000	0,000000	0,000000	0,000000
168	0,00000	-0,02596	0,00000	0,000000	0,000000	0,000000
169	0,00000	-0,02620	0,00000	0,000000	0,000000	0,000000
170	0,00000	-0,02644	0,00000	0,000000	0,000000	0,000000
171	0,00000	-0,02669	0,00000	0,000000	0,000000	0,000000
172	0,00000	-0,02693	0,00000	0,000000	0,000000	0,000000
173	0,00000	-0,02718	0,00000	0,000000	0,000000	0,000000
174	0,00000	-0,02742	0,00000	0,000000	0,000000	0,000000
175	0,00000	-0,02766	0,00000	0,000000	0,000000	0,000000
176	0,00000	-0,02791	0,00000	0,000000	0,000000	0,000000
177	0,00000	-0,02816	0,00000	0,000000	0,000000	0,000000
178	0,00000	-0,02840	0,00000	0,000000	0,000000	0,000000
179	0,00000	-0,02865	0,00000	0,000000	0,000000	0,000000
180	0,00000	-0,02890	0,00000	0,000000	0,000000	0,000000
181	0,00000	-0,02915	0,00000	0,000000	0,000000	0,000000
182	0,00000	-0,02940	0,00000	0,000000	0,000000	0,000000
183	0,00000	-0,02965	0,00000	0,000000	0,000000	0,000000
184	0,00000	-0,02990	0,00000	0,000000	0,000000	0,000000
185	0,00000	-0,03015	0,00000	0,000000	0,000000	0,000000
186	0,00000	-0,03040	0,00000	0,000000	0,000000	0,000000
187	0,00000	-0,03065	0,00000	0,000000	0,000000	0,000000
188	0,00000	-0,03090	0,00000	0,000000	0,000000	0,000000

Load step	Ux [m]	Uy [m]	Uz [m]	Theta x [rad]	Theta y [rad]	Theta z [rad]
189	0,00000	-0,03115	0,00000	0,000000	0,000000	0,000000
190	0,00000	-0,03140	0,00000	0,000000	0,000000	0,000000
191	0,00000	-0,03166	0,00000	0,000000	0,000000	0,000000
192	0,00000	-0,03191	0,00000	0,000000	0,000000	0,000000
193	0,00000	-0,03216	0,00000	0,000000	0,000000	0,000000
194	0,00000	-0,03241	0,00000	0,000000	0,000000	0,000000
195	0,00000	-0,03266	0,00000	0,000000	0,000000	0,000000
196	0,00000	-0,03291	0,00000	0,000000	0,000000	0,000000
197	0,00000	-0,03316	0,00000	0,000000	0,000000	0,000000
198	0,00000	-0,03342	0,00000	0,000000	0,000000	0,000000
199	0,00000	-0,03367	0,00000	0,000000	0,000000	0,000000
200	0,00000	-0,03393	0,00000	0,000000	0,000000	0,000000

3.2 Cap Plot in Y-direction

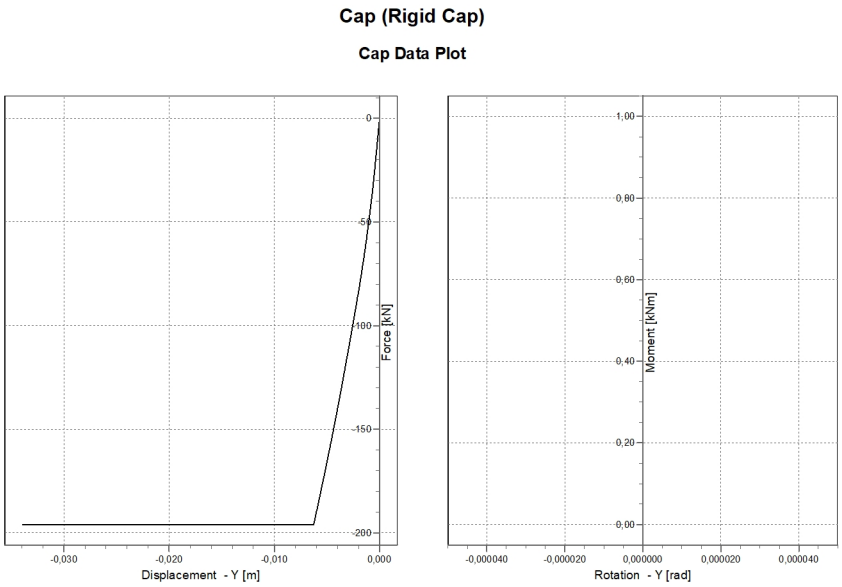

3.3 Piletop Results at Loadstep 100

3.3.1 Global Forces

Pile no.	Fx [kN]	Fy [kN]	Fz [kN]	Mxx [kNm]	Myy [kNm]	Mzz [kNm]
1	0,000	-196,000	0,000	0,000	0,000	0,000

3.3.2 Displacements

Pile no.	Global			Local		
	Ux [m]	Uy [m]	Uz [m]	Ux [m]	Uy [m]	Uz [m]
1	0,00000	-0,00626	0,00000	0,00000	-0,00626	0,00000

3.4 Piletop Results at Loadstep 200

3.4.1 Global Forces

Pile no.	Fx [kN]	Fy [kN]	Fz [kN]	Mxx [kNm]	Myy [kNm]	Mzz [kNm]
1	0,000	-196,000	0,000	0,000	0,000	0,000

3.4.2 Displacements

Pile no.	Global			Local		
	Ux [m]	Uy [m]	Uz [m]	Ux [m]	Uy [m]	Uz [m]
1	0,00000	-0,03393	0,00000	0,00000	-0,03393	0,00000

3.5 Force displacement tables for pile 1

3.5.1 Fy - y

Load step	Fy [kN]	uy [m]
0	0,000	0,00000
1	-1,960	-0,00004
2	-3,920	-0,00007
3	-5,880	-0,00011
4	-7,840	-0,00015
5	-9,800	-0,00018
6	-11,760	-0,00022
7	-13,720	-0,00026
8	-15,680	-0,00029
9	-17,640	-0,00033
10	-19,600	-0,00037
11	-21,560	-0,00040
12	-23,520	-0,00044
13	-25,480	-0,00048
14	-27,440	-0,00052
15	-29,400	-0,00056
16	-31,360	-0,00060
17	-33,320	-0,00064
18	-35,280	-0,00068
19	-37,240	-0,00072
20	-39,200	-0,00077
21	-41,160	-0,00081
22	-43,120	-0,00086
23	-45,080	-0,00091
24	-47,040	-0,00096
25	-49,000	-0,00101
26	-50,960	-0,00106
27	-52,920	-0,00111
28	-54,880	-0,00116
29	-56,840	-0,00121
30	-58,800	-0,00126
31	-60,760	-0,00132
32	-62,720	-0,00137
33	-64,680	-0,00142
34	-66,640	-0,00148
35	-68,600	-0,00154
36	-70,560	-0,00160
37	-72,520	-0,00165
38	-74,480	-0,00171
39	-76,440	-0,00177
40	-78,400	-0,00184
41	-80,360	-0,00190
42	-82,320	-0,00196
43	-84,280	-0,00203
44	-86,240	-0,00209
45	-88,200	-0,00216

Load step	Fy [kN]	uy [m]
46	-90,160	-0,00222
47	-92,120	-0,00229
48	-94,080	-0,00236
49	-96,040	-0,00242
50	-98,000	-0,00249
51	-99,960	-0,00256
52	-101,920	-0,00263
53	-103,880	-0,00269
54	-105,840	-0,00276
55	-107,800	-0,00283
56	-109,760	-0,00290
57	-111,720	-0,00297
58	-113,680	-0,00304
59	-115,640	-0,00311
60	-117,600	-0,00318
61	-119,560	-0,00325
62	-121,520	-0,00332
63	-123,480	-0,00339
64	-125,440	-0,00346
65	-127,400	-0,00353
66	-129,360	-0,00360
67	-131,320	-0,00367
68	-133,280	-0,00375
69	-135,240	-0,00382
70	-137,200	-0,00389
71	-139,160	-0,00397
72	-141,120	-0,00404
73	-143,080	-0,00411
74	-145,040	-0,00419
75	-147,000	-0,00426
76	-148,960	-0,00434
77	-150,920	-0,00442
78	-152,880	-0,00449
79	-154,840	-0,00457
80	-156,800	-0,00465
81	-158,760	-0,00472
82	-160,720	-0,00480
83	-162,680	-0,00488
84	-164,640	-0,00496
85	-166,600	-0,00504
86	-168,560	-0,00511
87	-170,520	-0,00519
88	-172,480	-0,00527
89	-174,440	-0,00535
90	-176,400	-0,00544
91	-178,360	-0,00552
92	-180,320	-0,00560
93	-182,280	-0,00568
94	-184,240	-0,00576
95	-186,200	-0,00585
96	-188,160	-0,00593
97	-190,120	-0,00601
98	-192,080	-0,00610
99	-194,040	-0,00618
100	-196,000	-0,00626
101	-196,000	-0,00680
102	-196,000	-0,00731
103	-196,000	-0,00781
104	-196,000	-0,00827
105	-196,000	-0,00868
106	-196,000	-0,00907
107	-196,000	-0,00946
108	-196,000	-0,00984
109	-196,000	-0,01022
110	-196,000	-0,01058

Load step	Fy [kN]	uy [m]
111	-196,000	-0,01093
112	-196,000	-0,01128
113	-196,000	-0,01162
114	-196,000	-0,01195
115	-196,000	-0,01227
116	-196,000	-0,01258
117	-196,000	-0,01288
118	-196,000	-0,01317
119	-196,000	-0,01346
120	-196,000	-0,01375
121	-196,000	-0,01404
122	-196,000	-0,01433
123	-196,000	-0,01461
124	-196,000	-0,01490
125	-196,000	-0,01517
126	-196,000	-0,01544
127	-196,000	-0,01571
128	-196,000	-0,01598
129	-196,000	-0,01625
130	-196,000	-0,01651
131	-196,000	-0,01677
132	-196,000	-0,01703
133	-196,000	-0,01733
134	-196,000	-0,01762
135	-196,000	-0,01791
136	-196,000	-0,01820
137	-196,000	-0,01848
138	-196,000	-0,01877
139	-196,000	-0,01905
140	-196,000	-0,01934
141	-196,000	-0,01962
142	-196,000	-0,01989
143	-196,000	-0,02017
144	-196,000	-0,02044
145	-196,000	-0,02070
146	-196,000	-0,02097
147	-196,000	-0,02122
148	-196,000	-0,02148
149	-196,000	-0,02172
150	-196,000	-0,02197
151	-196,000	-0,02221
152	-196,000	-0,02245
153	-196,000	-0,02268
154	-196,000	-0,02291
155	-196,000	-0,02313
156	-196,000	-0,02336
157	-196,000	-0,02358
158	-196,000	-0,02379
159	-196,000	-0,02401
160	-196,000	-0,02422
161	-196,000	-0,02442
162	-196,000	-0,02463
163	-196,000	-0,02483
164	-196,000	-0,02502
165	-196,000	-0,02525
166	-196,000	-0,02548
167	-196,000	-0,02572
168	-196,000	-0,02596
169	-196,000	-0,02620
170	-196,000	-0,02644
171	-196,000	-0,02669
172	-196,000	-0,02693
173	-196,000	-0,02718
174	-196,000	-0,02742
175	-196,000	-0,02766

Load step	Fy [kN]	uy [m]
176	-196,000	-0,02791
177	-196,000	-0,02816
178	-196,000	-0,02840
179	-196,000	-0,02865
180	-196,000	-0,02890
181	-196,000	-0,02915
182	-196,000	-0,02940
183	-196,000	-0,02965
184	-196,000	-0,02990
185	-196,000	-0,03015
186	-196,000	-0,03040
187	-196,000	-0,03065
188	-196,000	-0,03090
189	-196,000	-0,03115
190	-196,000	-0,03140
191	-196,000	-0,03166
192	-196,000	-0,03191
193	-196,000	-0,03216
194	-196,000	-0,03241
195	-196,000	-0,03266
196	-196,000	-0,03291
197	-196,000	-0,03316
198	-196,000	-0,03342
199	-196,000	-0,03367
200	-196,000	-0,03393

End of Report